DEVELOPMENT AND INVESTIGATION OF POLYMERIC VASCULAR GRAFT MATERIALS

Andrew G. Whitton, MSci, MRes

Bioengineering Unit,
University of Strathclyde

Supervisors:
Dr. Richard Black
Prof. David Flint

Thesis submitted for the degree of Doctor of Engineering (EngD)

This thesis is the result of the author's original research. It has been composed by the author and has not been previously submitted for examination which has led to the award of a degree.

Signed:

Date:

ABSTRACT

Vascular disease leading to stenotic or occluded arteries and subsequent ischemia is often treated using bypass grafts. Although autologous material, the preferred source for constructing a bypass graft, often provides a graft with satisfactory patency rates, it is not always available and suitable for use. In these cases synthetic material is often utilised but these rarely produce the patency of autologous material. The causes of their failure are compliance mismatch and thrombus formation.

For this reason, polyurethane was studied as a suitable graft material due to its compliant nature and excellent thromboresistance. Investigations into the effect of the material stiffness and potential to allow adsorption of blood-borne proteins were conducted, showing that an optimum combination of the two existed for the migration of vascular tissue onto the graft. As this migration can lead to restenosis and reocclusion of a graft, the ability to control the migration rate could limit the failure of the graft through these processes.

The electrospinning technique was utilised to develop a polyurethane processing method for producing fibrous materials which better replicate the geometry of the native vessel than do other materials commonly used. The effect of this fibrous structure was to maintain the differentiated state of the vascular cells resident upon it. This contractile state is consistent with that in which cells are found in a healthy vessel and is the opposite state to that of the synthetic phenotype in which cells are found when on planar surfaces *in vitro* and in diseased vessels. It therefore follows that the control of the phenotypic state can prevent the dedifferentiation of the cells into the synthetic state, whereupon they form a thickening of the vessel wall which, again, ultimately results in restenosis.

Mechanical deformation of these electrospun materials was conducted in a dynamic system, replicating the motion in the vascular system *in vivo*. The effect of this dynamic system was to further develop the degree to which the cells demonstrated a contractile phenotype. This highlights that the electrospun polyurethane graft

material represents a promising alternative to those commonly used, perhaps due to it somewhat recapitulating the topographical and mechanical nature of the native vessel.

I dedicate this thesis to my darling Anthea, we made this journey together.

ACKNOWLEDGMENTS

Firstly I would like to thank my supervisors Dr. Richard Black and Prof. David Flint for all of their help, guidance, and encouragement in developing my work. Their wisdom and insight have been much appreciated. Special thanks also go to Prof. Helen Grant for all the help and encouragement she has generously given. In addition, I would very much like to thank Biomer Technology Ltd and especially Simon Dixon for their help and support. I am also very grateful for the guidance and support given by Dr. Rachel Williams.

For their invaluable technical knowledge and experience and their generosity in sharing these I would like to thank Katie Henderson, Jo-Ann Smith and Elizabeth Tonner. I never failed to be surprised at the ingenuity with which they helped me develop feasible ways to conduct my experiments. This work would also not have been possible without Brian Cartlidge and Liz Goldie who worked tirelessly to help me use and understand the microscope that has formed such a large part of the work. This was in addition to expanding their own knowledge, and therefore usefulness of the machine. I would also like to thank Dave Smith and Liz Smith who have helped on numerous occasions to solve a wide variety of problems.

Last, but by no means least, I would very much like to thank Davie Robb, Steven Murray and John MacLean. Their skill and expertise have been behind the construction of almost all the pieces of equipment created in this work, including the prototypes from which they were developed. Their knowledge and patient explanations have helped me to develop the equipment as required and their dedication and generosity with their time has kept it all running. Their help has been invaluable.

CONTENTS

CHAPTER 1

GENERAL INTRODUCTION

Diseases of the cardiovascular system are responsible for more deaths in the western world than any other single cause. The most common route for mortality is through a process called atherosclerosis, whereby fatty deposits accumulate inside an artery. These deposits cause a thickening of the vessel wall which, in turn, causes a narrowing of the vessel lumen and a reduction in blood flow to the downstream organ or tissues, causing ischemia and subsequent tissue damage.

One method for treatment of narrowed or stenotic arteries is to provide a bypass graft to allow the blood to flow past the blockage by an alternate route. The preferred material for use when making a bypass graft is the patient's own vascular tissue, however, when this is not available or its use is not appropriate an alternative material is required. Currently, the two most frequently used synthetic vascular graft materials are expanded polytetrafluoroethylene (ePTFE) and woven polyethylene terephthalate (PET/Dacron®) as described by Xue and Griesler (2003). Although some success has been had in their use in peripheral and carotid artery grafts, the patency rates of coronary and small diameter (<6mm) grafts constructed of these two materials is significantly lower than with autologous arterial or venous material. The reasons postulated for these higher failure rates are due to their thrombogenicity and the compliance mismatch between the diseased vessel and the graft, sometimes accentuated by the sutures used (Tiwira et al., 2003, Zeebregts et al., 2004), which also leads to poor hemodynamics, as discussed by Brossolet (1992).

The number of coronary artery bypass surgeries is on the rise, leading to an increase in the need to perform repeat revascularisation procedures, and the availability of autologous donor tissue will subsequently decline in these repeat cases. Also, the use of autologous material has the drawback of donor site morbidity and the additional unnecessary procedure to facilitate its initial removal. Tissue engineered blood vessels have been heralded as the future for vascular graft applications (Kakasis et al., 2005) but are still in their infancy. For these reasons it is evident that the need for a suitable synthetic graft material that has an appropriate patency in applications other than peripheral and carotid bypass grafts is greater than ever before. As such it is important to understand the reasons why the current attempts to create such grafts

have failed and then find ways to improve upon the grafts to reduce this failure rate. The reasons that both ePTFE and PET grafts fail can be attributed to two main properties; their inherent thrombogenicity in the short-term and their lack of compliance in the mid- to long-term.

Both ePTFE and PET have elastic moduli significantly higher than that of the native artery with the synthetic materials being in the ranges 400-750MPa and 2-4GPa respectively, while the natural artery is in the range 100-1000kPa, depending on the type of the artery, age of the subject and the presence of a pathological state. This discrepancy in compliance at the join between the native and synthetic vessel, or anastomosis, which can cover four orders of magnitude, causes localised turbulent flow. When combined with the vessel calibre mismatch this turbulence produces shear stresses that cause endothelial cell damage and leads to a growth of tissue in the vessel in the region of the anastomosis. This growth continues onto the graft surface and forms a pannus of tissue, causing a narrowing of the lumen, as detailed by Zilla et al. (2007). The general non-compliance of the graft also disrupts the flow characteristics of the blood that travels along it.

Two methods previously used for altering the modulus of a vascular graft have been through the use of various polymer processing methods and through the choice of the material itself. The former only has a limited effect on the compliance of ePTFE and PET grafts, however the use of alternative polymers has been found to produce a graft with mechanical properties much closer to those of the native vessel. Polyurethane (PU), for instance can be created with a wide range of moduli from as low as 100kPa.

A problem common to all synthetic vascular grafts is the effect of thrombosis, the response of blood to any surface other than that formed by an uninjured endothelium. Graft materials elicit a thombogenic effect to a greater or lesser extent depending on their physicochemical nature. For instance, the electronegativity of ePTFE makes its failure rate due to thrombosis less than that of PET but still a significant limiting factor in terms of use in small diameter vascular grafts.

As with alterations to compliance, there are two main methods utilised to control and limit thrombus formation on the luminal surface of vascular grafts. The first is through designing the graft such that thrombus formation on its surface is reduced by selecting specific polymers that are inherently thromboresistant, chemical treatment of the surface of the polymer to make it more resistant to the deposition of the proteins that commence the formation of a thrombus (Francois et al., 1996) or by the inclusion of heparin on the surface. The second method is to design the graft such that endothelialisation of the graft occurs and this endothelial layer provides the resistance of the graft to failure due to thrombosis. Although this latter method has provided very promising results in animal models and in vitro as shown by Birchall et al. (2001), the same level of endothelialisation has not been recreated in clinical trials. For this reason, perhaps a more promising route for creating a thromboresistant synthetic graft in the near future is to create one that has this inherent property. Once again PU has excellent thromboresistant properties which can be further improved by the incorporation of heparin on its luminal surface.

The mechanical and thromboresistant properties of polyurethanes make these polymers look like the ideal material for use in vascular grafts. Initial trials using PU foams were less than successful due to, amongst other factors, the *in vivo* hydrolytic degradation of the polymer (Zhang et al., 1997). However, more modern PUs such as polyether urethanes (Labow et al., 1995) show far superior resistance to degradation and constitute a very promising choice for further investigation into their use in vascular graft applications. As the failure of PU grafts due to thrombosis is secondary to their failure due to the presence of tissue growth at the anastomotic regions it was the latter that was studied in this work, along with investigations into ways that the material can be processed in order to minimise this effect. More specifically, it was the aim of the work described in this thesis to answer the following questions:

How does the stiffness of the polyurethane graft material affect the patency of the graft? In particular, how does this affect the migration of the adjacent vascular

tissue onto the graft surface, an important first step in the formation of this pannus of tissue and the stenosis of the graft?

What is the effect of the polymer processing method on the formation of the tissue growth? Is there a way that the invasion and subsequent growth of the adjacent vascular tissue on the luminal surface of the graft can be controlled through the geometric properties of the polymer, which are in turn controlled by the way that the polymer is processed?

Does the compliant nature of the polymer affect the behaviour of the tissue that resides upon it? Arteries, due to their elastic nature, distend with the pulse pressure and this can have an effect on the resident cells. If an elastic vascular graft is used will its distension have an effect on the growth of the tissue attached to it?

In order to answer these questions an *in vitro* model of a vascular graft was created to replicate the environment *in vivo* while providing the ability to investigate a number of variables in a systematic investigation.

CHAPTER 2

BACKGROUND AND LITERATURE REVIEW

2.1 Structure and Function of Blood Vessels

The main function of a blood vessel is to transport blood around the body, providing nutrients and oxygen to the various tissues and removing metabolites, waste products and carbon dioxide for excretion. These vessels are divided into two types; arteries which transport oxygen to the body, taking blood away from the heart, and veins which carry deoxygenated blood back towards the heart, although the oxygenated state of the blood is the opposite in the pulmonary vascular system. All blood vessels are composed of up to three distinct layers as shown in figure 2.1; the tunicas intima, media and adventitia. These layers vary in thickness and even presence between arteries and veins and between different size vessels, with capillaries for example being only one layer thick.

The innermost and thinnest layer, the tunica intima is composed of an endothelium, a single layer of squamous endothelial cells (ECs) supported on the internal elastic lamina. The roles of the endothelium are numerous, but are based mainly on its barrier nature. Firstly, the endothelium acts as a selective barrier to the transport into and out of the blood of materials such as nutrients, metabolites and leukocytes. Secondly it forms a surface that prevents blood clotting and the formation of a thrombus. However, when the vessel is damaged the underlying surface is exposed, which elicits a thrombus formation and limits the loss of blood through the damaged vessel. Other functions of the endothelium are through control of vasoconstriction and vasodilation, in controlling inflammation and sensing of blood flow-induced shear stresses as illustrated by Ganguli et al. (2005) and Punchard et al. (2007).

The middle layer, the tunica media is the thickest layer in arteries and is composed of a fibrous material resident to numerous smooth muscle cells (SMCs). In arteries this layer is significantly thicker than in veins and the number of smooth muscle cells is substantial. These cells are elongated and oriented in the circumferential direction of the vessel and are able to contract and vary the calibre of the vessel, giving the vascular system the ability to control the flow of blood to the different parts of the

body. The elastic nature of these cells and the surrounding fibrous proteins confers to the artery its elastic nature which aids in the flow of blood (Bia et al., 2006).

Lastly, the tunica adventitia consists mainly of connective tissue which anchors the vessel to the surrounding tissue, providing stability. This layer is also innervated by nerves, through which the blood vessel calibre is controlled.

2.2 Vascular Disease

The underlying cause of a large proportion of all cases of cardiovascular disease is atherosclerosis, a condition where the vessel wall thickens due to the accumulation of fatty deposits. There are many risk factors known for atherosclerosis, such as diabetes, smoking, hypertension, being of the male gender and raised serum concentrations of low-density lipoproteins (LDL) (Fruchart et al., 2004). The disease process starts with a deposition and build-up in the arterial wall of LDL from the blood. When this LDL becomes oxidised by free radicals it can cause damage to the vessel wall, especially the endothelium. This, damage and the chemotactic effect of the LDL, attract monocytes to the area, which migrate through the endothelium and differentiate into macrophages which start to consume the LDL. As the macrophages have no way to metabolise or process the LDL their accumulation in the cells progresses to a point where the macrophages have a distinctive lipid-laden appearance, at which point they are referred to as foam cells. These foam cells continue to take up the LDL until they rupture, releasing a greater amount of LDL into the artery wall, inducing the accumulation of more monocytes and perpetuating the cycle. It has been shown that endothelial and smooth muscle cells too uptake, to some degree, this LDL and as it is cytotoxic, cell damage ensues.

One function of the endothelium not mentioned previously is its role to moderate the function of the underlying smooth muscle cells. Through the release of soluble factors such as nitrous oxide and platelet derived growth factors (Dardik et al., 2005) and through more direct contact, the endothelial cells maintain the SMCs in a state

where they are aligned, essentially non-proliferating, non-synthetic and non-migratory; a quiescent state. When the endothelium is damaged the ability of the ECs to control the behaviour of the SMCs is compromised, leading to a change in their characteristics. The change in the hemodynamic characteristics of a diseased vessel have also been implicated, by Dancu et al (2004), to influence the pathological state through the release of vasoactive agents and their subsequent effect on the surrounding vascular smooth muscle cell (VSMC). In addition the damage to the SMCs and that of the surrounding matrix disrupts the effect of the extracellular matrix (ECM) on the cells (Streuli, 1999) in that it normally maintains the cell in a quiescent state. The SMCs in the medial layer begin to migrate towards the intima whereupon the proliferation rate increases and the deposition of large quantities of EMC proteins ensues (Karim, 1998). This process, shown in figure 2.2, is termed intimal hyperplasia (IH) and, along with the deposits of fatty material, is the main cause for the thickening of the artery wall.

Normally an artery has the ability to distend to accommodate the wall thickening and, if composed mostly of intimal hyperplastic lesions the atherosclerotic plaque is stable and asymptomatic. However, if the accumulation of fatty deposits is more substantial a fibrous cap forms over the lesion, which is weak and easily ruptured by the shear stresses of blood flow. Once ruptured a thrombus formation can easily cause a substantial stenosis of the vessel and tissue ischemia. When this occurs in the coronary artery the ensuing event is termed a myocardial infarction or heart attack and can cause irreversible damage to the heart and easily lead to a loss of life. In addition, the embolus created from the breakdown of the fibrous cap and resulting thrombus can cause serious blockages in the downstream vessels.

The changes which occur in the VSMCs which lead to the process of IH are the consequence of a shift in the phenotypic state of the cells. Those resident in a healthy vessel with an intact endothelium demonstrate a contractile phenotype. In this highly differentiated state the cells are, as stated previously, quiescent; proliferation, migration and ECM deposition are attenuated. The cells possess a fusiform morphology, arranged in a spiral fashion but aligned almost

circumferentially around the vessel (as shown in figure 2.1) so as to experience the strain of the distending vessel to the maximal amount, providing vessel tone, while also using their contractile nature to alter the calibre of the vessel. When the cell is removed from this environment it will often convert to a more dedifferentiated, synthetic phenotype. Proliferation, migration and ECM production all increase while the spindle-shaped morphology transforms to a more stellate, fibroblastic one.

The response to injury of a blood vessel involves many of the same processes which work to prevent the loss of blood. Damage to the endothelium exposes the underlying vessel to the blood, causing a clotting cascade and the formation of a thrombus over the damaged endothelium, creating a barrier to the further loss of blood. The damaged endothelium and ECM lead to the phenotypic change in the medial smooth muscle cells whereupon they migrate to the site of injury, proliferate and deposit EMC. This provides the required reparation to the structure of the blood vessel and leads to the healing of the wound. When healing is complete the VSMCs, quiesced by the re-established endothelium and intact ECM, revert to their contractile phenotype. This is seen by many, such as Subbotin (2007), to be the same process as that involved in intimal hyperplasia with the latter being an uncontrolled version, perhaps due to the continued onslaught of damage due to the toxic accumulation of fatty materials.

When an artery is narrowed, particularly by the stenosis caused by atherosclerosis it is crucial that the blood flow is resumed either by reopening the vessel or by providing an alternative route for the flow. The former can be accomplished through angioplasty and stenting, where a balloon is inflated inside the vessel to mechanically reopen the blockage while the stent provides the support to hold the vessel open. This, like atherosclerosis itself, can cause endothelial (Nestor et al., 2006) and vessel (Batchelor et al., 1998) damage and as the underlying cause of the stenosis is not treated these vessels can easily reocclude (Kotani et al., 2006).

Figure 2.1. Schematic diagram of the blood vessel showing tunicas intima, media and adventitia. The cobblestone-like endothelial cells can be seen to cover the luminal surface of the vessel, while the walls are composed mostly of elongated smooth muscle cells, oriented circumferentially around the walls of the vessel.

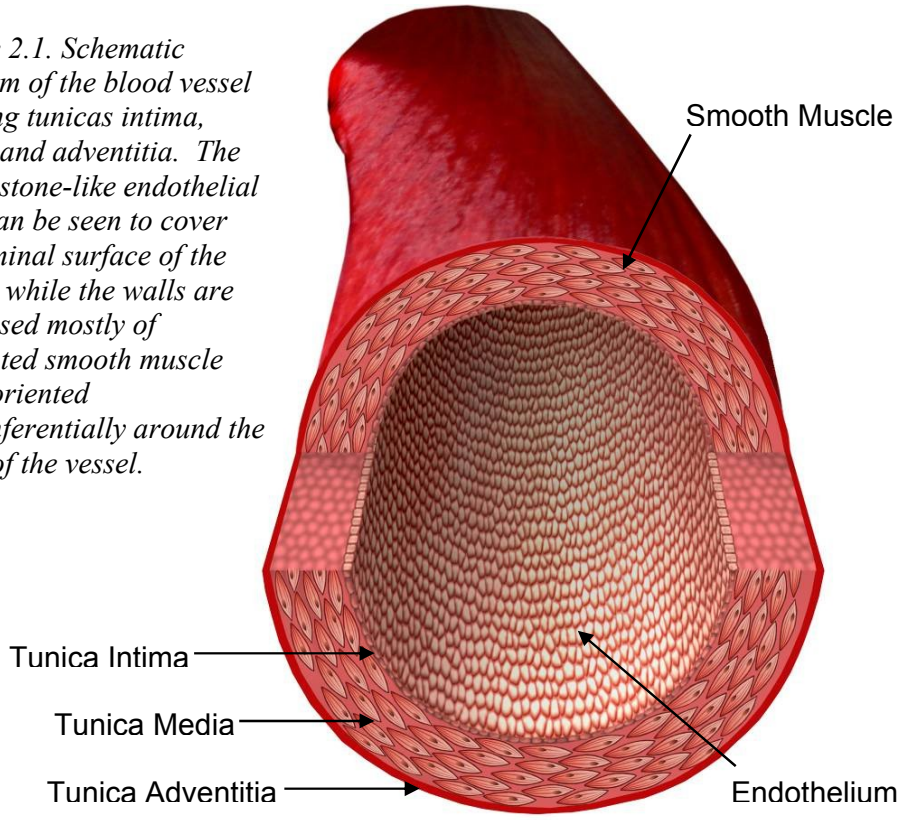

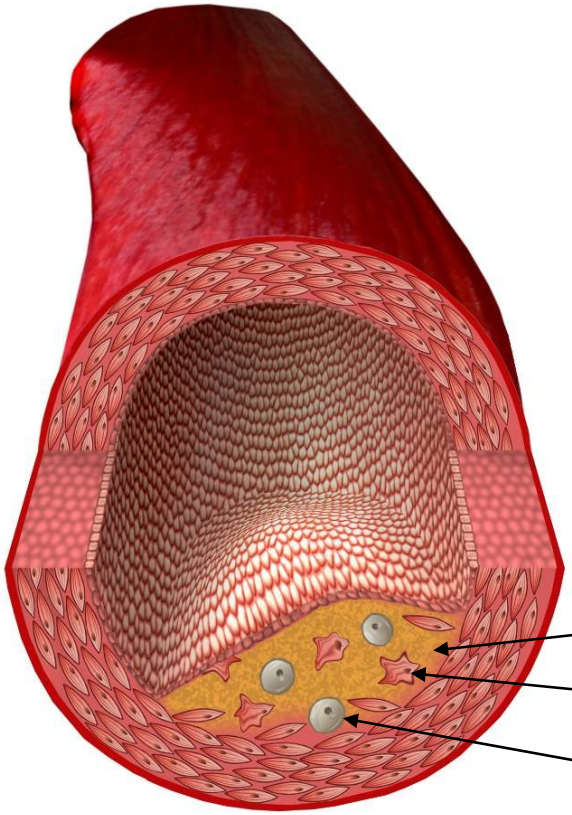

Figure 2.2. The vessel as shown in figure 2.1 after the development of an atherosclerotic plaque. The plaque can be seen to be filled with a fibrous or fatty substance and resident macrophages and synthetic smooth muscle cells are visible.

2.3 Bypass Grafts

In addition to stenting, there is a treatment method that involves a more invasive procedure. An alternative path for blood flow is created to bypass the blockage in the artery. This can be performed using the patient's own vascular material which, although occasionally failing due to damage to the endothelium of the replacement vessel (Mitra et al., 2006), are often successful at resuming blood flow. However, when the use of autologous tissue is contraindicated, synthetic materials are often used. The two most commonly used synthetic graft materials, ePTFE and PET are limited in their use and effectiveness due to thrombosis occurring on the luminal surface of the graft and the recurrence of intimal hyperplasia at the graft anastomoses. In particular, the use of these two materials in grafts with diameters less than 6mm has been found to be associated with significant reocclusion. This has been attributed to a number of factors including compliance mismatch and subsequent hemodynamic factors. Areas of localised high flow rate and therefore fluid shear stress can cause endothelial damage while low flow rates can cause a build-up of chemicals such as growth factors and can also lead to increased thrombus formation. The effect of the compliance mismatch can also cause unnatural stresses on the blood vessel wall and therefore the resident cells.

In a similar manner to the initial occlusion of the diseased blood vessel, the failure of ePFTE and PET grafts is partly driven by intimal hyperplasia. Damage to the blood vessel and endothelium from the surgical procedure itself (Tsui and Dashwood, 2002 and Fujita et al. 2006), as well as from the ensuing turbulent blood flow and subsequent endothelial damage, leads to a similar process which occurs in the atherosclerotic vessel. However, unlike in the bypassed intimal hyperplastic lesion, the VSMC growth is not restricted solely to the host vessel. A pannus of tissue is formed over the anastomotic ends of the graft, consisting again of mostly VSMCs and ECM proteins. This is predictably caused by the migration of VSMCs from the media of the adjacent artery onto the luminal surface of the graft whereupon it adopts a hyperproliferative state and deposits excessive quantities of ECM. For this reason

limiting the growth of the tissue over the graft surface may slow or help prevent the progression of the stenosis of the vessel.

One hope for success of bypass grafts is that they will become endothelialised by the transanastomotic migration of endothelial cells (Simmers et al, 2007). This endothelial layer, in principle, could lead to a loss of thrombosis on the vessel surface and provide control over the nearby smooth muscle cell phenotype. However, the promising results for endothelialisation of some grafts seen *in vitro* and in animal models (Tsuchida et al., 1997) have yet to be repeated in clinical trials.

The response of the resident VSMCs to the graft can be affected by a number of properties of the graft. By utilising these it may be possible to gain some control over the processes that lead to the failure of the graft. The following chapters introduce a number of these properties, the reasons why they may have an effect on the development of intimal hyperplasia and an overview of the relevant current investigations in that area.

CHAPTER 3

EFFECT OF POLYMERIC GRAFT MATERIAL STIFFNESS ON SMOOTH MUSCLE MIGRATION RATE

3.1 Introduction

Cardiovascular disease is the single greatest killer in the western world. Many of the surgical interventions used to treat this disease experience low patency rates due to IH (Lemson et al, 2000), whereby growth of vascular tissue surrounding the site of intervention leads to re-occlusion of the vessel. An important early stage in this process is the migration of vascular smooth muscle cells VSMCs out of the vessel wall and onto the surface of any implanted device used in the surgery (Pitsch et al, 2000, Gerthoffer, 2007). The ability to control or limit this migration may be a key tool in the reduction of the progression of IH and the maintenance of a viable vascular implant.

Immediately after the contact of blood with a foreign object, such as a polymeric vascular implant, the adsorption of proteins from the blood onto the surface of the object occurs as described by Goodman et al. (1990). In any subsequent attachment of cells to the object the cell-substrate interaction will be greatly influenced by the adsorbed proteins. When SMCs migrate onto a vascular implant from the surrounding tissue, the proteins adsorbed to the surface will have a significant impact on the cellular locomotion. One protein that is of particular relevance to this situation is fibronectin (Fn) which exists in relatively high concentrations in the blood, adsorbs readily onto implanted surfaces and has a significant effect on cell attachment and migration. The Fn molecule presents a site for attachment of the cell through its integrins and can influence the formation of focal adhesions and ultimately the ability of the cell to attach to the surface (Smith et al, 2004, Rajagopalan et al, 2004 and Koo et al, 2002).

Another factor which can affect the interaction between a cell and its substratum is the stiffness of the substrate as shown by Lo et al. (2000) and Yeung et al. (2005). It has been shown that a cell cultured on softer materials will attach poorly to the surface while showing a distinct lack of mature focal adhesions. Conversely a cell on a stiffer substrate will attach much more strongly and larger, more defined adhesion assemblies are produced. This has led to the discovery of a process termed

durotaxis or mechanotaxis in which a cell will migrate preferentially in the direction of increasing substrate stiffness (Lo et al, 2000, Jiang et al, 2006 and Wong et al, 2003).

The investigation of the combination of the effects of the surface density of adhesion sites and substrate stiffness on cell migration rate have been conducted in terms of models of cells in the extracellular matrix to explore the migration through tissue (Peyton and Putnam, 2005). The migration rate is maximal at intermediate values of both these variables, showing that there is an optimum substrate stiffness and adhesion site density for cell migration. However, the two factors are not independent, as an increase in the density of adhesion sites will lower the value of the substrate stiffness where migration is greatest, and vice versa. This relationship has been predicted theoretically and is based on the effect of both these factors on the attachment strength of a cell to a substrate and the consequential effect on the migration rate (DiMilla et al, 1991). The model surmises that at a low attachment strength the cell will be unable to provide sufficient traction forces to traverse the substratum while at higher attachment forces the adhesion complexes and actin filament framework will be more highly developed and take longer to release from the surface at the dorsal end of the cell. As DiMilla et al. (1993) have shown, the maximum migration rate occurs with a compromise between the two when the adhesion strength is at an intermediate value. However, so far no studies have been conducted regarding the effect of adhesion site density and substrate stiffness on migration rates in the context of implanted polymeric materials and adsorbed proteins. When it is considered that, in the case of polyurethane, when the polymer stiffness is altered there is also likely to be a variation in the wettability of the polymer and the subsequent protein adsorption, a study of this nature is even more important. For this reason the migration rate of SMCs across two grades of polyether urethane (PU) and tissue culture polystyrene after the adsorption of plasma Fn was measured in this study.

Numerous migration assays have been developed to study cell locomotion over surfaces (Decaestecker et al, 2007). Although many of them have been developed to

replicate the effect of migration through tissue, which is a rather crude representation, the use of a 2D model in this study is much more representative of the nature of the migration over an implanted surface. These assays can generally be divided into two groups; single cell and cell population assays. Generally, single cell migration assays (Berns and Berns, 1982) require the use in a microscope stage-top incubator and time-lapse microscopy (Roy et al., 2002), the acquisition and analysis of data can be time consuming and removing the interaction between cells provides less accurate a representation of the nature of the situation *in-vivo*. Two of the most popular cell population assays are the scratch (Liang et al, 2007 and Todaro et al, 1965) and Teflon fence (Pratt et al, 1984) assays, with the former having many potential problems due to inconsistencies in the scratch area, the effect of cell damage at the wound edge (Okada et al., 1995) and the removal of any adsorbed proteins from the surface, although some were overcome in the work conducted by Keese at al. (2004). A modification of the fence assay was therefore chosen to analyse cell migration as it does not rely on a microscope stage-top incubator, time-lapse microscopy, or transmitted light/phase contract microscopy. Removal of the reliance on transmitted light for microscopy is advantageous when working with opaque polymeric samples.

3.2 Materials and Methods

3.2.1 PU Substrata Preparation and Fn Adsorption

Solutions of PU grades Z1A1 and Z3A1 (Biomer Technology Ltd., Runcorn, UK) were produced at 15% w/w in dimethylformamide (DMF) by mixing on a roller mixer for 48 hours at room temperature (RT) and atmospheric pressure. Solvent cast PU films were produced in flat bottomed glass petri dishes by removal of solvent at 65ºC under a vacuum of 45kPa for a duration of 48 hours. PU sheets were removed from the petri dishes and soaked in deionised water for 24 hours before use for complete removal of all remaining solvent. In all following work the sheet surface in

contact with the air was used solely so as to minimise substrate variation due to the properties of the petri dish surface.

Fn solutions in phosphate buffered saline (PBS) were produced at a range of concentrations using bovine plasma fibronectin (Invitrogen, Paisley, UK). These solutions were applied to the surface of small sections of the PU sheets in addition to tissue culture-treated polystyrene (TCP) at a volume to adsorbing surface area ratio of approximately $0.4cm^{-1}$. Concentrations of Fn of 0.31, 0.63, 1.13, 2.5, 5, 10 and 20μg/ml were utilised to determine the relationship between this concentration and the amount of Fn adsorbed onto the surfaces. For all subsequent work in which adsorbed Fn was required, concentrations of 0, 1, 2 and 4μg/ml were used, as above this concentration range the rate of increase of the density of adsorbed protein with increasing concentration started to plateaux. After static incubation for 1 hour, the solutions were aspirated and washed twice with PBS. Treatment of the surfaces with solutions of bovine serum albumin (BSA), 1% (w/v) in PBS for 1 hour, without agitation, was performed in order to minimise any further adsorption of Fn from the subsequent addition of serum-containing media during cell culture work. At no point after the initial application of the Fn solutions were the surfaces allowed to completely dry so as to avoid creating a protein/air interface which could affect the conformation of the Fn.

A quantitative analysis of the density of adsorbed Fn was conducted with the enzyme-linked immunosorbent assay (ELISA) assay using an anti-fibronectin primary antibody (Invitrogen, Paisley, UK) and a horseradish peroxidase (HRP)-conjugated secondary antibody (Invitrogen). The maximum density of fibronectin detected on any combination of polymer and applied Fn solution concentration in this analysis was, for future comparison, labelled as '100% saturation'. This was used in all future analyses as a semi-arbitrary unit of measure of adsorbed Fn density as, in the absence of a reference or calibration sample, a definitive density in $\mu g/cm^2$ was not obtainable.

3.2.2 Measurement of the Mechanical Properties of PU Substrata

5mm x 20mm rectangular specimens of Z1A1 and Z3A1 were cut, using a scalpel, from sheets of the cast polymers (15% w/w in DMF), formed as previously described. 20 of each of these samples strips were loaded individually into an Instron tensile testing device (Instron, High Wycombe, UK) and stretched at a rate of 6mm/min. The force/extension relationship was determined using the device's software and used in conjunction with the sample geometry to measure the modulus of elasticity of the two polymers at an extension of 5%.

3.2.3 Determination of the Wettability of PU Substrata

Contact angle measurements of the three polymers were performed using the static sessile drop method (Uyama et al. 1991). Samples of Z1A1, Z3A1 and TCP were placed onto the stage of a DSA100 Drop Shape Analysis System (Kruss, Hamburg, Germany) and a 2μL drop of deionised water was deposited on top. Images of the 6 drops were obtained on each surface type from a horizontal viewpoint and used by the system software DSA3 to determine the contact angle between the drop and the surface.

3.2.4 Cell Culture

Human aortic smooth muscle cells (hASMCs) were obtained from Lonza (Slough, UK) and maintained in medium 231 supplemented with smooth muscle growth supplement (SMGS), both from Invitrogen (Paisley, UK), at 37°C with 5% CO_2. Cells were used between passage 2 and 4 and during this time the population doubling times remained constant if not allowed to reach confluence.

3.2.5 Migration Assay

The migration assay used, as illustrated in figure 3.1, had been adapted from the Teflon fence migration assay (Pratt et al., 1984). 1cm^2 square sections of Fn-coated Z1A1, Z3A1 and TCP were placed into 24-well tissue culture plates. Small sections of clear silicone membranes (10mmx7mm) were placed onto the polymer sections to mask approximately two thirds of the substrate. The force between the two smooth surfaces was sufficient to hold the two together without the use of an adhesive. An ELISA assay was performed to verify that the Fn surface density was unaffected by the application of the silicone membrane to the polymer surface. Phase contrast microscope images were obtained of each sample with an Axio Imager Z1 microscope (Zeiss, Hertfordshire, UK) in order to determine the position of the mask edge to facilitate the measurement of the migration rates.

1ml aliquots of hASMCs in medium 231/SMGS were seeded into the wells at $4x10^4 cm^{-2}$, corresponding to approximately 80% confluence and allowed to attach to the Fn-coated polymer substrate, the silicone mask and the base of the wells. Once confluence had been achieved on the substrata after 1-2 days, the masks were removed, the samples were washed in PBS to remove any unattached cells and transferred to a new 24-well plate containing fresh media at 1ml per well. Samples in which the cell population was damaged or had migrated under the silicone mask prior to its removal were discarded. Cells in the remaining samples were allowed to invade the unpopulated region, previously unreachable due to the mask. Three days after removal of the mask, the cell samples had their covering media removed, were washed twice with PBS and then fixed with 4% paraformaldehyde at RT for 10 minutes. Cells were then stained with 4',6-diamidino-2-phenylindole (DAPI, Invitrogen, Paisley, UK), 300nM in PBS at RT for 10 minutes.

Cell migration samples were imaged using the fluorescence imaging capabilities of an Axio Imager Z1 microscope (Zeiss, Hertfordshire, UK). Image analysis software, ImageJ (NIH, Bethesda, MD) was used to analyse the fluorescence images of the cells' nuclei. The 'Threshold' function and the 'Cell Counter' plugin were used to

determine the position of each cell nuclei in each image. The centre of a nuclei of a cell was used to represent the position of the cell. For each sample the migrated distance of the cell population was calculated as the average displacement perpendicular and relative to the mask edge of all cells occupying the area previously inaccessible due to the mask. The mean migration rate for each sample was calculated using the duration of the experiment which varied between experiments but was approximately 72 hours.

In order to determine the constancy of the migration rate and therefore obtain a measure of the effect of experiment duration on the resultant migration rate, a number of identical migration samples were created as described above. All utilised Z1A1 as the substrate without the application of Fn. Samples were fixed, stained and analysed 2, 4 and 7 days post commencement of the experiment to determine the migrated distance and migration rate at these times.

3.2.6 Proliferation Rate Measurement

As the migration assay used was a cell population assay and as the duration of the experiment was approximately three days it is conceivable that proliferation would occur and affect the migration rate result. Therefore, the proliferation rate was measured on the three polymers, without the application of a Fn solution.

hASMCs in medium 231/SMGS were deposited onto samples of TCP (24-well tissue culture plates), and sections of Z1A1 and Z3A1 PUs to achieve final densities of approximately $5x10^3$ cm^{-2}. Cell samples were cultured at 37ºC in 5% CO_2 for up to 5 days with a media change on day 3. Each day, a number of each sample were removed from culture, washed twice in PBS and fixed in 4% (v/v) paraformaldehyde before being mounted in a DAPI containing mountant. 200 fluorescence images were obtained of each cell sample using an Axio Imager Z1 microscope (Zeiss, Hertfordshire, UK), with each image representing an area of approximately $1.4mm^2$ and all images were analysed using the ImageJ software. The 'Cell Counter' plugin

was used to determine cell densities from the cell nuclei on each substrate at each time point and from these the proliferation rate of hASMCs on each surface was determined.

3.2.7 Attachment Assay

A centrifugal detachment assay as described by Chu et al. (1994) was used to study cell-substratum adhesive forces. As illustrated in figure 3.2, 96-well tissue culture plates were modified to allow the PU substrates to provide the base of the wells, unmodified plates were used as the TCP samples. Fn was then allowed to adsorb onto the bases from Fn solutions at 0, 1, 2 and 4μg/ml, as described in section 3.2.1. hASMCs were seeded at $2x10^4cm^{-2}$, at approximately 40% confluence, onto the Fn-coated polymer bases and allowed to attach for one hour, this seeding density was used to reduce cell-cell contact after spreading. The medium was then removed from the plates which were subsequently transferred into a Beckman Coulter centrifuge (Beckman Coulter (UK) Ltd, High Wycombe, UK) with a rotor designed to accept 96-well plates. The centrifugal force from the centrifuge was used to detach the cells from their substrata; each sample was exposed to one of 500, 1000, 1500, 2000 or 2500rpm centrifuge spin speeds for a duration of 5 minutes. The medium was removed before centrifugation to increase the difference in density between the cell and its surrounding environment, which would produce a larger detachment force for a given rotation speed. The effect of removing the media from the cell samples for the duration of the centrifugation was taken into account with the use of a control sample which was inverted for 5 minutes.

After cell detachment, cell samples were fixed and stained with DAPI and fluorescent images were obtained and analysed, all as described above. The number of cells removed was measured by comparing the cell surface densities of each sample at each spin speed with the density in the control sample (sample inverted for 5 min, equivalent to 1g). The spin speed which corresponded to the removal of 50% of the cells from the sample surface was determined for each sample. The average

volume of cells in suspension and a density of the cell of 1.07g/ml (Godin et al., 2007) were used to determine the median detachment force for cells on each sample.

3.2.8 Cytoskeletal Staining

hASMCs were seeded at $2x10^4 cm^{-2}$ onto the Fn-coated polymeric substrata and allowed to attach for 24 hours. Cells samples were then removed from media, washed twice with PBS, fixed with 4% paraformaldehyde before membrane permeabilisation with Triton X-100, 0.25% (v/v) in PBS. Cell samples were incubated for 1 hour with an anti-vinculin antibody (Sigma-Aldrich, Dorset, UK) and then an anti-mouse Texas Red-conjugated secondary antibody (Vector Laboratories Ltd., Peterborough, UK) and fluorescein isothiocyanate (FITC)-conjugated phalloidin (Invitrogen, Paisley, UK) for the visualisation of F-actin filaments, both followed by three washes in PBS. Samples were then mounted onto coverslips using a DAPI-containing mountant, Prolong Gold (Invitrogen, Paisley, UK).

Fluorescence images were obtained using the Apotome function of an Axio Imager Z1 microscope (Zeiss, Hertfordshire, UK). Cell spread area and focal adhesion size were analysed by manually outlining either on the image, using the ImageJ software and again using the software to calculate the given area.

3.2.9 Statistical Analysis

All values are expressed as means ± the standard deviation (SD). Student's t-test or one-way analysis of variance (ANOVA) and the multiple comparison test were used to determine statistical significance. The level of significance was taken as $P < 0.05$.

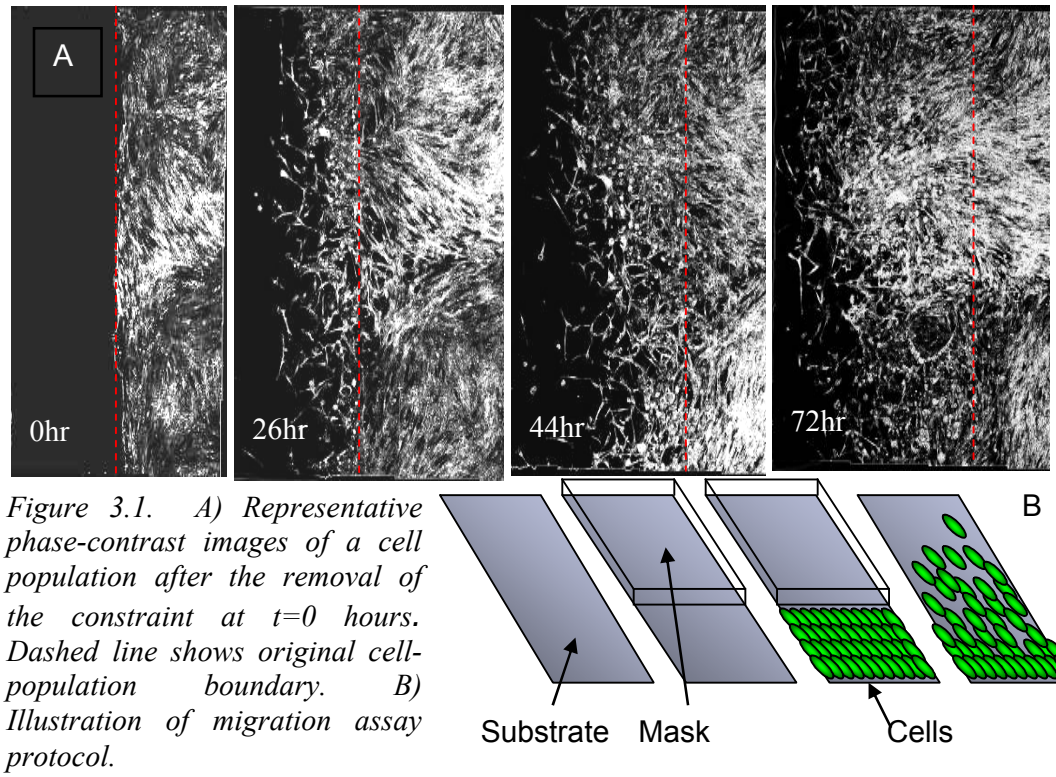

Figure 3.1. A) Representative phase-contrast images of a cell population after the removal of the constraint at t=0 hours. Dashed line shows original cell-population boundary. B) Illustration of migration assay protocol.

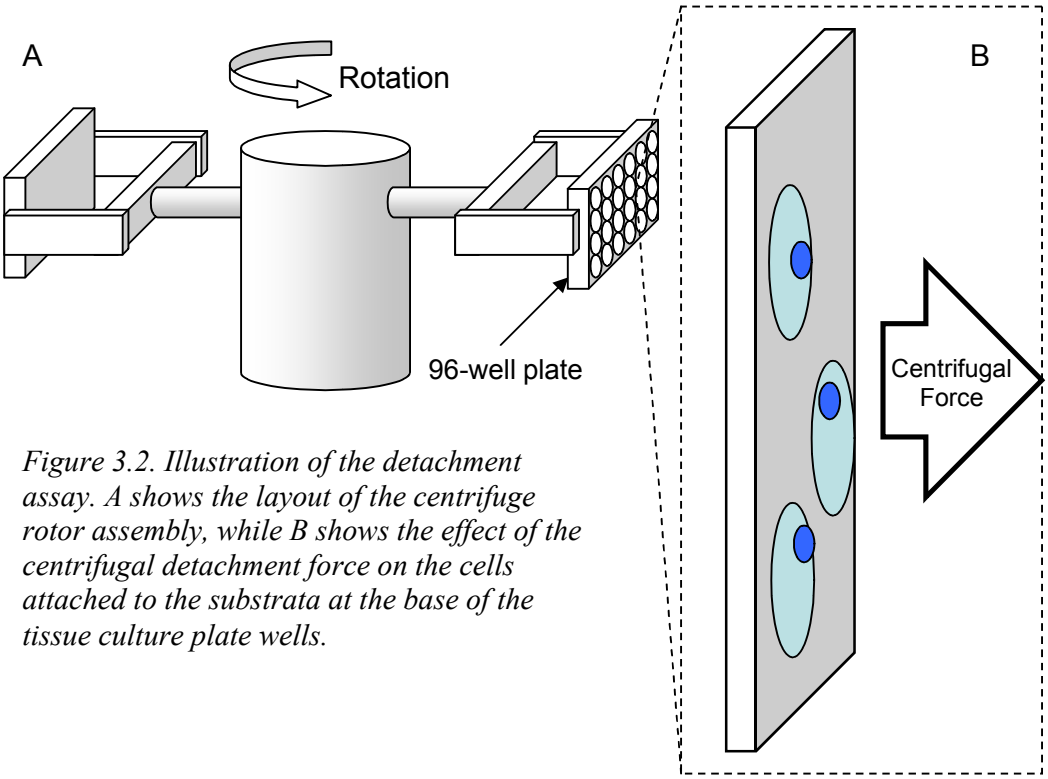

Figure 3.2. Illustration of the detachment assay. A shows the layout of the centrifuge rotor assembly, while B shows the effect of the centrifugal detachment force on the cells attached to the substrata at the base of the tissue culture plate wells.

3.3 Results

3.3.1 Fn Adsorption

Fn was adsorbed onto polymer surfaces from solution at a range of concentrations between 0 and 20μg/ml. Measurement of the quantity of adsorbed protein was determined using the ELISA assay as shown in figure 3.3. This shows that the quantity of Fn detected on each of the polymer surfaces increased asymptotically towards a threshold value with the concentration of the protein in the applied solution. This threshold value differed for each of the polymers investigated. In all following results the threshold level for Fn adsorption onto TCP was termed the 'saturation' level and all adsorbed Fn densities are expressed as a percentage thereof. The curves in figure 3.3 were used to determine the Fn surface density on all samples from the concentration in the solution applied.

In order to determine whether any further experimental steps remove adsorbed Fn from the surfaces, ELISA assays were repeated for surfaces after the application of Fn solutions at 4μg/ml for one hour at RT then exposure to a series of 12 washes with PBS, the application of the silicone mask utilised in the migration assay in the current study or scratching with a 1000μl pipette tip to represent the scratch migration assay used extensively elsewhere. No change in measured Fn density was found after any number of washes in PBS, up to 12 extra washes, over those required to perform the assay. The application of the silicone mask had no significant effect on the adsorbed Fn density, however scratching of the polymer surface removed approximately 50% of the Fn in a highly inconsistent manner as represented in figure 3.4.

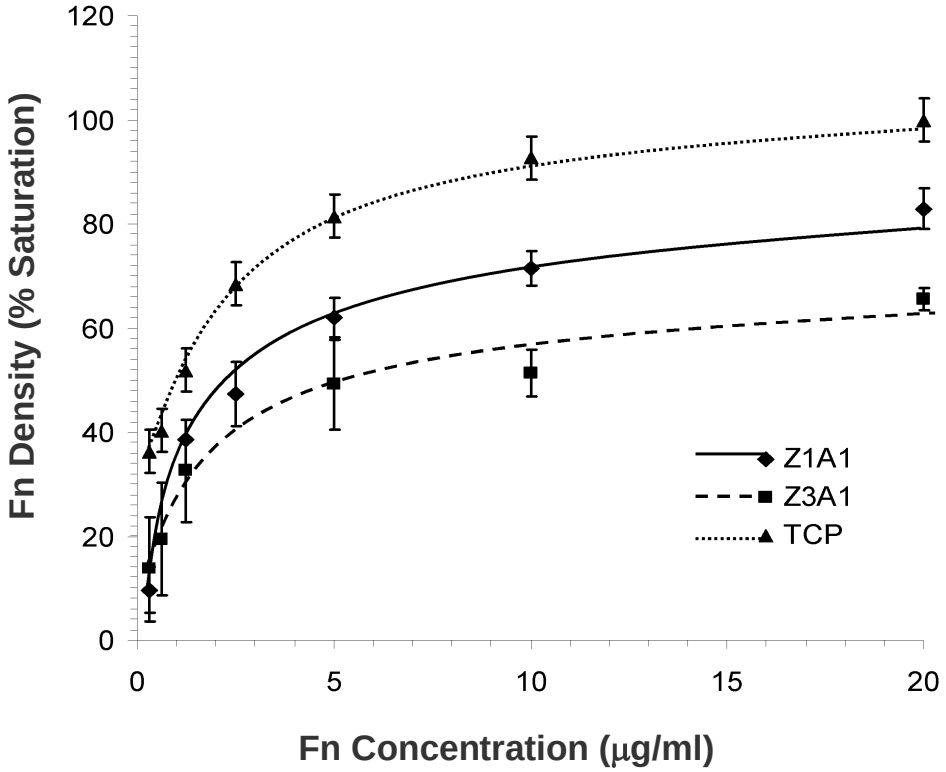

Figure 3.3. Effect of Fn concentration in PBS on the adsorption of the protein to the three polymer surfaces after 1 hour at room temperature. Fn densities were measured with the ELISA assay. All points represent mean values ± SD, n=6, and are expressed using the semi-arbitrary units of % of saturation where the maximum value of the Fn density found, on TCP after the application of a 20μg/ml solution of Fn was applied, was labelled as 100% saturation. These curves were then used to convert the concentration of Fn (in mg/ml) applied into an adsorbed surface density.

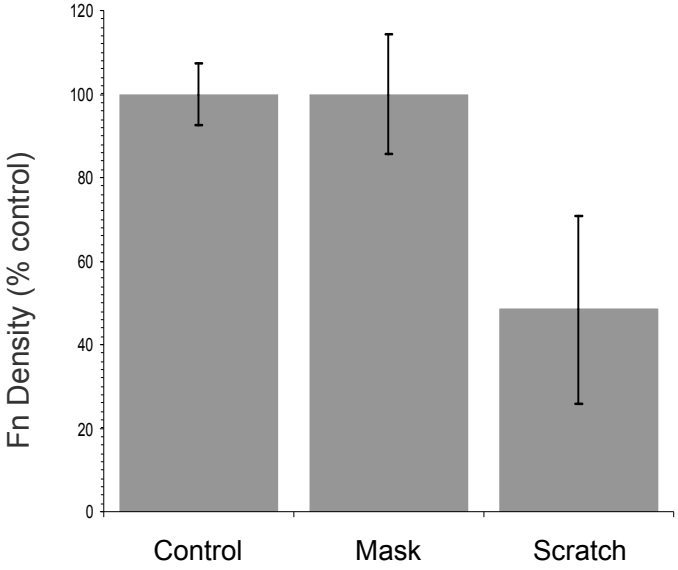

Figure 3.4. Effect of migration assay conditions on the amount of adsorbed Fn. ELISA assays were used to measure the remaining adsorbed Fn on TCP after incubation with 4μg/ml Fn, then the application of the silicone mask or scratching with a 1000μl pipette tip versus untouched control samples. Bars represent mean values ± SD, n=6.

3.3.2 Elastic Moduli Measurements

Force-extension measurements of the two polyurethanes, Z1A1 and Z3A1, as shown in figure 3.5, were used to determine their elastic moduli. These were found to be 2.04 ± 0.41 MPa and 12.35 ± 1.24 MPa respectively (n=20). The modulus of the polystyrene tissue culture plastic was not measured as it was too stiff to be compatible with the method of testing. However, the bulk stiffness of polystyrene used in tissue culture applcations has been shown to be 3.37 ± 0.52GPa but the surface stiffness can decrease to 2.6 ± 0.39GPam due to the surface treatment (Lubarsky et al., 2004), but is still approximately three orders of magnitude greater than the two polyurethanes.

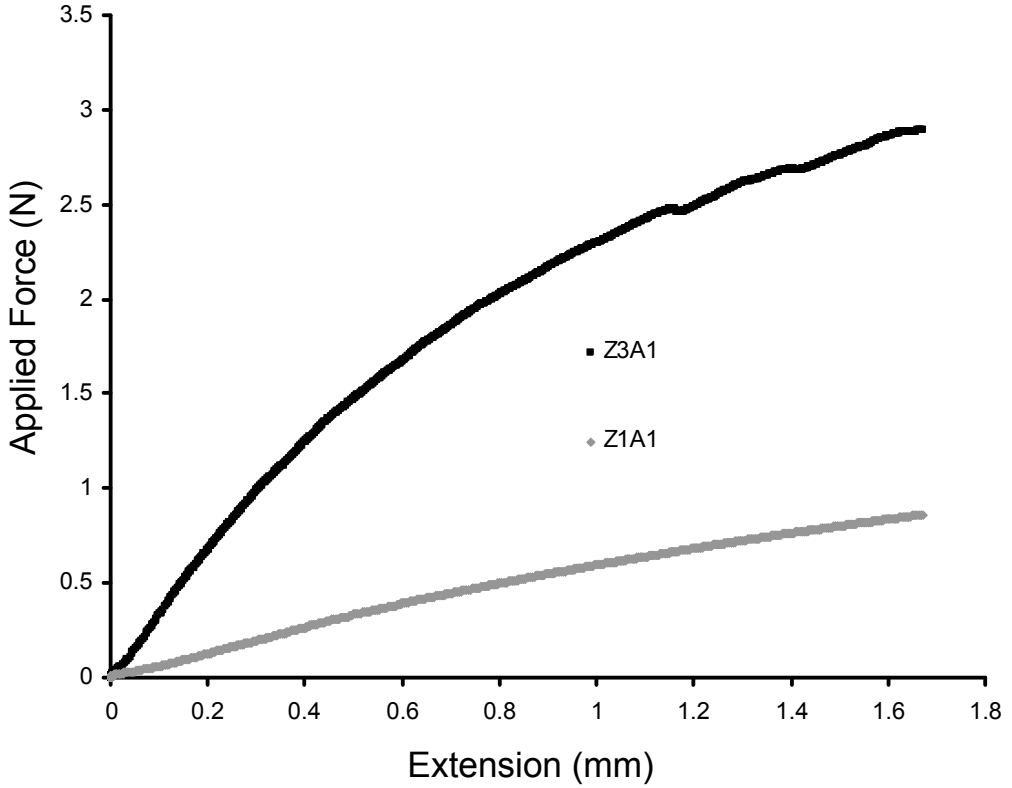

Figure 3.5. Representative force-extension relationships for the two grades of PU, Z1A1 and Z3A1. A measurement of the stiffness of the two were obtained at a strain of 5%.

3.3.3 Contact Angle Measurements

The ability of a protein to adsorb to a solid surface is strongly associated with the wettability of the surface as shown by Macdonald et al, (2002), Wei et al. (2009) and Grinnell et al. (1981). To determine whether the variations in Fn adsorption to the three polymers is due to this effect the relative hydrophilicities were measured. The contact angle of a static drop deposited onto each of the polymers was used as a measure of the wettability of the polymers. As seen in figure 3.6, no significant difference in the contact angle was measured on the two polyurethanes, while the contact angle on the TCP surface was markedly lower, indicating it to be a more hydrophilic surface than either of the PUs.

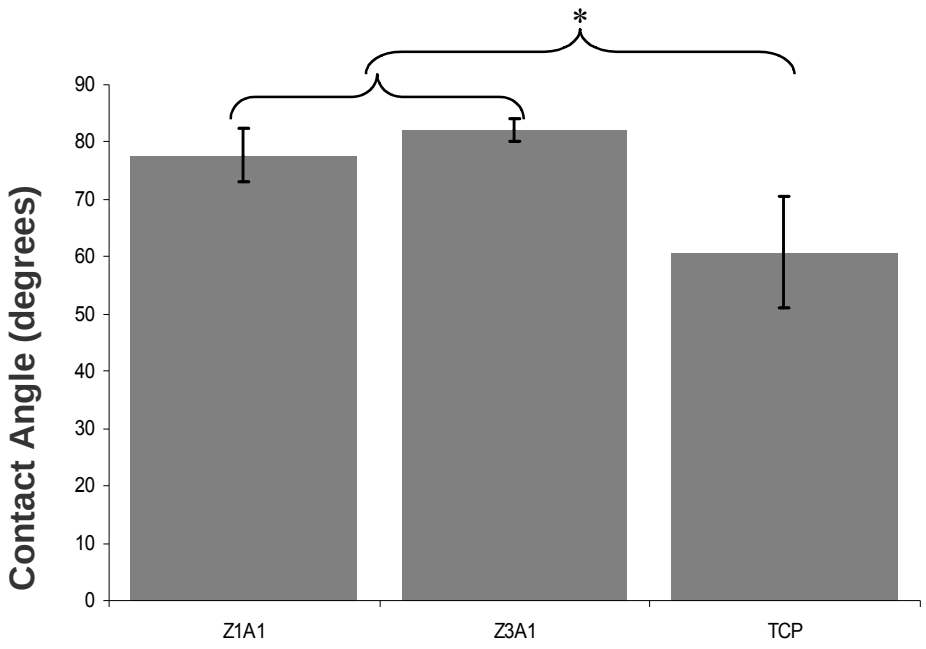

Figure 3.6. Contact angle measurements on polymer samples before Fn adsorption. The static sessile drop method was used to determine surface wettability. Bars represent mean values ± SD, n=6. Asterisk shows statistically significant differences in contact angle ($p<0.05$) between TCP and both Z1A1 and Z3A1, analysed using the Student's t-test.

3.3.4 Mask Migration Assay

The mask migration assay developed was found to be a simple and reliable method for determining the migration rate of whole cell populations across a surface. The migration rates across a range of surfaces were constant during all experiment durations investigated, up to 7 days post mask removal, as shown in figure 3.7, with the coefficient of determination of the linear relationship being 0.998. Therefore, the migration rate can be said to be independent of the duration of the experiment, thus removing inter-sample variations due to the experiment duration.

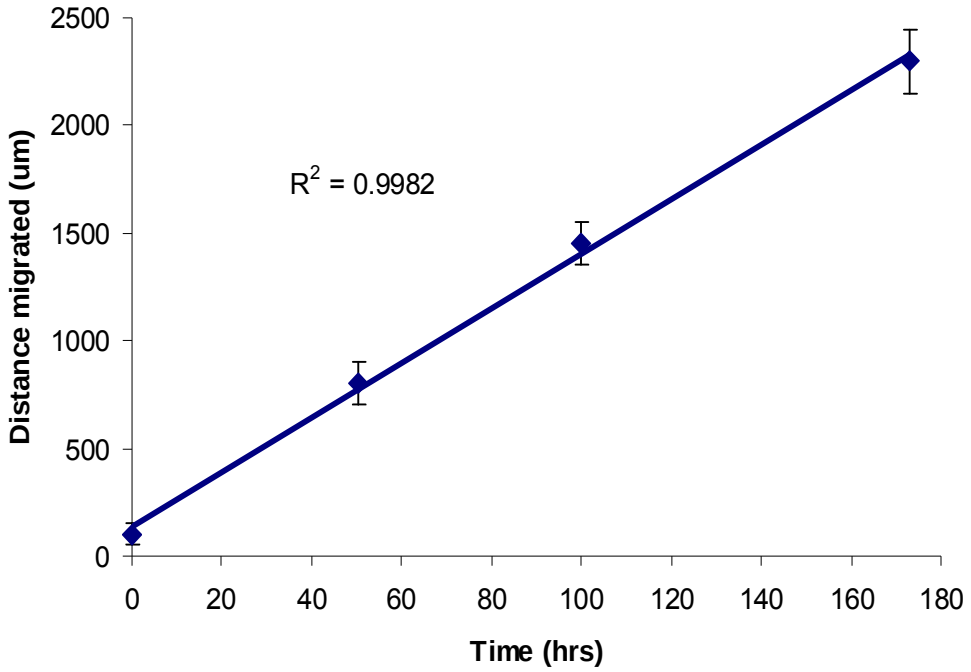

Figure 3.7. The migratory distance of hASMCs over Z1A1 at a number of time points. The migration rate can be seen to be constant to a good approximation during the entire duration of the experiment, that is, up to 7 days. n=16.

3.3.5 The Rate of Proliferation Does Not Vary Significantly on the Three Polymers Investigated

Through the use of cell density measurements from fluorescent images of cell nuclei, the proliferation rate of the cells on the various substrata was measured. The proliferation rate, as seen in figure 3.8 showed no significant difference over the duration of the experiment.

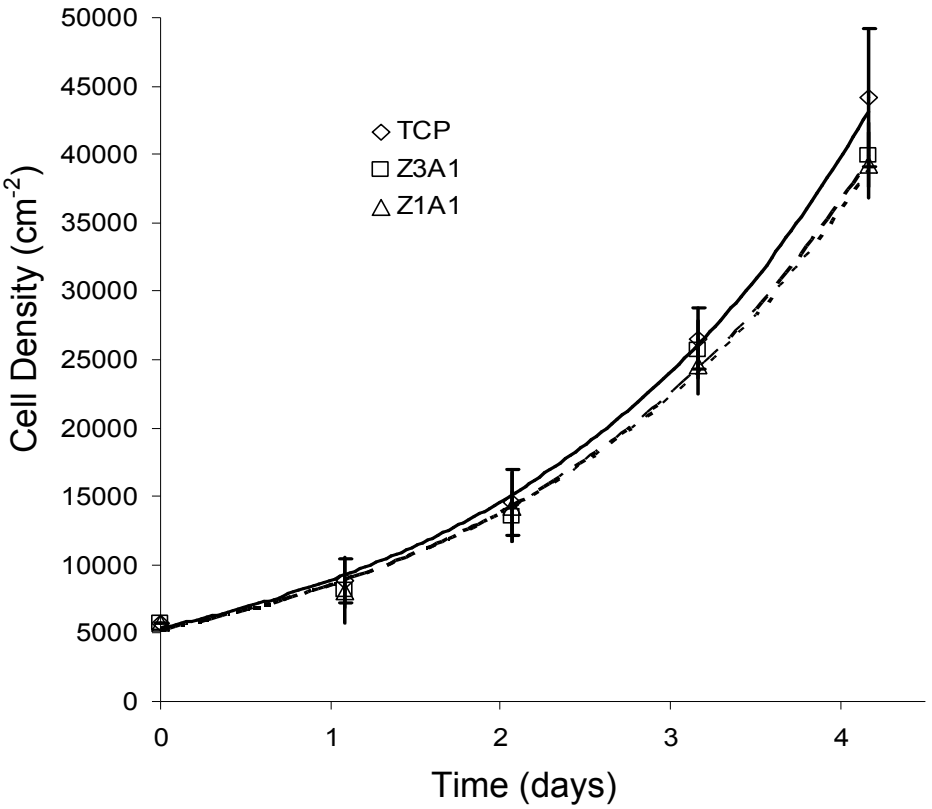

Figure 3.8. Graph showing the change in cell density over time due to proliferation. It was found that there was no significant difference in the proliferation rates of hASMCs on the three polymers without the application of a Fn solution. In addition, the population doubling time was found to be 1.3 ± 0.2 days. n=200.

3.3.6 Migration Rate is Highest at Certain Fn Densities and Substrate Stiffnesses

Using the mask migration assay, a measurement of the migration rate of hASMCs over Fn-coated PU and TCP was obtained. Figure 3.9 illustrates that for all three polymers investigated, there is a variation in migration rate with adsorbed Fn density. On TCP this can be seen to take the form of a decrease in migration rate with increasing Fn density and on the PU samples the migration rate peaks at an intermediate Fn coverage. The Fn density at which the migration rate peaks differs for each polymer, decreasing as the polymer stiffness increases. There was no statistically significant difference, as determined by ANOVA, between the value of the maximum migration speed on the three polymers, being 16.9 ± 0.7, 18.3 ± 1.2 and 18.5 ± 0.8 μm/hr for Z1A1, Z3A1 and TCP respectively (n=16).

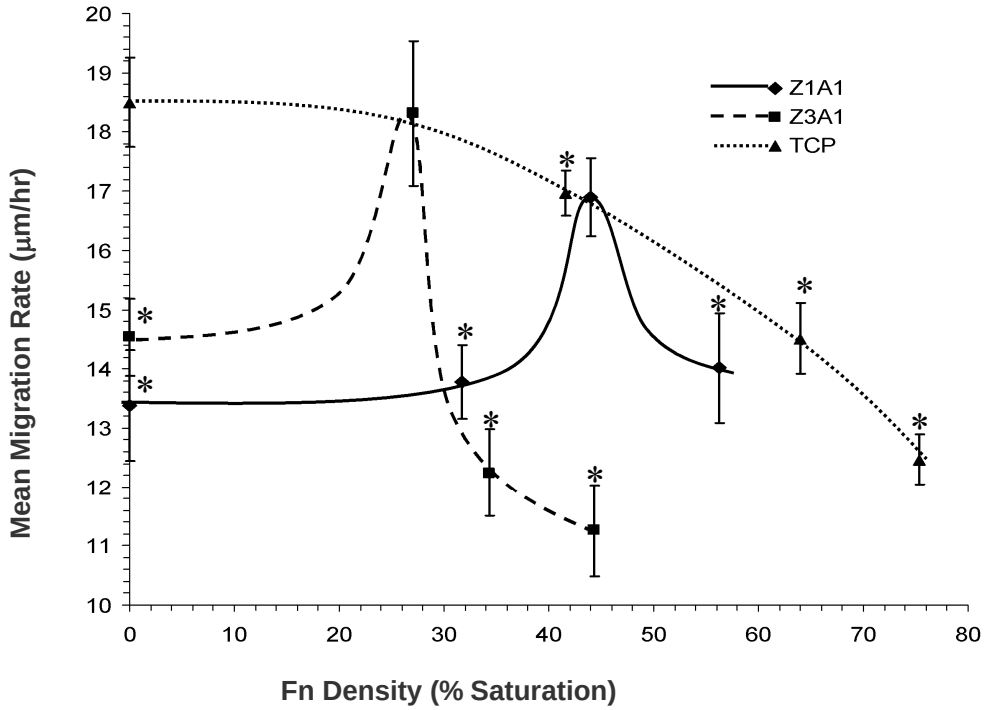

Figure 3.9. Variation in hASMC migration rate with adsorbed Fn density on the three polymers investigated. Fn density is expressed using the semi-arbitrary units of % of saturation where the maximum value of the Fn density found, on TCP after the application of a 20μg/ml solution of Fn was applied, was labelled as 100% saturation. The mask migration assay developed here was used to measure the migration rate on the three polymers at various Fn densities over 72 hours. Data points represent mean values ± SD, n=16. Asterisks show statistically significant differences in migration rate ($p<0.05$) compared to that on TCP at a Fn density of zero, analysed using the Student's t-test.

3.3.7 Cell Attachment Strength Increases with Substrate Stiffness and Fn Density

The link between the short-term attachment strength of a cell to a surface and its migration over it is well documented (Palacek et al, 1997). In order to measure the average attachment force of hASMCs to the three polymers a centrifugal detachment assay was used. As seen in figure 3.10, the attachment force of the cells to the three substrates increases with Fn surface density. The attachment force of the cells to TCP is also greater than that of cells to both grades of PU at all Fn surface densities, while the attachment force differs on the two grades of PU when the surface density of Fn is greater than 44% saturation.

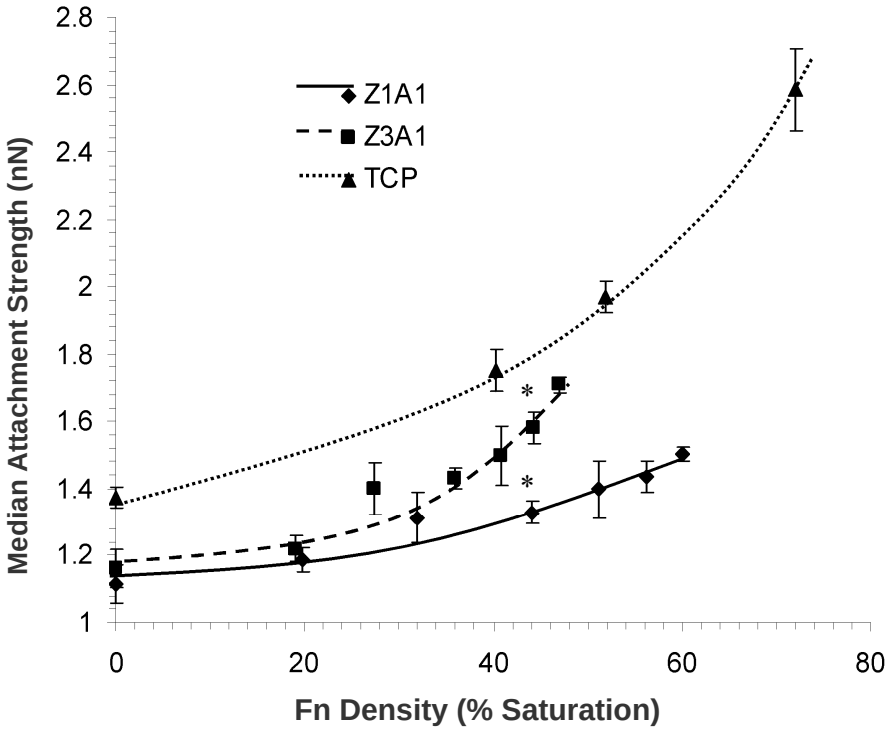

Figure 3.10. Adhesion strength of hASMCs to polymeric substrata after Fn adsorption, as measured with the centrifugal detachment assay. Fn density is expressed using the semi-arbitrary units of % of saturation where the maximum value of the Fn density found, on TCP after the application of a 20μg/ml solution of Fn was applied, was labelled as 100% saturation. Median detachment forces were determined for each surface. Data points represent mean values ± SD, n=32. Asterisk represents a significant difference in attachment strength ($p<0.05$) as determined using the Student's t-test.

3.3.8 Migration Rate is Maximal at a Particular Attachment Strength

As a comparison of how the attachment strength of cells affects their migration rates the two data sets (figures 3.9 and 3.10) were mapped one onto the other. The resultant graph is presented in figure 3.11, where it can be seen that the peaks in migration rates for the three polymers exist at the same attachment strength. In other words, the cells appear to migrate at a maximal rate when their attachment strengths to their substrates are at a particular, perhaps optimal value.

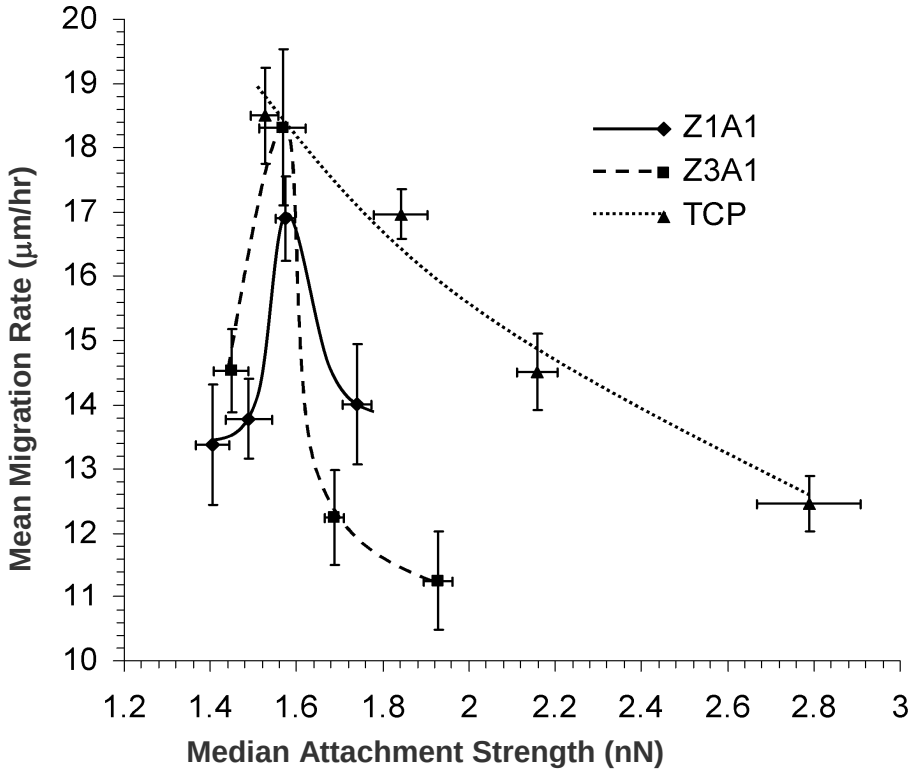

Figure 3.11. Comparison of migration and attachment strength data. The results shown in figures 3.9 and 3.10 were compared to show the relationship between these two. Data points represent mean values ± SD.

3.3.9 Cell and Focal Adhesion Area Increase With Fn Density and Substrate Stiffness

Fluorescence microscope images of hASMCs attached to substrata were analysed to determine cell spread area and focal adhesion size as shown in figures 3.12 and 3.13 respectively. Both cell and focal adhesion area is generally greater on stiffer substrates at the majority of Fn densities. Both of these also tend to increase with Fn density; the areas of both are larger at the highest Fn density on each polymer than at the lowest Fn density, with the exception of TCP, where the focal adhesion size showed no statistically significant change with increasing Fn density. Figure 3.14 shows representative fluorescence images of hASMCs on the three substrata at the lowest Fn density to illustrate the effect of substrate stiffness on cell area and focal adhesion size.

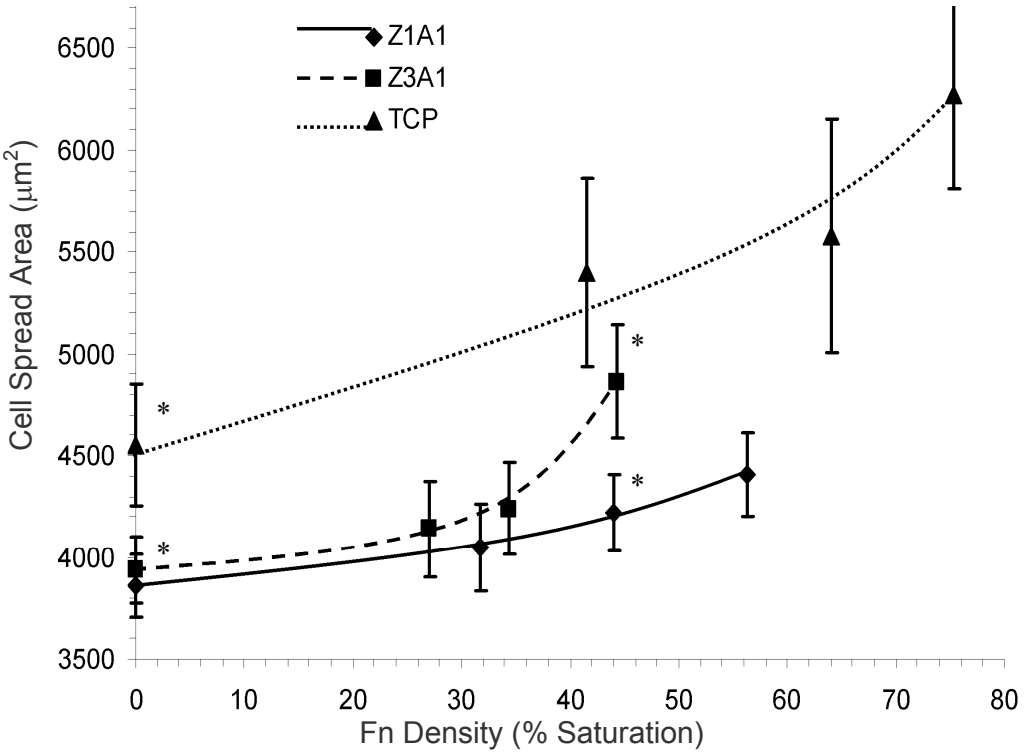

Figure 3.12. Variation in cell spread area with substrate stiffness and Fn density, as measured manually from immunofluorescence images. Fn density is expressed using the semi-arbitrary units of % of saturation where the maximum value of the Fn density found, on TCP after the application of a 20μg/ml solution of Fn was applied, was labelled as 100% saturation. Data points represent mean values ± SD, n=250. The asterisk denotes a significant difference ($p<0.05$) in cell spread area between two polymers at a particular Fn density as determined by the Student's t-test.

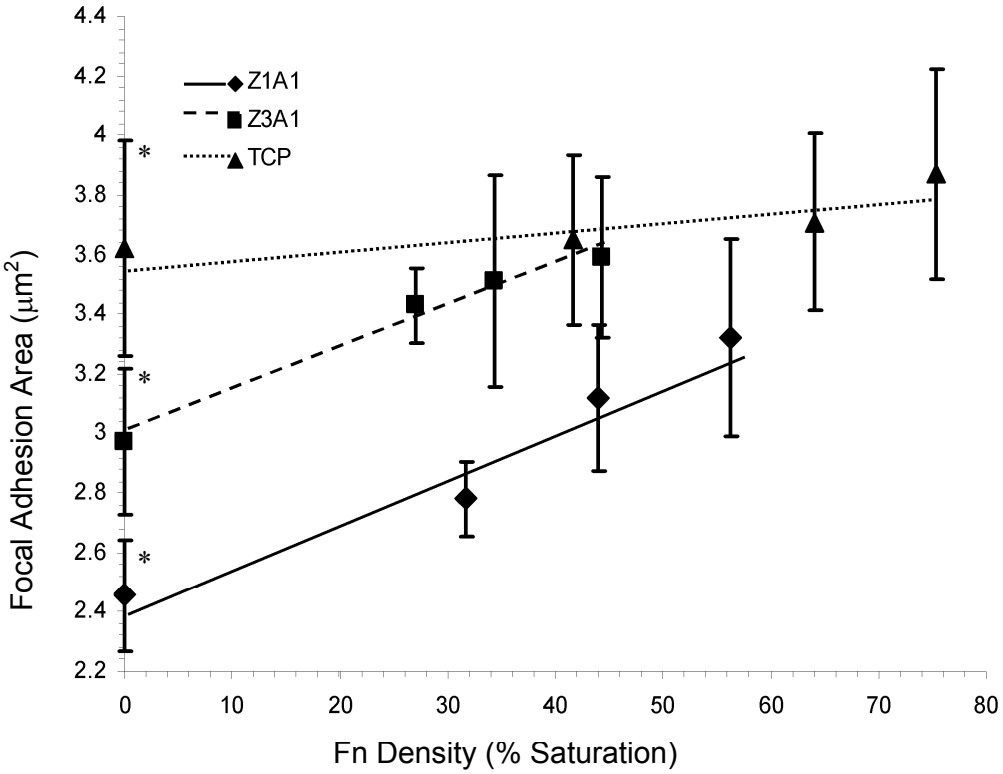

Figure 3.13. Change in focal adhesion area with substrate stiffness and Fn density, as measured manually from immunofluorescence images of cellular vinculin. Fn density is expressed using the semi-arbitrary units of % of saturation where the maximum value of the Fn density found, on TCP after the application of a 20μg/ml solution of Fn was applied, was labelled as 100% saturation. Data points represent mean values ± SD, n=200. The asterisk denotes a significant difference ($p<0.05$) in focal adhesion area between two polymers at a particular Fn density as determined by the Student's t-test.

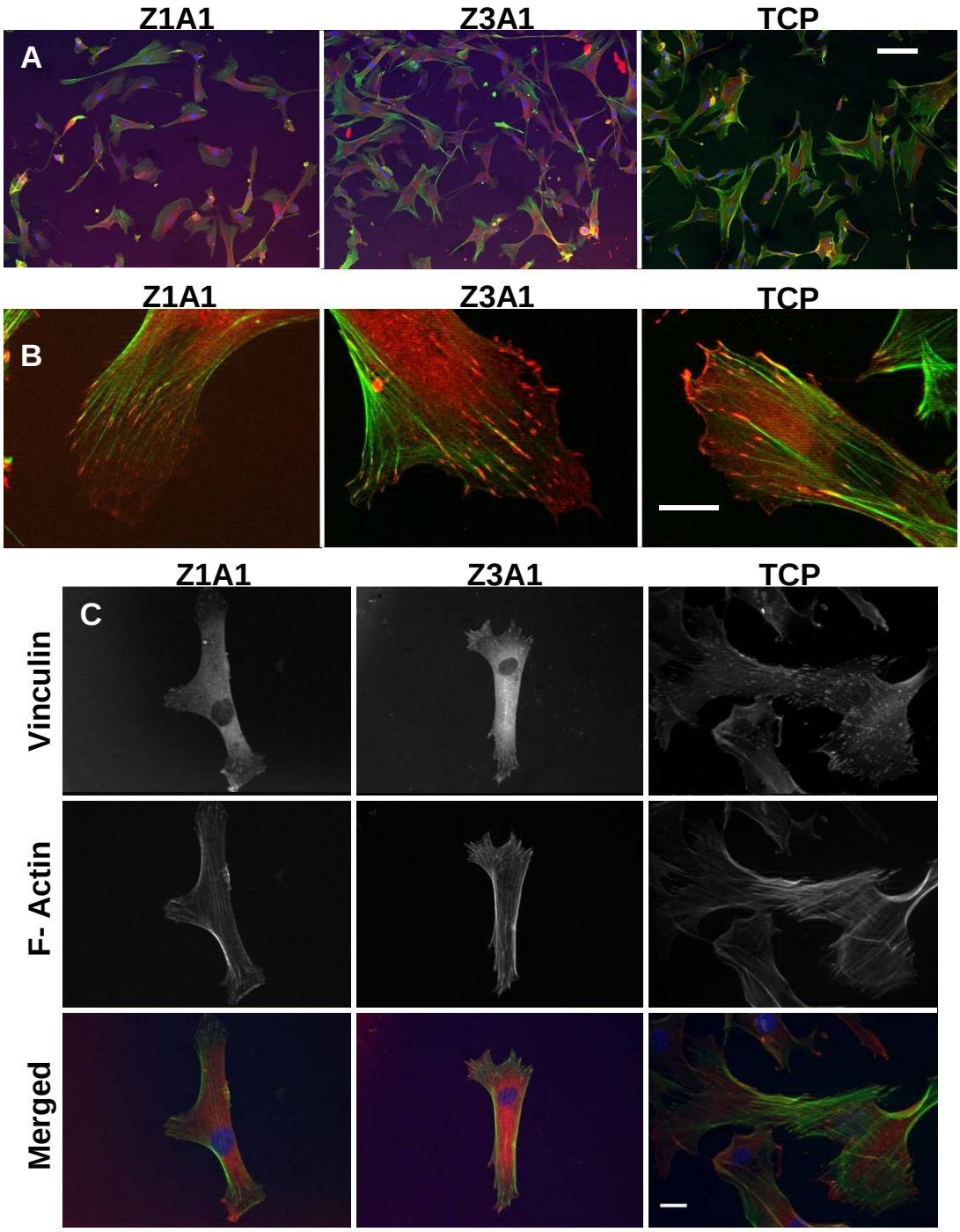

Figure 3.14. Representative immunofluorescence images of hASMCs on the three polymeric substrata with no adsorbed Fn in order to show the effect of substrate stiffness on vinculin location (red in A and B and top row and stained red in merged images in C), actin fibres (green in A and B and middle row and stained green in merged images in C) and cell spread area. Scale bar=100μm in A and =20μm in B and C. Vinculin can be seen to be dispersed throughout the cytoplasm as well as concentrated in regions at the tips of the actin filaments. These regions correspond to the locations of focal adhesions.

3.4 Discussion

The effect of substrate stiffness and surface-bound adhesion sites on cell migration rates are well known (Peyton and Putnam, 2005, DiMilla et al, 1991). However, no previous studies have addressed the effect of these factors on the migration rate of the surrounding tissue across implanted polymeric surfaces. For this reason the current work has employed two grades of biocompatible polyurethane to test for this effect, using tissue culture polystyrene by way of a control surface.

Fibronectin plays a major role in the coagulation of blood on foreign surfaces and also on the adhesion and migration of cells (Smith et al, 2004, Rajagopalan et al, 2004). It will adsorb to varying extents onto a surface to which it is presented. As with all protein adsorption the physicochemical nature of the surface affects the quantity of adsorbed protein. One of the main factors in this process is the wettability of the surface which has an effect on protein adsorption in a manner which can be either proportional or reciprocal in nature (Macdonald et al, 2002, Wei et al, 2009 and Grinnel et al, 1981). The adsorption of Fn to the surfaces of the three polymers investigated increased asymptotically with increasing Fn concentration in solution towards a threshold which differed for the three polymers. The difference in Fn adsorption between the two PUs and with TCP could potentially be due to the difference in wettability as determined by contact angle analysis. However, as no significant difference in wettability exists between the two grades of PU the difference in the adsorption characteristics on these two surfaces could be due to other factors. Variations in surface roughness could potentially cause such a difference as it has in the work such as by Deligianni et al. (2001), although as the processing of the polymer films is identical this may not be likely. However, the contact angle measurement technique used may also have limitations due to the phase separation of the polyurethane surfaces used and the differences in the hydrophilicities of the hard and soft segments. This situation could be remedied by the use of dynamic contact angle measurements, where determining the advancing and receding contact angles may expose a difference in the wetability of the two polyurethanes that was not found with the static sessile drop technique. Also of note

is the fact that the ELISA assay used to measure the protein adsorption has a limitation due to its sensitive to the conformation and orientation of the adsorbed Fn molecule (Grinnel et al, 1981); if a Fn molecule is adsorbed in such a way as the corresponding antibody cannot bind to it, then this molecule will not contribute to the result obtained in the ELISA. The nano-scale properties (Bahader, 2001 and Garrett et al, 2001) of the surfaces may have more of an effect on such factors than the bulk material wettability. Likewise, the conformation and orientation of the Fn molecule will likely also have an effect on the ability of a cell to bind to it (Stephansson et al, 2002). At the time of writing, work is ongoing, utilising Atomic Force Microscopy, to measure the surface features of the various surfaces and also to provide an insight into the adsorption conformation of the Fn onto the surfaces.

A migration assay was developed to provide a simple and reliable method to measure the migration rate of hASMCs across polymeric surfaces after the adsorption of proteins. The assay was also designed to replicate the nature of the migration that is likely to occur when a foreign object is placed in contact with tissue in the body, that is the migration of a large number of cells from the tissue onto the object. One noteworthy point concerning this assay is that the measured migration rate may be influenced by cell proliferation in addition to pure migration; a cell which has migrated past the initial mask edge and subsequently undergone mitosis would count for two cells in the analysis as opposed to one, conversely, a cell in a mitotic state may not migrate as fast as one that is not. It was determined that there was no significant difference in the rate of proliferation of cells on the three polymers investigated at low cell densities or as cells approach confluence, as in the conditions of this assay. Therefore, even though the measured migration rates may be impacted upon by the cellular proliferation, the presence of proliferation is assumed not to influence the differences in migration rate observed.

The migration rate of the SMCs across Fn-coated surfaces was found to vary with different combinations of surface Fn density and substrate stiffness by using the mask assay. A certain adhesion molecule density on each polymer produced a maximum migration rate of 18.3 ± 1.2 μm/hr, which was similar for all three

polymers. The Fn density at which this maxima occurred decreased with increasing substrate stiffness. Therefore, a certain combination of substrate stiffness and Fn density provide optimum conditions for cell migration.

Using a centrifugal detachment assay the median attachment force was determined for hASMCs attached to the three polymers at a range of Fn surface densities. The short-term attachment strength was found to generally increase with both Fn density and substrate stiffness at certain Fn densities. The conditions which allow for the maximum migration rate of hASMCs over the surfaces also resulted in attachment strengths of the same value. Therefore, it can be concluded that a cell will only migrate at its maximum speed when the attachment strength is at an optimum value for migration, 1.57 ± 0.065 nN in this case.

These results are consistent with the tensegrity hypothesis which predicts force balance between a cell and its environment (Ingber, 1993, 2003a and 2003b). On compliant substrata there is insufficient resistance to the cell's internal tension for the cell to develop such robust actin fibres or focal adhesions. On stiffer surfaces the cell can develop these to a much higher extent before a balance in tension in the cell and substrate is reached (Putnam et al, 2001). Along the same lines is the effect of surface-bound adhesion molecule density. A higher density of adhesion sites promotes the formation of larger, more developed adhesion complexes and therefore the associated actin fibres can develop a greater force on the substrata through the focal adhesion contact with the surface. As such a decrease in either the stiffness in the substrate or the adhesion site density will decrease the magnitude of the force of the cell on the substrate. This cell-substrate force and the resulting development of the actin fibres and focal adhesions of the cell directly affect the ability of the cell to migrate. At low attachment strength the cell is unable to provide the traction force to migrate at its maximum rate, the forces generated by the actin fibres or the focal adhesions being insufficient. Conversely, at high attachment strengths the adhesion complexes and actin filaments form and develop quickly. These structures, when at the dorsal end of the migrating cell must be dissociated and released to permit the continued migration of the cell, and if more robust, a greater amount of time is

required for this to happen (Nicolas et al, 2008 and Diener et al, 2005). At intermediate attachment strengths there are sufficiently developed actin fibres and focal adhesions to provide attachment and traction forces for migration but not so well developed that their dissociation is a limiting factor in migration. This is well illustrated by the peak in migration rate observed in figure 3.11.

3.5 Conclusion

In conclusion, the effect of substrate stiffness and adsorbed fibronectin density on the migration rate of SMCs over implantable polymeric materials has been investigated. A maximal migration rate of 18.3 ± 1.2 μm/hr was found to occur with each polymer at a certain Fn density, which varied reciprocally with substrate stiffness, as seen in figure 3.9. The substrata which yielded these peaks in migration rate also provided surfaces to which cells attached to at the same strength of 1.57 ± 0.065 nN. The immunocytochemical analysis showed that certain elements of the internal migratory apparatus of the cell, namely the focal adhesions, developed more when on surfaces to which it adheres to more strongly. These results are important for the development of vascular prosthetics where the migration of smooth muscle cells onto the surface of the implant is an important first step in intimal hyperplasia which can ultimately lead to the failure of the device. Also of import is the effect of cell migration in other implantable structures, particularly in tissue engineering, where tissue migration into the construct is vital and time-critical. Being able to control cell migration speed, by engineering both the mechanical and physicochemical properties of the material, in both these instances could prove to be hugely beneficial to the particular application.

CHAPTER 4

CONTROL OF SMOOTH MUSCLE PHENOTYPE THROUGH SUBSTRATE STRUCTURE

4.1 Introduction

One significant distinction between the environment of a VSMC resident in a natural vessel wall and one on the surface of an implanted synthetic surface is in the substrate geometry. Such surfaces, on the length scale of a cell, can be flat, as with a stent, or of a fibrous nature when expanded polytetrafluoroethylene (ePTFE) or woven polyethylene terephthalate (PET) are used. None of these replicate the three dimensional structure of the native vessel where an aligned fibrous structure of ECM proteins is found. Although ePTFE woven PET are also fibrous, the constituent fibres are of a diameter some one to two orders of magnitude greater than those found in a natural vessel. One possible avenue for improving the cellular response to such surfaces may lie in the development of implants that mimic this fine, aligned fibrous structure.

As discussed in chapter 2, one of the causes of the failure of vascular implants is through the hyperplasia of the resident VSMCs, which is preceded, and caused, by a shift in the phenotypic state of the cells. This shift from the normal contractile phenotype to a more synthetic one brings about a loss of the high quantity of contractile proteins contained in the cell, as well as an increase in the migration and proliferation rate and in the amount of ECM proteins produced by the cell. It is also accompanied by a change in the morphological appearance of the cell, from spindle-shaped to a more spread arrangement. The ability to influence the differentiation of a VSMC has distinct advantages; by limiting the migration and proliferation rate, the ability of the cell to form a pannus of tissue over the implanted surface would be compromised, while maintaining the contractile apparatus of the cell allows the vessel to preserve more of its natural tone.

The measurement of cellular migration and proliferation rate is a relatively straightforward matter. However, to measure the contractile proteins that will indicate the differentiated state of the cell, first the most relevant proteins must be selected. There are a number of proteins that are required to perform the process of contraction in a smooth muscle cell and most are attenuated when the cell

dedifferentiates into a more synthetic phenotype, however the magnitude and timing of this decrease varies with each protein. Some of the more commonly chosen proteins that are used as markers for the phenotypic state are listed below:

- Alpha smooth muscle actin (αSMA) is one of the isoforms of actin that form the actin filaments and one of the main components of the contractile apparatus of a cell. It is one of the last proteins to disappear when a cell loses its contractile ability, or equivalently, the first to be produced in a synthetic cell during differentiation (Drew, 1991 and Hungerford, 1993).

- Smooth muscle myosin heavy chain (MHC) is also a major contributor to the motor ability of a smooth muscle cell. It forms part of the myosin molecule that, alongside actin, performs the smooth muscle contraction. Unlike αSMA, myosin heavy chains 1 and 2 are two of the last proteins to be upregulated in the differentiation of VSMCs as shown by Aikawa (1993) and Kuro (1989).

- Smoothelin is a regulatory protein involved in muscle contraction (Niessen et al., 2004). It is also a late developer in the differentiation of VSMCs (van Eys et al., 2007).

- Calponin and caldesmon are also involved in the regulation of smooth muscle contraction. Both proteins inhibit the ATPase activity of myosin and according to Drew (1991) both appear as intermediate markers of the phenotypic state during the differentiation of the cell.

Of the choices of smooth muscle contractile phenotypic markers above, αSMA, myosin heavy chain 1 and 2 (MHC1/2) and calponin were selected as they represent the full spectrum of when a protein is upregulated during the differentiation of the cell.

In addition, the choice of controls for the contractile VSMC must be selected. It is well documented that this cell type de-differentiates when cultured *in vitro* on a flat

surface such as tissue culture polystyrene when in the presence of serum, but will revert to a more contractile phenotype when serum is removed from the culture medium (Ma, 1998). These are therefore useful samples to provide controls for cell phenotype.

A significant amount of work has been performed on the response of smooth muscle cells (SMCs) to the topography of the surface to which they are attached. A number of techniques are now at the disposal of the researcher which allows one to create a range of different substrate structures as discussed by Norman and Desai (2006). One such technique is surface patterning which can be divided into micropatterning and nanopatterning depending on the scale of the features produced. This is performed by either photolithographic techniques (Hsieh et al., 2010), where a light-sensitive material is illuminated in a certain pattern to provide features on the materials surface, or through imprint lithography (Truskett and Watts, 2006), whereby a mould or stamp with a specific pattern is used to produce the complementary pattern in the material of choice. Due to the inherent limitations in the diffraction limit of light, photolithographic techniques are mainly limited to micropatterning, while imprint lithography can be used to produce features on the scale of less than a micron.

In the majority of the work performed using substrata micropatterned with grooves SMCs have been observed to align in the direction of the grooves. Isenberg (2008) showed that cells attached to 50μm wide grooves adopted the same alignment as the grooves, while Vernon (2005) showed a similar effect on a variety of different shaped but relatively wide microgrooves, but only on those deeper than 1μm. However, on 10μm wide grooves, as shown by Williams (2011), not only did VSMCs align along the direction of the grooves but the cells developed a more fusiform shape and also increased their expression of αSMA and MHC. This substrate also prevented the increase in MHC from the addition of transforming growth factor beta 1 (TGFβ1), perhaps because the patterned surface prevents the action of TGFβ1 or because the level of MHC could not be increased any further by the cell. Similar effects of morphological change, and contractile protein expression

in addition to a decrease in proliferation rate were observed by Cao (2010) on 300μm wide channels but only at confluence. This is perhaps more likely due to the influence of the confluent state, well know for producing a contractile phenotype in SMCs (Chamley-Campbell and Campbell, 1981), than due to the effects of the microchannels. Similarly, Thakar (2003) showed that micropatterned collagen channels 20, 30 and 50μm wide all produced a cell alignment but only the 20 and 30μm wide channels caused a reduction in proliferation rate of SMCs, while all substrates caused a decrease in αSMA expression relative to unpatterned surfaces, rather than an increase, indicating that the effect on the cells does not extend to a change of the phenotypic state. With regards to nanopatterned surfaces, Yim (2005) showed that nanogrooves, 350nm wide and deep produced cell and cytoskeletal alignment alongside a reduction in the proliferation rate.

In addition to surface-patterning techniques, cell samples can be formed inside gels of natural proteins, such as collagen. The work by Oishi et al. (2000) has shown that VSMCs in reconstituted collagen gels contract in response to the application of certain agonists. While the work by Beamish et al. (2009) has demonstrated that VSMCs in RGD-bearing hydrogels maintain a contractile phenotype. However, the use of collagen in implantable vascular grafts has met with significant problems due to source variability, the possibility of bacterial or viral contamination, the possible antigenicity (Venkatraman et al., 2008), the complication of harvesting the collagen if from animal sources, the rate at which the resident cells degrade the protein structure and their resulting mechanical properties (Sell et al., 2009). This rate of degradation has also been shown to depend on the dynamic nature of the graft as an increasing frequency of stretch slows the rate of enzymatic degradation of a collagenous construct (Jesudason et al., 2007).

Micropatterning has previously been investigated in the context of vascular graft applications by Uttayarat et al. (2010) and although micro- and nanopatterning has allowed a wide variety of surfaces to be produced, their shapes and size appear to be rather limited and their fabrication process becomes much more difficult when three-dimensional structures are required. In addition, microgrooves are distinctly

different from the fibrous structures found in the blood vessel. However, a process called electrospinning can be used for this purpose.

4.2 Electrospinning

Electrospinning is a process in which electrostatic forces are utilised to create a fibrous structure from a polymer solution or melt. The technique has been known for over 100 years and was initially introduced as a production method in the textiles industry. However, as it was further developed, the formation of thinner fibres became possible and opened up other possibilities, not only in textiles but in areas such as filtration, catalysis, power (Dong et al., 2011) and medicine (Liang et al., 2007). The latter of these consists of drug delivery devices, wound dressings and tissue engineering scaffolds (Zhang et al., 2007). For this reason it is possible that electrospinning may have a place in the creation of vascular graft materials. The use of polymer melts, however, has been found to only produce fibres of a diameter larger than a few microns which is too restrictive for use in replicating the structure of a native blood vessel and as such the focus in this thesis will be on electrospinning using polymer solutions.

Electrospinning has been used previously to produce cell substrata from a range of materials. When used as a scaffold for VSMC culture the cells have been shown, by Xu (2004) amongst others, to display some characteristics of a contractile phenotype although a rigorous analysis of the differentiated state has not been conducted. The fibrous nature also appears to have a diameter-dependent effect on cellular morphology and migration as demonstrated by Liu et al. (2008, 2009).

In a typical electrospinning configuration, such as the one illustrated in figure 4.1, the polymer is delivered through a needle which is brought within a certain distance of a collector or target. A large potential difference created between the collector and needle, and therefore the polymer solution, causes an electrostatic attraction between the polymer and the collector. If the attraction is sufficient, the polymer

droplet at the needle tip forms into a cone, the so called 'Taylor Cone', from which a fibre jet ejects in the direction of the collector as shown in Taylor's work (1969). The jet travels through the intervening space and in the process the evaporation of the solvent occurs, leading to the collection of solid polymer fibres on the target. After travelling a short distance from the needle, the jet becomes unstable due to electrostatic repulsion at small bends in the fibre and a whipping instability is created, causing the fibre to bend and turn rapidly, giving the impression to the naked eye that the fibre is splitting into many diverging fibres. When these fibres deposit onto a stationary target, they will lie facing every direction and a random mesh of fibres is produced.

There exist many factors which affect the electrospinning process and therefore the resultant fibrous structure. These variables must be optimised in order to create the desired product in terms of fibre size and geometry. Suboptimal parameters can lead to indistinct fibres, fibres with a non-circular cross section or the inclusion of bead defects, with an extreme example of this being electrospraying, a discrete process whereby solid polymer drops are deposited instead of fibres, that can be performed with the same apparatus as electrospinning but with a different choice of operating parameters. A short overview of some of these variables and how they influence the electrospinning process is given in the following sections.

4.2.1 Applied Voltage

The applied voltage is the driving force for the formation of fibres and for pulling them towards the collector. As such the importance of the magnitude of the potential difference is paramount in creating the optimum fibrous construct, as shown by Deitzel (2001) and Meechaisue (2006). If the voltage is below a certain level no fibres will be formed at all from the solvent solution. As this is increased, fibres will start to form but only intermittently and they will bring with them a large number of bead defects. This absence of continuity of a steady fibre exists due to the time taken for the accumulation of charge on the polymer droplet. The time taken for this to

occur also allows the drop to reach a relatively large size and the subsequent ejection of an above optimum amount of polymer leads to incomplete solvent evaporation.

A further increase in applied voltage reduces the effect of beading and simultaneously can alter the diameter of the deposited fibres. This has been found to increase or decrease the diameter, depending on the polymer solution and electrospinning apparatus used. Reasons for increasing the fibre diameter have been postulated to be due to the increasing electric potential pulling to a greater extent on the polymer solution and leading to a higher mass flow rate. The converse has been attributed to the greater potential leading to a higher electrostatic repulsion of the polymer and greater stretching of the jet and more rapid evaporation of the solvent.

4.2.2 Flow Rate

As with the applied voltage, the polymer flow rate also has an important effect on the electrospinning process. A threshold flow rate is required to replenish the solution on the Taylor Cone at the rate that it is being removed by the fibre jet. Below this threshold Taylor (1969) demonstrated that the cone is not allowed to form and the production of fibres is discontinuous. As the flow rate increases above this threshold the fibre diameter and the associated pore size also increase as shown by Megelski (2002). When increased to a certain level, the flow rate does not allow for complete solvent evaporation before deposition onto the collector, resulting in bead formation and the formation of flat, ribbon-like fibres, created when the evaporating solvent bursts through the edges of the drying fibre.

4.2.3 Capillary-Collector Distance

The main effect of the displacement of the polymer outlet from the collector is in allowing the solvent to have sufficient time to evaporate while the fibre traverses the distance. Megelski (2002) found that if the gap is too small beads appear on the

fibres and the fibres attain a flattened morphology. A decrease of the fibre diameter is generally found with an increase of the separation (Doshi, 1995 and Jaeger, 1998), perhaps due to the stretching of the fibre that occurs as it traverses the gap.

Certain arrangements of the apparatus pair the capillary-collector distance with the applied voltage as it is electric field strength rather than the magnitude of the applied potential that dictates the driving impetus of the jet formation. One particular situation where this would be the case is when the electric potential is applied to the collector and the capillary and solvent are earthed rather than the reverse. In these cases the two variables are more inextricably linked than normal.

4.2.4 Polymer Concentration

Polymer concentration has an effect on the electrospinning process, not only directly but also through its effect on the solution viscosity and surface tension. Doshi (1995) describes the effect if too thin or thick a solution is used. If it is too dilute polymer chain entanglement will not occur and the effect of surface tension will cause the fibre to break up into droplets before it can reach the collector. Too high a concentration increases the viscosity of the solution to a point where it is difficult to deliver through the capillary and therefore control the delivery process. It has been found in general (Megelski, 2002 and Deitzel, 2001) that increasing the polymer concentration increases the fibre diameter and prevents bead formation due to the lower quantity of solvent that requires evaporation.

Along with concentration, the molecular weight of the polymer has a very similar effect on the result of the electrospinning process, both directly and through its influence on viscosity and surface tension.

4.2.5 Solvent Volatility

Megelski (2002) has performed much work on the effect of solvent volatility on the electrospinning process. Solvent volatility, as would be expected, can dictate whether the solvent has completely evaporated before deposition on the collector. A low volatility leads to incomplete evaporation, the presence of bead defects and can cause ribbon shaped fibres. A highly volatile solvent can lead to a high degree of phase separation and subsequently leads to a porous fibre surface.

4.2.6 Solution Conductivity and Polarity

The conductivity of the polymer solution dictates its charge carrying capacity and as such affects the shear forces felt due to the electrostatic forces present. A high conductivity leads to high shear forces and causes an increased amount of fibre thinning to occur. As with other parameters, extremes of solution conductivity can cause problems with the process, with low values preventing fibres being formed and high values leading to extreme shear forces that cause the fibres to break in transit (Hayati, 1987). Work by Baumgarten (1971), Zhang (2005) and Jiang (2004) have also shown that the resulting fibre diameter decreases with increasing solution conductivity.

In certain processing arrangements the solvent polarity plays a crucial role. An example of this is where the collector is charged and the polymer solution earthed. In this instance the polymer solution must have a polar nature so that charge separation can occur and an electrostatic attraction of the polymer to the collector is created.

4.2.7 Type of Collector

One of the most common collectors used is a piece of aluminium foil due to its simplicity of use. However, many different types and shapes of collector have been

used to influence the structure and nature of the resultant fibrous material. As previously mentioned the native ECM is of an aligned fibrous nature. In order to mimic this with the electrospinning process it would be advantageous to be able to produce aligned electrospun fibres instead of the random matrix that is ordinarily produced.

One method of aligning fibres is to use two collectors, both held at the same electric potential and equidistant from the polymer capillary. This way the fibres are drawn to one collector and then the other in quick succession. The passage back and forth causes the deposition of aligned fibres to occur between the two collectors.

Another method would be to form the collector into a drum which is then rotated at high speed such that when the fibres hit the surface they are pulled into alignment. This requires the collector to be rotated at very high speeds because the velocity that the fibres impinge on the collector can be near the speed of sound.

4.2.8 Electrospinning Arrangement

The primary distinction between two possible setups is whether the electric potential is applied to the collector and the polymer solution is earthed or whether the reverse is used. Most experimentalists favour the latter, while some of the effects of the former arrangement are discussed elsewhere in this section.

Whichever arrangement is used, the effect of charging one of either the collector or the polymer results in the other, as well as any other earthed conductors in the vicinity, attaining the opposite charge. The resultant electrostatic attraction forms the driving force that leads to fibre formation. However, in the case where the collector is charged it is crucial that the solvent used in the polymer solution is of a polar nature as this allows the charge separation to occur in the polymer.

4.2.9 Ambient Parameters (temperature, humidity and air velocity)

The effect of the ambient conditions of the electrospinning, although often difficult to control, can have a significant effect on the process. This primarily has an effect on the evaporation of the solvent with an increase in temperature and air velocity and a decrease in humidity all increasing solvent evaporation. High air humidity can also lead to the discharge of the fibres which has unpredictable effects on the process.

4.3 Materials and Methods

4.3.1 Electrospinning Apparatus

The first step in obtaining electrospun materials for investigating their suitability in a vascular graft was to develop a set of apparatus that can be used to create such materials. The configuration used was as illustrated in figure 4.1. The main components of this system were; the polymer delivery system, the collector and power supplies, the motion control system, and the safety mechanisms. All of these components are described below.

4.3.1.1 Polymer Delivery System

The polymer delivery system, the first component of the electrospinning system, was composed of a 100ml stainless steel syringe, a syringe pump (PHD 2000, Harvard Apparatus, Kent, UK), fluorinated ethylene propylene tubing, a needle manifold and an array of needles. The polymer solution was deposited inside the syringe, which was subsequently placed onto the syringe pump. The tubing was then connected between the syringe and the needle manifold, which had a specified number of needles attached. The syringe pump compressed the syringe, delivering the polymer solution through the tubing, into the needle manifold and out of the array of needles.

A stainless steel needle and fluorinated polymer O-rings and tubing were chosen so as to be chemically compatible with the solvents used in the polymer solution, namely dimethylformamide (DMF), dimethylacetamide (DMAc) and tetrahydrofuran (THF). All of these solvents can cause corrosion or degradation of less inert metals and polymers, leading to contamination and inefficient delivery of the polymer solution. The size of the syringe was chosen to allow the uninterrupted production of a large amount of electrospun material, either covering a large area, of a large thickness or in applications where a considerable amount of the fibrous material is wasted, for example because it deposited onto surfaces other than that of the collector.

The pump had a versatile syringe mount and a powerful motor, permitting the use of the 100ml syringe. It allowed the controlled delivery of the polymer at specified rates and also the ability to be controlled remotely, such that a computer with the appropriate software could be programmed to vary the flow rate of the polymer over time. This has benefits if the electrospinning is being performed over extended periods of time and the flow rate needs modifying in response to, for example the amount of polymer deposited. Also, some electrospinning protocols require the flow to be periodically interrupted, such as if two polymers are being deposited sequentially in layers, and this remote control of the pump would also be advantageous in this situation.

As with the choice of syringe O-rings, the material of the tubing connecting the syringe to the needle manifold was chosen to be a fluorinated polymer to withstand attack from the solvent of the electrospinning polymer. The internal diameter of the tubing had an effect on both the priming volume of the system with the polymer solution as well as the force required to push the solution through it. To minimise both, the internal diameter was kept low as was the length of the tubing, while still allowing it to span the distance between the syringe and the needle manifold without any kinks.

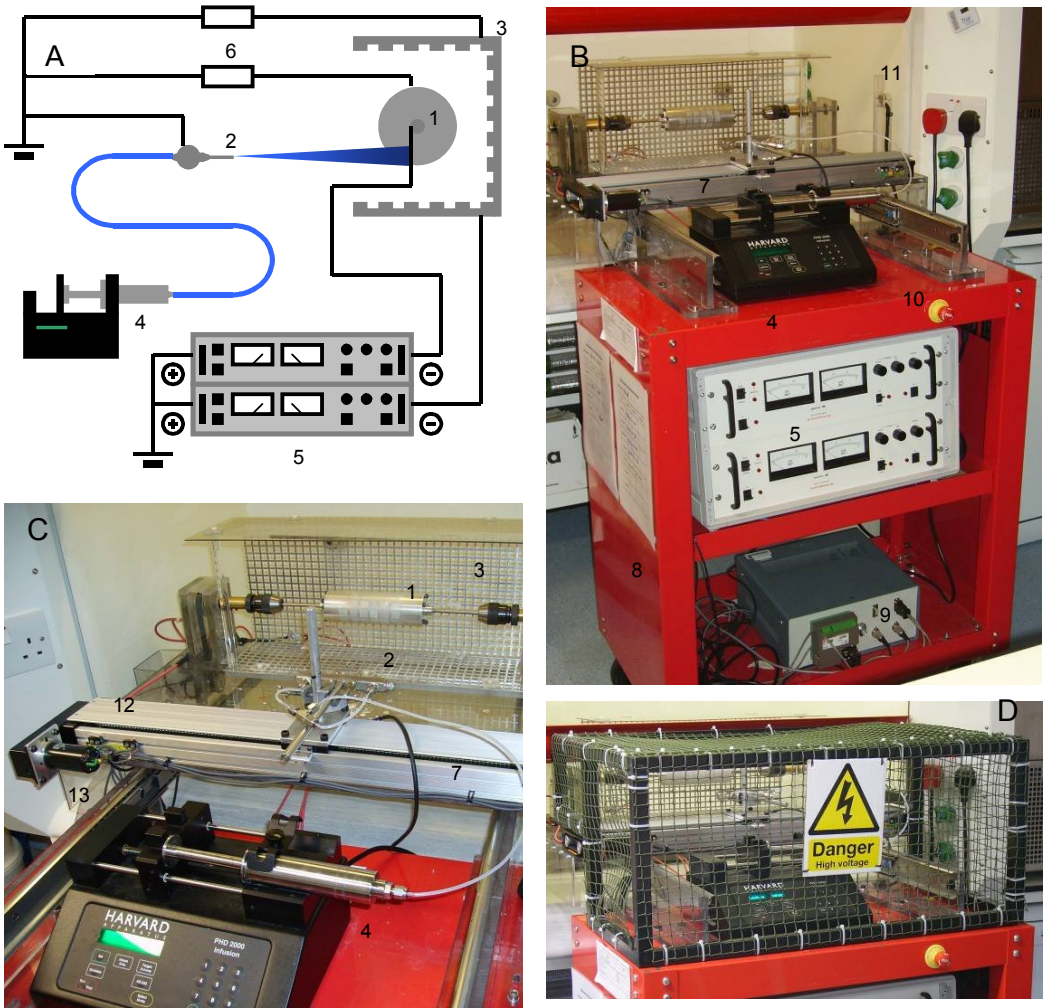

Figure 4.1. Diagram and photographs of the electrospinning apparatus. A) Diagram of polymer delivery and high voltage system. B) Entire electrospinning rig. C) Polymer delivery system. D) Safety cage. E) Needle and collector.

Guide to labels: 1-collector, 2-needle assembly, 3-grid, 4-syringe and pump, 5-high tension power supplies, 6-high voltage and resistance resistors, 7- linear positioning table, 8-trolley, 9-motion controller, 10-emergency stop button, 11-safety switch, 12-table limit switch, 13-positioning table motor, 14-fume cupboard sash.

When considering the limiting factor of bead defects on the maximum allowable flow rate for a particular electrospinning setup it is important to remember that the maximum flow rate is only limited per needle that the polymer is ejected through. In order to overcome this it is merely a case of increasing the number of needles used in parallel. However, this solution is hampered by the interaction of the fibre jets as they tend to diverge due to their like charges, but can be minimised by ensuring a sufficient displacement between adjacent needles. The needle manifold was created to allow a high flow rate of polymer onto the collector while preventing the interaction of the polymer jets but still keeping the deposition site from each needle relatively close. Each needle position could be filled with a blank so that the number of needles used simultaneously could be varied between one and four.

The needles used were again made of stainless steel and were gauge 25. The needle was cut to a convenient length and the tip filed flat to allow the Taylor cone to form uninterrupted. The needles and manifold were bolted onto a platform which was electrically connected to ground and was adjustable, allowing the positioning of the needles relative to the collector.

4.3.1.2 Collector and Power Supplies

As previously mentioned, the setup used here was designed such that the charge is applied to the collector and as such the collector and high voltage power supply form one component of the electrospinning apparatus. However, in order to provide an extra level of control over the path of the electrospun fibres toward the collector a separate grid was placed around the collector and attached to a separate power supply.

The collector system was designed so that it would be able to accept a number of different shape collectors. This was accomplished by attaching two rotatable chucks at either end of the system that could accept a stainless steel rod up to 13mm in diameter. To this rod could be attached a plate to provide a flat target while the

chucks were prevented from rotating. Alternatively the rod could pass through an aluminium drum with a diameter of 50mm which would rotate with and about the same axis as the rod. This drum was designed to be used in aligning the deposited fibres as the large diameter translates into a high surface velocity, which is essential for this purpose. The drum was used exclusively for obtaining the electrospun materials used in this study as its large surface area provided a sufficient quantity of material for use and the degree of alignment of fibres could be changed with the speed of rotation. Sheets of aluminium foil could be wrapped around the collector in most of its forms to make it easier to remove the deposited polymer matrix.

The three-sided aluminium grid which was used to obtain control over the fibre trajectory was placed such that the collector ran straight through the middle of the box that it created, as shown in figure 4.1. By adjusting the electric potential of the collector and grid it was possible to vary the attraction of the polymer fibre to one relative to the other.

In order to provide the electric potential to the collector and grid, two high-voltage Alpha III power supply units (Brandenburg, Dudley, UK) were used, one connected to each of the two. These units were capable of providing a voltage of up to 30kV and, like the syringe pump, could be controlled manually or automatically by a computer running suitable software. This would have similar benefits to the remote control of the syringe pump; slowly varying the parameters over time as required for long deposition times or varying quickly for more elaborate electrospinning techniques.

4.3.1.3 Motion Control System

The motion control apparatus consisted of two separate systems. The first controlled the rotation of the collector drum. This was required to be able to cover a range of speeds, from the relatively slow, when a random mesh of fibres is desired, to a much

higher speed in order to align the fibres. The speed was also required to be measurable so that reproducibility was maintained.

Fibres deposited onto a stationary target when drawn from a stationary needle form a spot with the greatest amount of fibres, and hence matrix thickness, at the centre and decreasing along the radius of the spot. For this reason the second motion control system was used to translate the needle laterally in the direction parallel to the axis of the collection drum. A linear positioning table was attached in the direction of the required motion with the needle manifold affixed on top of the attached stage. The table utilised a ballscrew arrangement to vary the position of the stage, and therefore the manifold in the direction parallel to the length of the collector rod. When combined with the rotation of the drum, this lateral motion coats a section of the drum with a uniform thickness of matrix, with only the periphery of the deposited area having an attenuated thickness.

Both of these systems were driven by a DC electric motor, attached to an encoder which was used for monitoring the position and therefore the rotation speed of the motor. The motor and encoder for both systems were connected directly to a servoamplifier which, using the encoder signal, provided the correct power to the motor to make it run at the desired speed. This feedback system was crucial for ensuring the motors ran at a continuous speed when the applied load varies.

In the typical electrospinning method used for this work the collector motor would need to have run at a constant rate during the deposition as even with a deposition of the thickest useable fibrous materials the effective diameter of the collector did not change significantly during deposition. In order to maintain this speed the relevant servoamplifier required a certain voltage input in order to set this rotation speed. This was achieved through the use of a constant voltage supply and a voltage divider with a variable output. Manually setting the input signal to the servoamplifier with the variable resistor dictated the rotation speed of the collector, which the feedback loop maintained.

The lateral motion of the needle manifold required a higher level of complexity. As it is a reciprocating motion, the periodic reversal of the motor direction is required. In addition to the encoder mounted on the motor on the positioning table, another encoder was also affixed to the table itself, both providing information about the location of the stage and needle manifold. The signal received from the table encoder was found to be more useful than that from the motor encoder because the former gave a position relative to a fixed point on the table whereas with the latter it was relative to the starting point of the motor which is more arbitrary. In order to control the reciprocation of the needle manifold a motion coordinator system MC302X (Trio Motion Technology, Gloucestershire, UK) was used in combination with the control software MotionPerfect. A programme was created to allow the system to monitor the lateral position of the manifold and vary it as required, in this case reciprocating, with the starting position, speed and range of motion all selectable by the user.

In order to prevent damage caused by the motor driving the table to the limit of its motion, perhaps due to a faulty electrical connection, a number of failsafes were included and controlled by the control software. These all consisted of push-button switches located near the limit of travel of the table's stage, with two at each end and activated by the stage passing by. The inner two of these switches caused the direction of travel of the stage to reverse and then refind the start of its reciprocatory motion. If these fail, and the stage moves past either of the inner two switches they will hit one of the outer two, whereby the power to the motor will be cut.

This motion controller was also useful for measuring the collector rotation speed. Although the controller could not vary it directly, the combination of manual control and the feedback of the collector motor encoder meant that the exact speed of rotation could be set.

4.3.1.4 Safety Mechanisms

The electrospinning apparatus combines a number of diverse and highly dangerous hazards, including high voltage sources, polymer solutions containing solvents that are often toxic, corrosive and carcinogenic and which are rapidly vapourised as well as rapidly moving parts. Therefore, arguably the most important parts of the equipment are the safety features, which ensures the risks posed to the user and those in the vicinity are kept to a minimum.

Firstly the whole system was designed so that the most hazardous parts can be moved into a fume cupboard. This ensures that all of the solvent evaporating from the system is drawn away from the work area and also it provides some protection from accidentally touching the elements of the system that are charged. The whole system is mounted on a trolley, but the main workings of the system are attached to a movable shelf, which is pushed back into the fume cupboard and the cupboard sash closed over it when the system was in use.

A safety feature of the power supplies was that if the current increased suddenly, for example due to a short circuit from being accidentally touched, the unit would trip before a dangerous surge in current could occur. For the units to do this it was necessary for a small 'trickle' current to operate. This was obtained by connecting the two power supply outputs to ground each through two high voltage 15kΩ resistors in series.

The third safety feature was a large cage with warning sign attached which was placed over the rest of the most dangerous pieces of equipment. This cage, combined with the fume cupboard, completely enclosed the polymer delivery system, all exposed elements which were charged by the high-voltage power supplies and all moving parts, ensuring that no one could accidentally touch any of it.

The last safety features were an interlock system which would shut down the power to the entire system should anyone try to gain access to the equipment whilst it was

running. The interlock system was activated by removal of the protective cage, lifting of the fume cupboard sash, sliding the shelf out of the fume cupboard and moving the trolley away from the cupboard. This was complemented with a cut-off switch located on the front of the trolley for use in emergencies. Any one of these interlock or emergency switches would cut out the high voltage power supplies, cease the delivery of the polymer solution and stop all moving parts.

4.3.2 Scaffold Formation

The purpose of the work in this chapter is to develop and test an electrospun material for use in vascular implant applications. The material should, as closely as possible, replicate the structure and mechanical properties of the native blood vessel. As outlined previously in this chapter the correct parameters must be sought for running the electrospinning process in order to make the desired product. The effect of the alignment of the fibres on the phenotype of the VSMCs was also sought, and as such two different fibrous structures were made, the aligned and the unaligned variety. The processes for developing the two structures were run relatively independently.

The choice of the first parameter, that of the polymer, was made to be polyurethane, Z1A1, (Biomer Technology Ltd. Runcorn, Cheshire) as this has already been proven to be a promising polymer for use in the culture of vascular smooth muscle cells as demonstrated in the proliferation results in figure 3.8. In addition, the compliant nature of this polymer means that the mechanical properties of the construct would be closer to those of the native vessel that was to be replicated than if a stiffer polyurethane, such as Z3A1, was used.

Subsequent to the selection of polymer is the choice of solvent. The two solvents that have been tested previously with this grade of PU are DMF and DMAc. Both of these dissolve the polymer well and are highly polar molecules, which is an important property for use in this electrospinning configuration. However both have relatively high boiling points, being at 153ºC and 165ºC for DMF and DMAc

respectively. The high boiling points mean that there is a higher probability that as the fibre traversed the gap to the collector, not all of the solvent would evaporate and bead defects would form. To overcome this shortfalling, another solvent, THF, was mixed with each of these solvents. The THF, while not a particularly effective solvent for the PU was adequate while mixed with either of the other two solvents and is also a highly polar molecule. The benefit of the THF was that it has a much lower boiling point of 66ºC, increasing the chance of total evaporation of the solvent before fibre deposition on the collector with increasing ratios of THF to DMF or DMAc. The use of THF did aid in the creation of fibres without bead defects but also resulted in the tips of the polymer ejection needles becoming fouled with a polymer or solvent residue that had to be cleaned off regularly. This prevented the electrospinning process from running without continued supervision and as it was required to run for up to 16 hours for creation of certain materials, this drawback was considered to be prohibitive for the use of THF. Finally, a 13% solution of PU in only DMF was used due to the lower boiling point of DMF relative to DMAc and as this solution did not produce a residue on the needle. Also a 13% concentration was found to be the highest one that was still practical for pumping through the tubing and needle assembly due to the viscosity of the solution at higher concentrations.

The remainder of the experimental parameters had to be selected by a careful process of iteration. These parameters, the applied voltages, the polymer flow rate and the needle-collector separation, all have a similar effect on the electrospinning process by varying the fibre diameter and, if not properly optimised can cause bead defects to occur. Only when all three were optimised simultaneously would the required results be obtained. They were all, therefore varied sequentially and the resulting material produced was analysed using SEM, as described in the following section.

The parameters that were obtained for electrospinning unaligned fibrous materials were 18kV for the collector voltage, 12kV for the grid voltage, 0.3ml/hour per needle for the polymer flow rate and 150mm for the separation of the needle from the collector surface. The needle translatory speed was not found to affect the fibres produced but was set at 20mm/s. The collector rotary speed was set at 500rpm.

These parameters were the only ones that lead to the production of fibres without bead defects and any small change in the parameters caused these defects to occur. As such only a small range of fibre diameters could be produced without the inclusion of these defects.

The effect of environmental changes, such as temperature and humidity variations, on the electrospinning process meant that the parameters of the electrospinning must be constantly revised such that the fibres are produced as desired.

Creating the aligned fibres was more problematic than the unaligned ones. Simply using the parameters obtained for the latter and increasing the speed of rotation of the collector did not produce the desired result, even when the maximum speed of 2000rpm was reached. This is mainly due to the speed of the fibres upon impact being much faster than the surface velocity of the collector, the former being near the speed of sound (~300m/s) and the latter in this case being roughly 5m/s at maximum. As the rotation speed of the collector cannot be increased further, the reduction in the speed of the fibres relative to the surface of the collector was attempted. The way this was performed was to use the attraction of the fibres towards the grid to draw the fibres into the gap between the grid and the collector instead of straight towards the collector. The fibres were postulated to follow a spiral path towards the collector instead of impinging perpendicularly onto its surface. This spiral path would mean that, although the speed of the fibres may not be significantly different than when travelling directly towards the surface of the collector, the speed in the direction perpendicular to its surface will be greatly reduced and the aligning effect of the rotation of the collector will be heightened. In addition, if the direction of travel of the spiral path is aligned with the direction of rotation of the collector the spiral path may also provide additional alignment of the fibres.

The modified path of the fibres was created by lowering the needle manifold by 3cm and moving it towards the collector such that the separation remained unchanged. The voltage of the grid was raised to the same level as the collector, 18kV and the attraction of the fibres towards the grid would then be more similar to that of the

collector and the path of the fibres would travel in the direction described. The direction of travel of the collector was also chosen to match the assumed direction of travel of the fibres and its speed was set to the maximum of 2000rpm. This arrangement also lead to the deposition of fibres onto the grid as well as onto the collector, as would be expected, and this means that longer deposition times are required to produce the same amount of fibrous material on the collector.

When performing fluorescent light microscopy analysis of cells attached to the electrospun materials a significant degree of autofluorescence of the fibrous material made the imaging impossible. To overcome this limitation the electrospun PU was deposited onto thin sheets of cast PU. The sheets were produced, as described in chapter 3, by pouring Z1A1 PU, 15% in DMF into glass flat-bottomed petri dishes and drying them in a vacuum oven at 65ºC at a vacuum pressure of 550kPa. Sections of these sheets were then cut and adhered to the collector. Immediately prior to electrospinning the cast PU was washed with acetone to clean its surface and to increase the adhesion of the electrospun PU fibres. The electrospinning process was then performed but only for a short duration so as to only deposit a small number of layers of fibrous material onto the cast PU. These sheets were found to not be autofluorescent to a noticeable degree and did not interfere with the fluorescence microscopy imaging, they were also transparent enough to allow transmission light microscopy of the samples. These thin fibrous layers on cast PU were used for all further work on electrospun materials.

4.3.3 SEM Analysis of Scaffolds

In order to investigate the structure of the fibrous materials, small sections of the material were imaged within a Hitachi TM1000 SEM. The microscope does not require any sample preparation so sections of the electrospun material could be imaged directly and immediately, facilitating the speedy acquisition of the correct electrospinning parameters described in the previous section.

The presence of bead defects could be detected easily with the microscope at magnifications of 5000 and over. When bead-free materials were made the SEM images also were used to gain measurements of fibre diameter, pore size and fibre alignment. The images were exported into ImageJ (NIH) and these measurements taken manually.

Due to the variable nature of the electrospinning process, particularly from temperature and humidity variations, the resulting materials were occasionally inadequate. Therefore, for each run of electrospinning, a sample was taken and analysed with the SEM to ensure that it was as required.

4.3.4 Cell Culture

In order for the electrospun materials to be used with cell culture they must first be sterilised. Of the options available, autoclaving was ruled out as the temperatures attained during the process would melt the polyurethane and UV sterilisation was disregarded as it can change the chemical nature of the polymer. Sterilisation with 70% ethanol and with microwave irradiation were both compared, and the samples after treatment were again analysed using SEM. The microwave sterilisation technique was found to be the less destructive towards the fibrous structure of the two and as such was chosen in all future work.

Square sections of solvent-cast PU, 10mm wide were attached to the collector of the electrospinning apparatus and the electrospinning process run to create either aligned or unaligned fibres. These sections were subsequently cut from the collector using a scalpel and placed onto the bases of the wells of a 24-well tissue culture plate. The adhesive used to secure the materials to the electrospinning collector was also used to attach the materials to the bottom of the plate. The adhesive used was a double sided adhesive tape that was found to be compatible with cell culture. To provide control surfaces small sections of Twillweave polyester graft material (PET) obtained from Vascutek (Glasgow, UK) was attached to the base of the wells in the same manner.

The base of these wells was also used as a control surface for the culture of cells. The plates were then placed in a microwave for 5 minutes at 800W in order to sterilise the materials. The materials were then washed twice with sterile filtered deionised water and then with Dulbecco's Modified Essential Medium (DMEM).

Human aortic smooth muscle cells (hASMCs) were maintained in DMEM, supplemented with 10% (v/v) fetal calf serum (FCS) and were used between passage 2 and 4. These cells were deposited into the bases of the 24-well plate wells at $2x10^4 cm^{-2}$, corresponding to approximately 40% confluence, and allowed to adhere.

4.3.5 Microscopy of Cells/Morphology

HASMCs were cultured in DMEM/FCS for 7 days on aligned and unaligned electrospun materials as well as on tissue culture polystyrene (TCP), in the form of the base of the 24-well plates with media changes every 3 days. PET samples were not used as a comparison as the material was opaque and too autofluorescent to allow visualisation of the attached cells

At the end of the 7 days, cells and substrate samples were removed from media, washed twice with PBS, fixed with 4% paraformaldehyde before membrane permeabilisation with 0.25% (v/v) Triton X-100. Cell samples were incubated for 1 hour with an anti-vinculin antibody (Sigma-Aldrich, Dorset, UK) and then an anti-mouse Texas Red-conjugated secondary antibody (Vector Laboratories Ltd., Peterborough, UK) and FITC-conjugated phalloidin (Invitrogen, Paisley, UK) for the visualisation of F-actin filaments, both followed by three washes in PBS. Samples were then mounted onto coverslips using a DAPI-containing mountant, Prolong Gold (Invitrogen, Paisley, UK).

Fluorescence images were obtained using the Apotome function of an Axio Imager Z1 microscope (Zeiss, Hertfordshire, UK), an alternative method to using a confocal laser scanning microscope for obtaining optical sections from biological specimens.

The shape of the cells was qualitatively analysed from the images and if they appeared to be of an elongated morphology the images were further analysed using ImageJ. The orientation of each cell in each image that was analysed was ascertained manually and recorded automatically by the analysis software.

4.3.6 Protein Expression: Immunocytochemical Analysis

The introduction to this chapter described how the phenotypic state of a vascular smooth muscle cell determines the protein expression of the cell, with the expression of certain proteins differing between the phenotypes more than others. Of those most commonly used to distinguish the phenotypic state, three were chosen for use in this work; alpha smooth muscle actin (αSMA), myosin heavy chain 1 and 2 (MHC1/2) and calponin.

In order to assess the antibodies to the selected proteins, test samples of hASMCs were created, consisting of the cells adhered to 8-well chamber slides and cultured in DMEM without any fetal calf serum. This medium promoted the differentiation of the cells into a more contractile phenotype whereby the cells should produce a greater quantity of the three proteins. After 7 days the cells on the chamber slides were fixed and stained with antibodies to one of the three phenotypic markers at varying concentrations of both primary and secondary antibodies. The samples were subsequently mounted in a DAPI containing mountant. Fluorescence microscopy analysis of each of the samples was performed to see which combination of primary and secondary antibody concentration was the most effective at producing a high degree of fluorescence. From this analysis it was found that the antibodies selected to measure MHC1/2 were ineffective and therefore not used in further analyses, whereas the antibodies against the other two proteins worked well and the optimum concentrations were determined.

To determine the phenotypic state of hASMCs on the various substrata, the cells were cultured, as before, in DMEM containing 10% (w/v) BSA for 7 days on aligned

and unaligned electrospun materials and woven polyester (PET) graft material as well as on tissue culture polystyrene (TCP), in the form of the base of the 24-well plates, with media changes every 3 days. Samples were again cultured on TCP in the absence of serum in order to provide a positive control for αSMA and calponin.

After 7 days, cells and substrate samples were removed from media, washed twice with PBS, fixed with 4% paraformaldehyde before membrane permeabilisation with 0.25% Triton X-100. One group of cell samples were incubated for one hour with an anti-αSMA antibody (Abcam, Cambridge, UK) and then with a FITC-conjugated anti-rabbit secondary antibody (Vector Laboratories, Peterborough, UK). The other group of samples were incubated for 1 hour with an anti-calponin antibody (Invitrogen, Paisley, UK) and then a Texas Red-conjugated anti-mouse secondary antibody (Vector Laboratories, Peterborough, UK). Both of these groups were washed 3 times in PBS between antibody applications and were subsequently mounted onto coverslips using a DAPI-containing mountant, Prolong Gold (Invitrogen, Paisley, UK).

Equivalent fluorescence images were obtained of all cell samples using the Apotome function of an Axio Imager Z1 microscope (Zeiss, Hertfordshire, UK) and all images were analysed using the ImageJ software. For each image, the total intensity of the channel relating to the colour of the fluorescent marker was determined. The number of cells in the particular field of view was then determined using the blue colour channel which relates to the DAPI nuclear stain and the cell counter plug in of the ImageJ software. The average amount of fluorescence per cell was then calculated from these two values and was used as a measure of the average protein expression per cell.

4.3.7 Protein Expression: Western Blot Analysis

The same three proteins were chosen as markers of the phenotypic state for Western blot analysis as in the immunocytochemical analysis detailed previously. As before the three corresponding antibodies were tested using a sample taken from cells

maintained in serum-free media. Of the three tested, only one worked with this method of measuring protein content; this being the anti-αSMA antibody, and during these tests the optimum concentrations of this, and the secondary antibody were obtained.

hASMCs in DMEM supplemented with 10% (w/v) FCS were deposited onto samples of TCP (24-well tissue culture plates), aligned electrospun PU, unaligned electrospun PU and Twillweave polyester (PET) graft material (Vascutek, Glasgow, UK) to achieve final densities of approximately $1x10^3$ cm^{-2}, $2x10^4$ cm^{-2}, $2x10^4$ cm^{-2} and $1x10^3$ cm^{-2} respectively. The medium in half of the samples on TCP were replaced with serum-free media one hour after deposition to allow time to adhere. All cell samples were incubated at 37ºC in 5% CO_2 for 7 days with a change of media every 3 days. No cell populations had sufficient time to reach confluence during this time. After the 7 days, cell lysates were obtained by physical removal of the cells from the surface into sodium phosphate (NaPi) buffer before homogenisation. Total lysate protein concentrations were analysed using the Lowry protein assay (Lowry et al., 1951). 20μg of protein from each cell sample was loaded into each of the wells of a 10% Bris-Tris electrophoresis gel, separated using electrophoresis and transferred onto nitrocellulose membrane. The proteins on the membrane were incubated in an anti-αSMA antibody (Abcam, Cambridge, UK) and then in an HRP-conjugated anti-rabbit antibody (Invitrogen, Paisley, UK) both for 2 hours at room temperature with constant agitation and with washes in phosphate buffered saline with tween (PBST) in between. The membranes were then placed into the development buffer, thereby defining the αSMA bands. Images of the bands were collected and analysed using the gel analysis function of ImageJ, which was used to determine the quantity of protein from the area and intensity/density of the bands.

4.3.8 Proliferation Measurement

Another mechanism affected by the phenotypic state of a cell is proliferation. This generally occurs at a greater rate in cells occupying a more synthetic phenotype. For

this reason the proliferation rate can be used as a measure of the phenotypic state of a cell population.

hASMCs in DMEM supplemented with 10% FCS were deposited onto samples of TCP (24-well tissue culture plates), aligned electrospun PU and unaligned electrospun PU to achieve final densities of approximately $5x10^3$ cm^{-2}. Half of the samples on TCP were changed to serum-free media one hour after deposition to allow time to adhere to the surface. As described in section 3.2.6, cell samples were cultured at 37ºC in 5% CO_2 for up to 5 days with a media change on day 3. Each day, a number of each sample were removed from culture, washed twice in PBS and fixed in 4% (v/v) paraformaldehyde before being mounted in a DAPI-containing mountant. 200 fluorescence images were obtained of each cell sample using the Apotome function of an Axio Imager Z1 microscope (Zeiss, Hertfordshire, UK), with each image representing an area of approximately $1.4mm^2$ and all images were analysed using the ImageJ software. The 'Cell Counter' plugin was used to determine cell densities on each substrate at each time point and from these the proliferation rate of hASMCs on each surface was determined.

4.3.9 Migration Rate Measurement

Not only is the migration rate a measure of the differentiated state of a VSMC but also has important implications in other processes, as detailed in the previous chapter. Therefore the migration rate measurement assay developed previously was used to measure the motility of hASMCs across the electrospun materials and TCP controls. The method described in section 3.2.5 was used to determine the migration rates of these cells across TCP in the presence and absence of serum, random electrospun fibres and aligned fibres in the directions both parallel and perpendicular to the fibre direction. On the aligned electrospun materials the mask edge was placed parallel to the direction of fibre alignment on some samples and perpendicular to it on others in order to measure the migration rate in both directions.

4.4 Results

4.4.1 Scaffold Formation

The electrospinning apparatus that was created proved to be a reliable source of electrospun material. Once the appropriate parameters were found, electrospun materials were formed without any bead defects. However, when trying to form fibres with different diameters, samples were instead formed with bead defects again. As such only fibrous samples with a very small range of fibre diameters were created. The use of the grid voltage was effective in creating aligned scaffolds as this was not possible without it even with the collector rotating at maximum speed.

The analysis of the fibrous structures with the SEM showed that the fibre diameter of the unaligned materials was 570 ± 20nm, while fibre diameter of the aligned materials was 587 ± 25nm. There was no significant difference between the diameters of the fibres in the two material types, whereas the fibre diameter of the woven polyester fibres from Vascutek were significantly larger at 13.0 ± 1.35μm. The representative images shown in figure 4.2 illustrate the structure of the two electrospun polyurethane materials with an image of the Twillweave polyester (PET) graft material (Vascutek) for reference. The unaligned fibres are random in orientation, crossing each other and apparently adhered at these junctions but relatively straight between the joins. In contrast, the aligned fibres, all running in a parallel direction, cross each other with a far lower frequency and, as opposed to being straight, were markedly undulating. The difference in alignment can be quantified by comparison of the angle which each fibre in a sample makes with the circumferential direction of the electrospinning collector. The unaligned fibres had a mean angle of 49.5 ± 26.3º, while the aligned fibres had a mean angle of 4.3 ± 7.9º. The former is consistent with a random orientation of fibres, while the latter shows that the aligned fibres are, in fact, highly aligned.

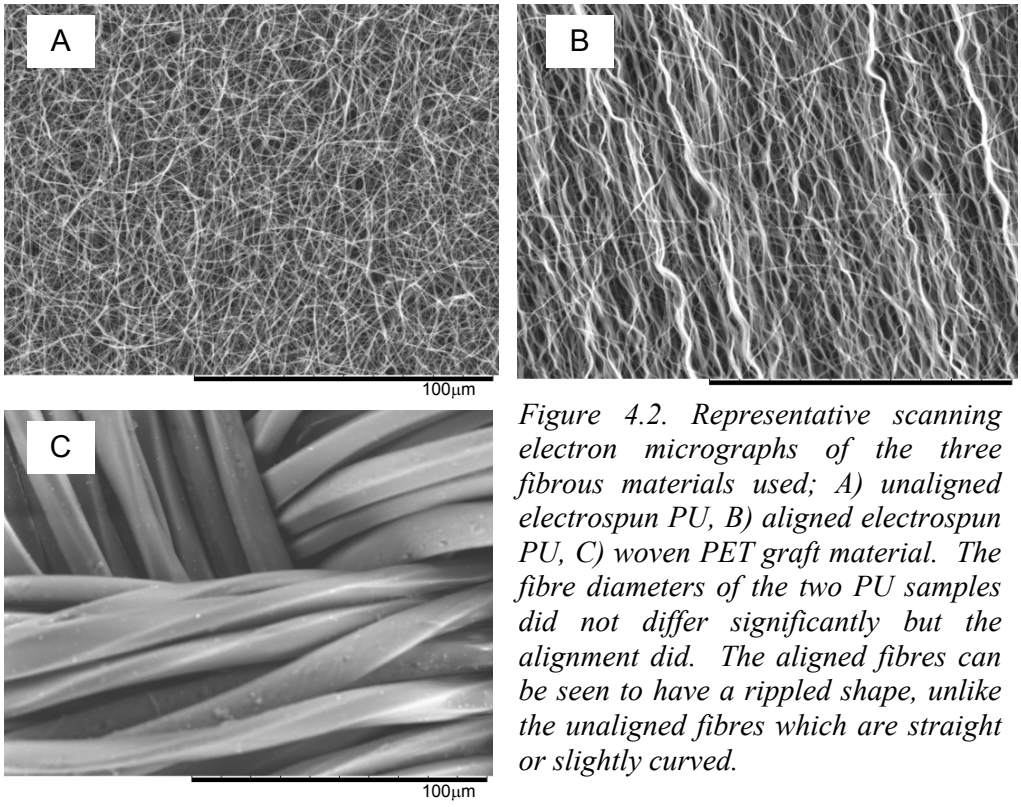

Figure 4.2. Representative scanning electron micrographs of the three fibrous materials used; A) unaligned electrospun PU, B) aligned electrospun PU, C) woven PET graft material. The fibre diameters of the two PU samples did not differ significantly but the alignment did. The aligned fibres can be seen to have a rippled shape, unlike the unaligned fibres which are straight or slightly curved.

4.4.2 Microscopy/Morphology of Cells

Cell samples attached to the three surfaces; TCP, aligned electrospun PU and unaligned electrospun PU, were cultured for 7 days in DMEM with FCS and, in the case of the cell samples on TCP, also in DMEM in the absence of FCS. These samples were probed with a fluorescently labeled antibody for vinculin and with FITC-conjugated phalloidin for f-actin. Representative images from each sample type are shown in figure 4.3.

The fluorescent images of the cells on TCP which had been maintained in serum-containing media showed them to have a spread morphology, as seen previously in figure 3.14. The images show the f-actin filaments mostly outlining the periphery of the cell with a few detectable filaments running across the cytoplasm. Conversely, cells attached to TCP which had been cultured in the absence of serum possessed a

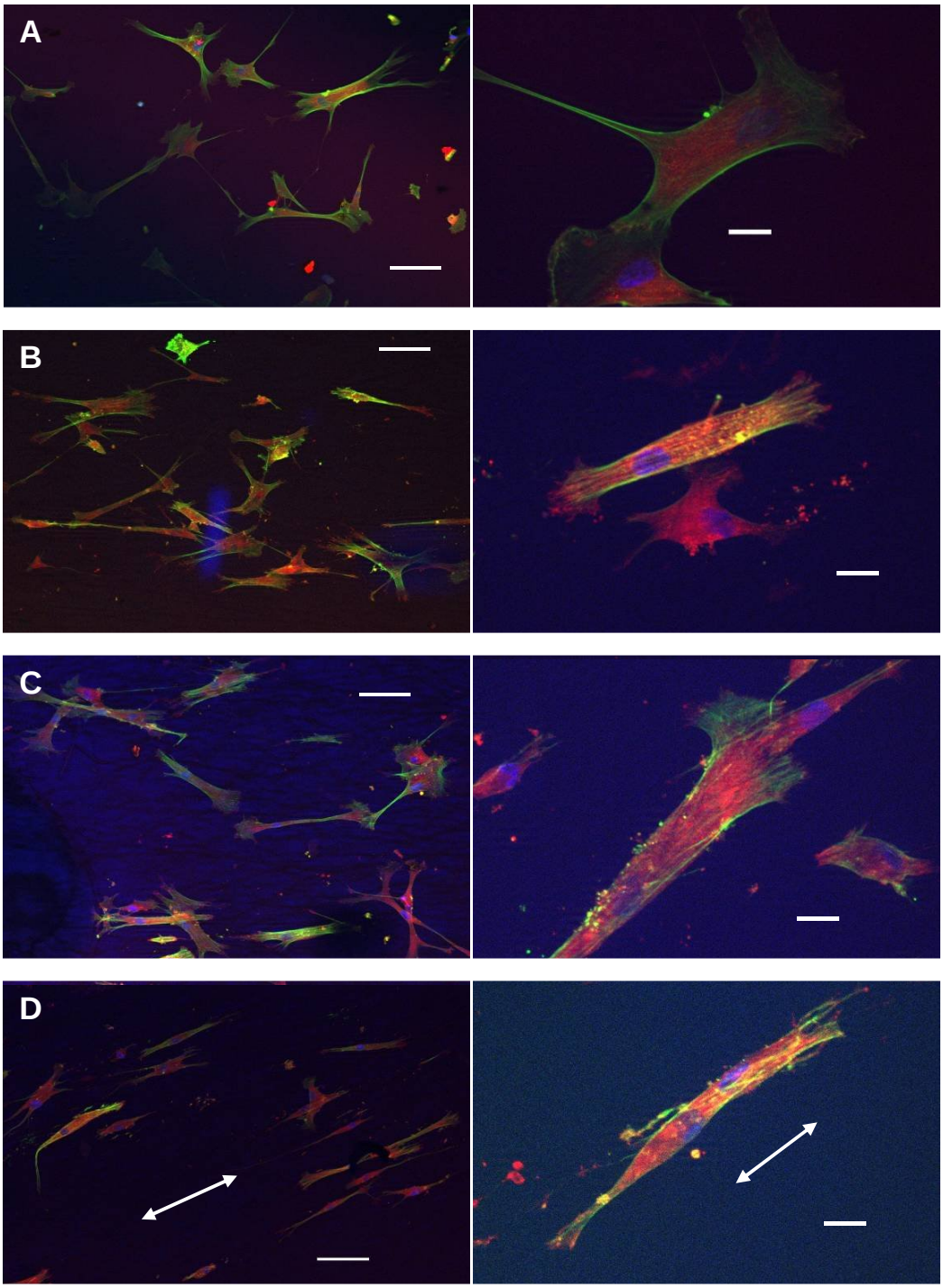

Figure 4.3. Fluorescence microscopy images of cells grown on TCP in the presence (A) and absence (B) of serum and on electrospun polyurethane, both unaligned (C) and aligned (D). Left and right images show the cell samples at different magnifications. Cells on TCP in the presence of serum assumed a flattened, spread morphology, while those on TCP in the absence of serum and on electrospun PU were more elongated, even fusiform in shape. Cells on aligned electrospun PU assumed the same direction of alignment as the fibres, the arrow in D indicates the direction of the fibre alignment. Green colour in the images corresponds to actin, red to vinculin and blue to nucei. Scale bar = 100μm in the left images and 20μm in those on the right.

vague spindle-shaped morphology; elongated with the nucleus in the middle and processes extending in either one or both opposing directions. The actin filaments can be seen to extend in the direction of the cell alignment.

When attached to electrospun Z1A1 polyurethane, both aligned and unaligned, the hASMCs, as seen in the immunofluorescence images, were also of a fusiform morphology, but more so than the cells on TCP in the absence of serum as shown by the proportion of elongated cells and the degree to which they were elongated. Again, the actin filaments could be seen to extend along the length of the cell. The cells that were attached to the aligned electrospun fibres, as evident in figure 4.3, were found to be aligned along the direction of the fibres. This is shown from the angle between these cells' directions and the fibre direction being $3.0 \pm 2.46^{\circ}$.

4.4.3 Protein Expression: Immunocytochemical Analysis

Through the use of immunofluorescent labeling of hASMCs on TCP and electrospun PU, as shown in figure 4.4, the quantity of both αSMA and calponin in the cells was measured. The analysis of both the intensity of fluorescence and the number of cells in each image provided a measurement of the content of both of these proteins per cell. The results of these measurements are shown in figure 4.5 where it can be seen that the quantity of these two proteins varied by similar amounts across all the samples. The amount of these proteins in the cells on the woven PET was similar to that in the cells on the TCP in the presence of serum, that is, a relatively low amount, as demonstrated by the lack of red or green in the images in figure 4.4 C and D. However, when cultured on electrospun PU, the cells produced similar amounts of these proteins to the cells maintained in the absence of serum on TCP. In the case of αSMA content of cells on aligned electrospun PU this was significantly higher than the content of this protein in the hASMCs in the positive control of the cells on TCP in the absence of serum.

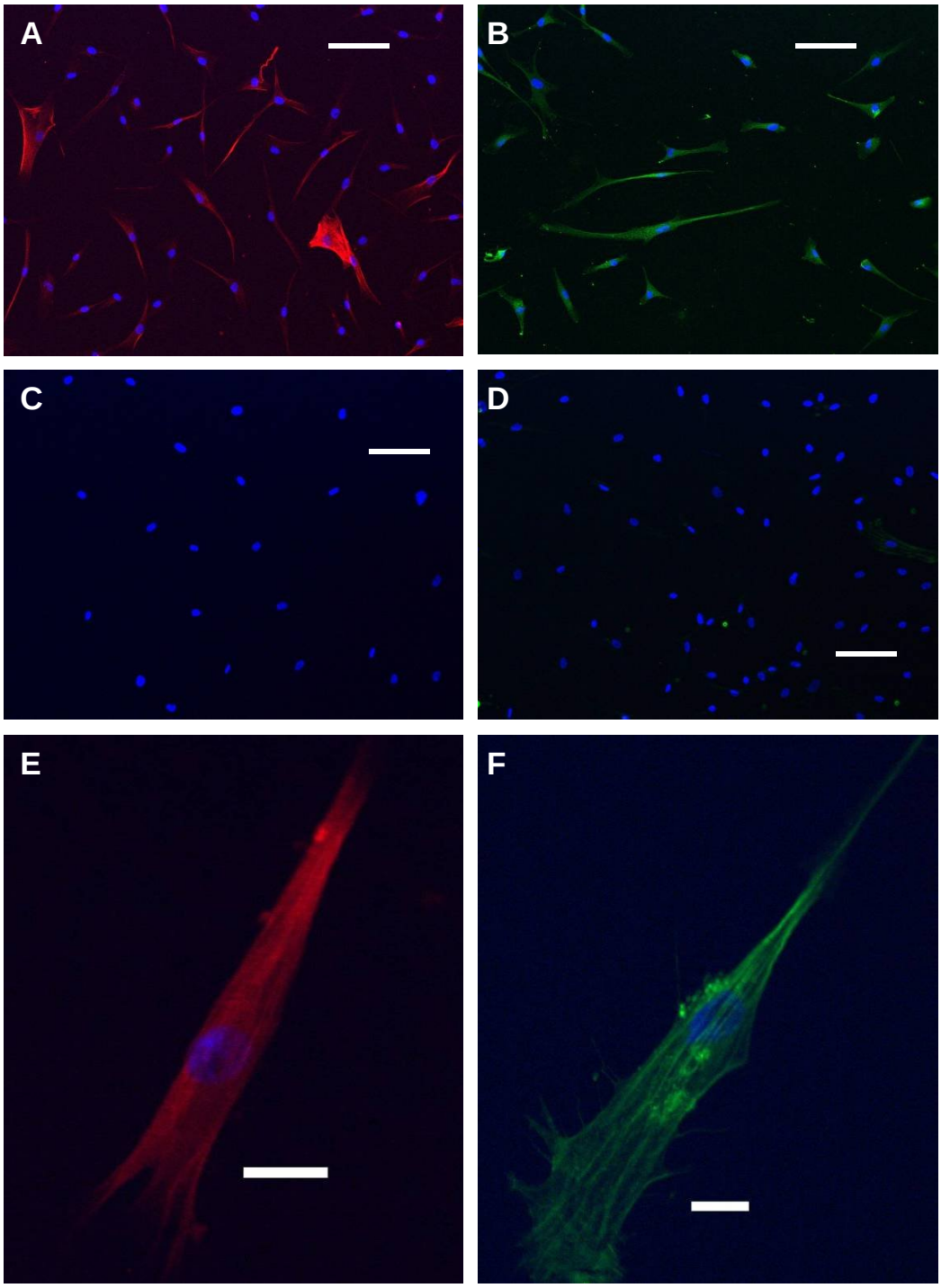

Figure 4.4. Representative fluorescence micrographs of cells on unaligned electrospun PU (A, B, E and F) and on TCP (C and D) all grown in the presence of serum and stained for calponin (red; A, C and E), and for αSMA (green; B, D and F) scale bars = 100μm (A-D) and 20μm (E and F). It can be seen in C and D, from the lack of any noticeable red or green fluorescence that cells on TCP have produced a low level of calponin and αSMA, whereas on electrospun surfaces the levels of these proteins produced is much more noticeable.

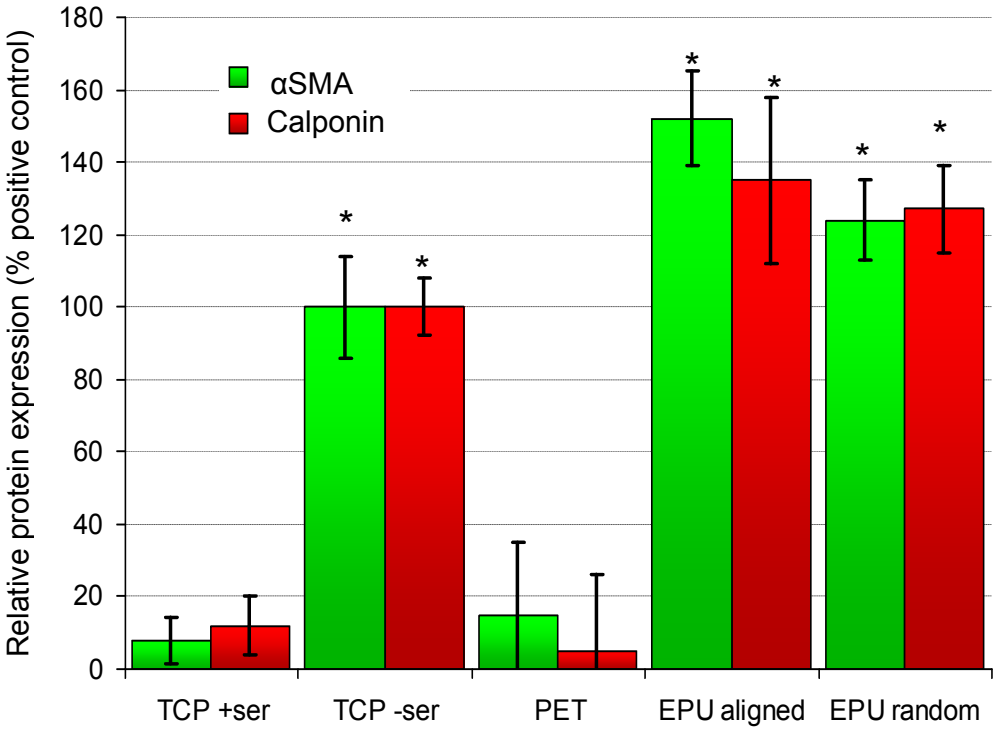

Figure 4.5. Relative quantity of the two proteins αSMA and calponin produced per cell on the various substrata, measured from images of the intensity of fluorescence of the stained proteins as exemplified by figure 4.4. Protein quantities were normalised for cell number by using ImageJ to count the number of cells in each image. The positive control sample for protein expression, to which all others were compared was the cells on TCP, cultured in the absence of serum. The asterisks show significance ($p<0.05$) relative to the negative control (on TCP in the presence of serum) as determined by ANOVA, n=160.

4.4.4 Protein Expression: Western Blot Analysis

The αSMA protein content of the hASMCs was measured using the method of Western Blot analysis. Homogenates from cells attached to TCP, PET and electrospun PU were analysed and the results shown in figure 4.6. As with the immunocytochemical analysis, the protein content of the cells attached to PET and TCP in the presence of serum were similar, while the content of the cells on the electrospun PU was similar to that of cells on TCP in the absence of serum. The difference between the two groups was also found to be significant.

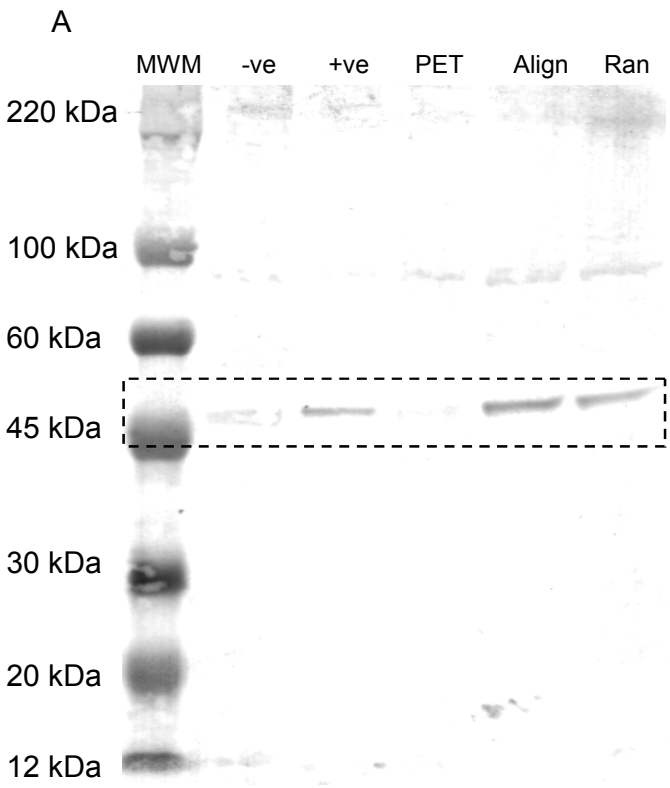

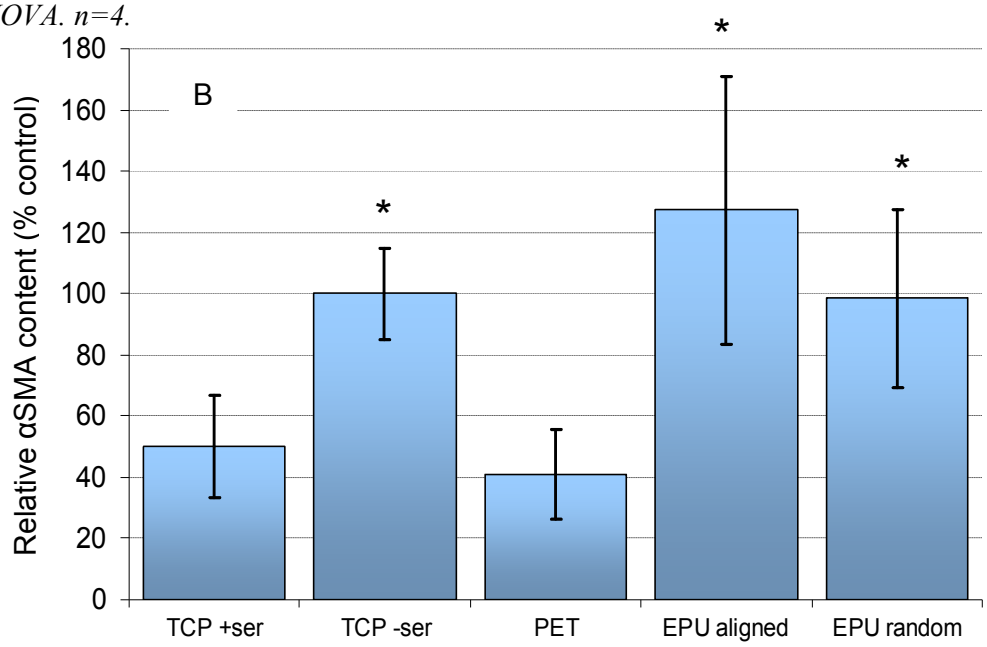

Figure 4.6. Cellular content of αSMA as measured by Western blot. A) example of a set of bands for αSMA with lanes corresponding to the molecular weight marker (MWM), cells on TCP in the presence of serum (-ve control), absence of serum (+ve control), on Dacron (PET), aligned (Align) and random (Ran) electrospun surfaces. The MWM shows that the bands for αSMA (42kDa) are in the correct position and as such correspond to this protein. B) graphical representation of band intensity relative to negative control. The asterisks show significance ($p<0.05$) relative to the negative control as measured using ANOVA. n=4.

4.4.5 Proliferation Measurement

Through the use of cell density measurements from fluorescent images of cell nuclei, the proliferation rate of the cells on the various substrata was measured. The proliferation rate, as seen on figure 4.7 was significantly higher in cells on TCP cultured in DMEM with serum than without, while cells on electrospun PU had an intermediate proliferation rate, but still significantly different from the other two sample groups.

Figure 4.7. Graph showing the mean change in cell density ±SD over time due to proliferation. The proliferation rate can be seen to be highest in cells on TCP in the presence of serum with the other cell samples exhibiting significantly lower rates. n=200

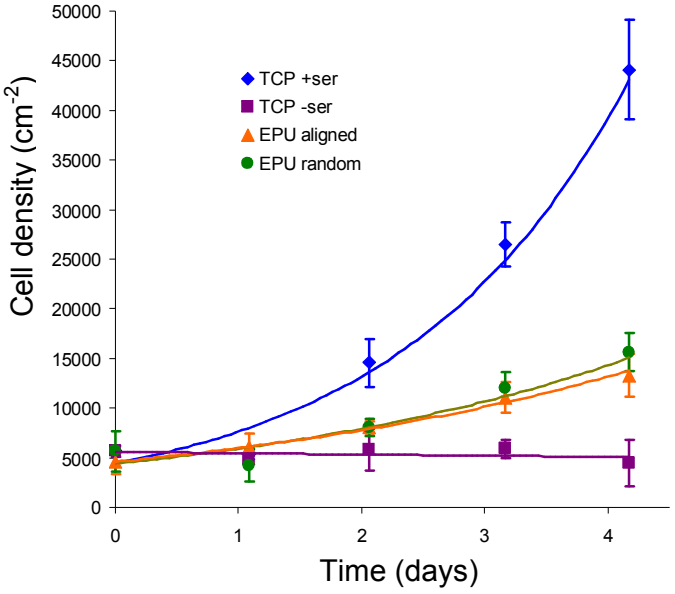

4.4.6 Migration Rate Measurement

The migration assay developed in the previous section was used again to determine the migration rate of hASMCs on the various substrata and the results are shown in figure 4.8. The migration rates were measured on TCP in the presence and absence of serum, as well as on electrospun polyurethane with unaligned fibres and aligned fibres, both parallel and perpendicular to the direction of fibre alignment. The migration rate of cells on TCP in the presence of serum was significantly higher than that in all other sample groups. One other difference was that the migration rate of cells in the direction of fibre alignment on aligned electrospun PU was significantly higher than that of cells in the perpendicular direction.

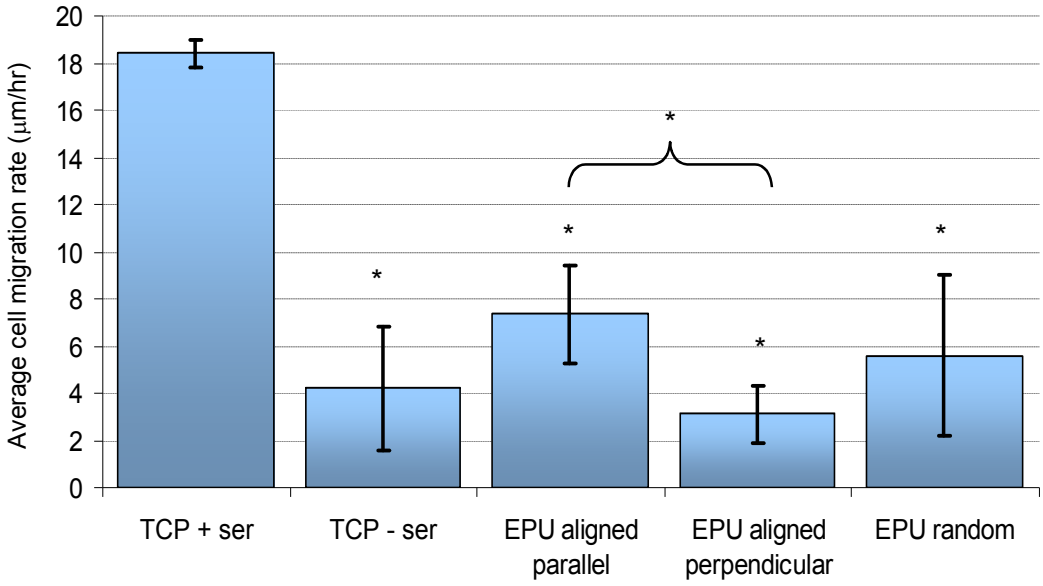

*Figure 4.8. Bar chart showing the mean cellular migration rate ±SD across various surfaces. This was found to be significantly higher on TCP than on other surfaces, including on TCP in the absence of serum. A significant difference in the migration rate was also found to exist between cells moving in the directions parallel and perpendicular to the aligned fibre direction on electrospun polyurethane. * shows significance ($p<0.05$) relative to the negative control as determined by ANOVA. n=16.*

4.5 Discussion

In order to create a vascular graft material which replicates the native environment for vascular smooth muscle cells the electrospinning technique was utilised. This process is widely used in medicine and tissue engineering to produce fibrous materials, as a wide variety of fibre and material geometries can be created. Z1A1 polyurethane was once again chosen as the material for use in the electrospinning due to its excellent mechanical properties and biocompatibility. The fibrous material geometry was intended to replicate that of the native vessel as closely as possible; having fibres with sub-micron diameters and a highly aligned orientation.

An electrospinning rig was designed and constructed for producing this fibrous material and was used to create both aligned and unaligned fibrous PU with a fibre diameter of approximately 580nm. This fibre diameter is within the range associated with extracellular matrix proteins found in the vasculature. The alignment was also consistent with that found in a blood vessel, being oriented circumferentially around the vessel and parallel to the direction of orientation of the VSMCs. This may also prove to be beneficial by providing the anisotropic mechanical properties found in the native blood vessel, as shown by Lillie et al. (2010), but further investigations would be required to determine this. The electrospinning apparatus proved to be reliable and consistently produced fibrous materials of the desired geometry.

The affinity of human aortic smooth muscle cells for cast Z1A1 was shared with that for the electrospun version. The cells cultured on this fibrous scaffold adopted a spindle-shaped morphology consistent with a more contractile or differentiated phenotype found in VSMCs in healthy vessels. This morphology was also observed, though to a slightly lesser extent, in hASMCs cultured on tissue culture polystyrene in the absence of serum. These latter samples were created in order to provide a positive control for the differentiated cell type and their morphological similarity to healthy cells *in vivo* shows that this had been accomplished. By contrast, the negative control for the differentiated cell type, hASMCs attached to TCP and maintained in the presence of serum, possessed a flattened, spread morphology.

Staining the cell samples with FITC-conjugated phalloidin illustrated the difference in cytoskeletal arrangement in the two cell morphologies as shown in figure 4.3. The flattened cells had an f-actin arrangement which encircles the periphery of the cell's cytoplasm. However, in the spindle-shaped cells, the actin filaments were orientated along the length of the cells, showing that the contractile proteins were aligned to be able to allow the cell to provide a contractile force.

The arrangement of cells on electrospun materials mimicked the orientation of the fibres to which they are attached; on unaligned fibres hASMCs adopted a random orientation, while on aligned fibres the cells were also aligned. This allows a higher

degree of similarity of these aligned electrospun scaffolds to the native vessel, with both cells and fibres being aligned circumferentially around the blood vessel. This arrangement of both cells and proteins in the native vessel is responsible for providing the vessel tone and, through the contraction of the VSMCs, allows the vessel to regulate the inner diameter and control the blood flow around the body. Although the reinstatement of vessel diameter control with the implantation of a synthetic, or part synthetic vascular graft would be quite improbable, the improvement in vessel tone with a vessel that contains normally aligned VSMCs may be more likely. This improvement in vessel tone over a graft without aligned VSMCs would aid in the transmission of blood along the vessel.

In addition to the morphological similarity between hASMCs attached to electrospun material and differentiated VSMCs, these cells' contents of contraction-related proteins were also similar. This was measured through the use of two methods; immunocytochemical staining and Western blot analysis. Both of these methods were found to provide consistent and reliable results for the detection of alpha-smooth muscle actin and, in the case of the immunocytochemistry analysis, for calponin too. The amount of these two proteins was found to be significantly higher in cells when attached to electrospun materials than in the negative control; on TCP in the presence of serum. The amount of αSMA and calponin in cells on these fibrous structures was much closer to the positive controls, cells on TCP in the absence of serum. Conversely, when hASMCs were cultured on woven PET graft materials the amount of these two proteins present in each cell was much less than the positive control but did not differ significantly from the cells in the negative control.

The presence of high levels of contractile proteins in the hASMCs on electrospun materials is another indicator that they have adopted a differentiated, contractile phenotype. This implies that if a vascular graft was composed of electrospun materials it could promote this state in any VSMCs that migrated onto its surface. In addition, if taken one step further, these materials, if used as a scaffold in tissue engineering applications, could perhaps maintain any resident SMCs in a contractile

state. The benefit of maintaining this state may be that the effects of intimal hyperplasia are limited. These would include the increased proliferation rate and rate of ECM deposition, both contributors to IH growths that cause the occlusion of vessels. In contrast to the electrospun samples, hASMCs on PET samples possessed a more synthetic phenotype. This could be implicated as a reason for the failure of grafts made from such materials. In addition to the use of electrospun Z1A1 as a cell substrate it would be an interesting extension of this work to utilise other polymers such as Z3A1, the other PU used in the previous chapter, in the same way. Some success had been gained in the production of electrospun Z3A1 materials but these had not, at the time of writing, been utilised in the manner in which electrospun Z1A1 had been in this chapter. However, it is feasible that the equivalent experiments could be performed with this other grade of PU. As the results in the previous chapter have demonstrated, the stiffness of a substrate can determine the way in which a cell can attach to it and migrate across it. It would also be of interest to see how the stiffness of the electrospun polymer affects the phenotypic state of any SMCs attached to its surface.

As myosin heavy chain 1 and 2 could not be detected by either immunocytochemistry or Western blot analysis in the cell samples on electrospun materials, it could be the case that either insufficient differentiation was promoted in these cell samples or that the anti-MHC1/2 antibody used in these experiments was not sensitive enough. Due to the fact that the positive control for a differentiated phenotype also appeared to be devoid of these proteins and as cells maintained in these conditions by Worth (2004) and Ma (1998) showed positive for MHC1/2, it would appear that the latter explanation is the more likely.

To further investigate the effect of the electrospun surface and therefore the differentiated state on the proliferation rate of hASMCs, samples were analysed for cell density at various time points. As expected, the proliferation rate on these fibrous surfaces was greatly reduced from those on TCP. This low proliferation rate, as described above, could be beneficial in the limitation of the growth of hyperplastic lesions if these electrospun materials were used as graft materials.

The migration rate of hASMCs was determined to be significantly lower across electrospun Z1A1 than across TCP, illustrating a differentiated phenotypic state of the cells on the fibrous PU. In addition the lower migration rate could be useful in limiting the invasion of VSMCs onto any implanted materials from the adjacent vascular tissue. As this is one of the first steps in the progression of intimal hyperplasia, electrospun materials could also prove useful for limiting the development of this condition. The migration rate of the cells across the aligned electrospun materials differed in the two directions parallel and perpendicular to the direction of the electrospun fibres. The cells migrate preferentially in the direction of the fibre alignment, rather than across them. This could be advantageous if the aligned electrospun materials were utilised in a vascular graft setting as VSMCs invading the graft from the surrounding tissue would have to migrate across the fibres, rather than along them. The apparent difficulty that the cells experience in doing this could further limit the progression of IH in these situations. Additionally, and as shown by Telemeco et al. (2005), the control over cell migration rate via fibre alignment could become a useful tool in regulating cellular infiltration into a tissue engineered scaffold comprised of electrospun materials.

Although the alignment of fibres could prove beneficial in limiting the migration of VSMCs onto an implanted graft and therefore the subsequent hyperplastic growth, it may be less useful if the same applied to the migration of the resident endothelial cells. It is well documented that the patency of a vascular graft is improved if its luminal surface can become endothelialised. However, if the alignment of fibres in the graft was perpendicular to the length of the graft; the direction in which endothelial cells would have to migrate to cover the luminal surface, and if these endothelial cells were also resistant to migrating across the alignment of the fibres, the endothelialisation would become more limited. Previous work by Uttayarat (2008) and Bouta (2011) conducted on the response of endothelial cells on aligned electrospun fibres and micropatterned surfaces shows that the response of these cells is similar to that of the hASMCs shown above. Although the fibre diameter differs from those in this work, the endothelial cells aligned along the fibre direction and

migrated preferentially in this direction as well. This suggests that a graft material with an aligned fibrous structure may have advantages in preventing invasion of VSMCs or allowing endothelialisation, but not both.

Previous work by Miyamoto (2009) has also determined that VSMCs transform to a more differentiated phenotype when attached to electrospun materials. In this case it was elastin that was used and the fibre diameter was an order of magnitude greater than the PU fibres created in the current work. The effect of the electrospun elastin scaffold on the phenotypic state appeared to be lesser than the one observed here, with the increase in αSMA being substantially less than the increase in αSMA in hASMCs on electrospun Z1A1. The use of the elastin material, proposed by Miyanoto et al, as a vascular graft material may prove to be problematic due to the rate of reconstruction of the graft by the resident cells and the inherent loss of mechanical integrity of the graft.

The effect of phenotypic modulation through substrate structure must be transmitted through the cell-surface integrins, with the work by Zargham (2007) implicating the α8 integrin, for example, in the differentiation of VSMCs. Very little work has been conducted into the signalling pathway that allows the nature of the surrounding topography of a cell to have an effect on its phenotypic state. However, it seems plausible, and has also been proposed by other researchers such as Cao et al. (2010), that they are the same signalling pathways as those responsible for mechanical stretch of a cell's substratum causing a VSMC to adopt a more differentiated state. As such the MAPK (Tock et al., 2003) and FAK phosphorylation transduction pathways (Gahtan et al. 1999), for instance, may also be responsible for the effects seen in this chapter, but further work would be required to verify this.

4.6 Conclusion

A set of apparatus was designed and built for the purpose of electrospinning polyurethane and was used to create both aligned and unaligned fibrous materials. Human aortic smooth muscle cells cultured on these materials assumed a more contractile phenotype than they do when maintained on tissue culture polystyrene. This was observed through the spindle-shaped morphology of the cells, the increased expression of the contraction-related proteins alpha smooth muscle actin and calponin and the decreased proliferation and migration rates. The ability of the electrospun material to modulate the phenotypic state of the hASMCs is not only useful for gaining additional insight into how a cell regulates its state of differentiation but it may also prove to be a useful tool in *in vitro* analysis of the behaviour of the cell as well as in vascular graft applications.

CHAPTER 5

EFFECT OF MECHANICAL STIMULATION ON SMOOTH MUSCLE PHENOTYPE

5.1 Introduction

The elastic nature of a healthy blood vessel and the pulsatile nature of the blood pressure mean that the arteries are continuously distending and retracting with the heart beat. The main stretch of the vessel is in its circumferential direction (Lillie et al., 2010), however there is also a systolic axial contraction, as measured by Tozzi et al. (2001) but this has been shown to be insignificant when compared to the circumferential distension. The stretching of the vessel influences all of its components; both the fibrous proteins that form the scaffold of the vessel, as well as the resident cells themselves, all undergo a deformation. For any *in vitro* model of the artery wall to provide an accurate representation of the situation *in vivo* the dynamic nature of the blood vessel must be considered. Therefore, the work in this chapter focuses on the addition of a mechanical stimulus to the investigation of vascular graft materials that were studied previously in a static model.

The effects of applying a force to biological systems or models have been studied extensively (Bader, 2008), partially due to their importance to many parts of the body such as the heart (Shyu, 2009), vasculature (Li et al., 2005), lungs (Hasaneen, 2005), bladder, gastro-intestinal system (Tanaka et al., 2000), skin, bones (Basso and Heersche, 2002), joints (Lee et al, 2005) and cartilage, to name a few. This stimulus has many and varied effects on the nature of the resident cells and the consequent change of the surrounding environment, as shown by Boerboom et al. (2008) and Asanuma et al. (2003). In the case of vascular smooth muscle cells, numerous cellular functions are modulated by cyclic stretch, including proliferation (Hipper, 2000), apoptosis, migration (Sweeney, 2004), cell alignment (Standley, 2002) and the differentiated state (Altman et al, 2002). This is activated through a number of sensing mechanisms by the cell. Firstly, the stretch of the substrate is felt through the cell's integrins through which the cell attaches to it. These integrins span the membrane and transmit the mechanical force of the substrate in the extracellular environment to associated intracellular molecules in the focal adhesion. Another mechanism for force transduction is the activation of ion channels. The stretching of the VSMC activates nonselective cation channels in the cell membrane and can also

open Ca^{2+} channels in intracellular Ca^{2+} stores, increasing the cytoplasmic concentration of this ion (Rosales et al., 1997). Lastly, receptor tyrosine kinases have also been implicated in the mechanical force transduction (Hu et al., 1998).

The effect of stretch on VSMC phenotype has been found to depend on both the nature of the extracellular environment and that of the strain. For instance, with cells on 2D surfaces, Birukov et al. (1998) and Reusch et al. (1996) have shown that uniaxial stretch increases the amount of smooth muscle differentiation markers such as MHC1/2 and caldesmon. Although, as shown in the work by Butcher et al. (2006), when an equibiaxial stretch is applied to a VSMC-seeded membrane the resident cells attain a more fibroblastic or synthetic phenotype. In addition, the work by Birukov et al. (1995) shows that VSMCs under cyclic stretch increase both their rate of proliferation and their production of h-caldesmon, although not their production of calponin or α smooth muscle actin, simultaneously showing both a move to a more contractile phenotype as well as to a more synthetic one, however this could be due to the fact that the strain field was not well characterised in this study. In 3D cultures (Pedersen and Swartz, 2005) both differentiation and dedifferentiation have also been observed. The work conducted by Sharifpoor et al. (2010) shows that VSMCs cultured inside a porous polyurethane scaffold increased their DNA mass and calponin content when exposed to cyclic stretch and Zeidan et al. (2003) have shown that the distension of rat portal veins also maintains the contractile phenotype of the resident VSMCs. In collagen gels Kim et al. (2000) has found that stretch causes a more differentiated state in VSMCs while in polyglycolic acid a phenotypic shift towards a more synthetic state is caused by the stretch.

In a similar way to the differential effect of stretch on VSMC phenotype due to environmental conditions, its effect on cellular alignment is also similarly affected. Cells cultured on a planar substrate will align perpendicular to the direction of strain in order to minimise the effect of the strain on the cell as shown by Chen et al. (2003) and Standley et al. (2002). This is in stark contrast to the cellular alignment in cells in 3D culture or *in vivo*, where the cellular orientation is parallel to the direction of strain. The work by Jeong et al. (2007) using blood vessel models composed of

freeze dried collagen and electrospun PLGA and seeded with both VSMCs and endothelial cells showed a circumferential alignment of the former cell type in response to a cyclic radial distension, coupled with an adoption of a contractile phenotype.

Both of these examples show the importance of considering the environment of the cell and the nature of the mechanical deformation on the impact of the applied stretch. In addition, the effect of the applied strain in *in vitro* models shows the importance of a deformable support for VSMCs *in vivo* so that the cells can take advantage of the effect of strain on their phenotypic state and help modulate the progression of a pathological condition.

The fact that *in-vitro* mechanical deformation systems have been used extensively to investigate the effect of strain on cell populations is due to their relative ease of use, flexibility and lack of the interpretational complexity of the results obtained when compared to *in vivo* systems. A number of types of system are used, as described in the review by Brown (2000) and there are numerous similarities across many of the systems in each type. One particular type is where in-plane longitudinal strain is applied, usually on a thin rectangular membrane held between two clamps. The motion of the clamps can be driven by a stepper motor through a cam, pulley system (Langelier, 1999) or lead screw system (Yost et al. 2000) or by a linear motor (Cacao et al, 2000). Another type utilises out of plane distension driven through the application of pressure or vacuum to a circular membrane restrained around its circumference to apply a biaxial strain field. The popular Flexercell system (Flexcell International Corporation, Hillsborough, NC, USA) is one such device, although it also has attachments which can be used for the purpose of applying uniaxial strain. Perhaps the most relevant system for the investigation of hemodynamic forces on a blood vessel is the tubular distension model, as used by Sipkema et al. (2003), where a vascular replica is stretched using the pressure of the media perfusing it. However, as shown in the work by Yoshigi et al. (2003), only the in-plane strain systems combine versatility and simplicity of use with the possibility of microscopic visualisation of the resident cell samples.

5.2 Materials and Methods

5.2.1 Construction of Mechanical Stimulation Apparatus

A number of considerations were taken into account when designing the mechanical stimulation apparatus based on the system requirements. These are outlined in the following subsections, with the final subsection explaining how these were brought together in the final design:

5.2.1.1 Ability to Provide the Desired Mechanical Stimulation

The initial consideration in the design of a mechanical stimulation device must undoubtedly be the provision of the mechanical stimulation. There are numerous properties of the applied stretch that must be controlled in order to properly replicate the mechanical environment *in vivo*.

The first quality of interest that has an effect on the cellular response, as shown by Boerboom et al. (2008) is the magnitude of the stretch. The normal maximum strain (Veress et al. 2002) is generally considered to be approximately 10% for a healthy vessel but could be substantially lower for a calcified, atherosclerotic vessel (Humphrey and Na, 2002) and much higher for an aneurismatic one, while hypertension can decrease arterial distensibility (Laurent et al, 1994). Likewise, the maximum strain for an implanted synthetic graft will also depend on the graft material stiffness. The maximum strain required for the device in this work to provide was chosen to be 20% of the original length of the membrane or cell substratum. In order to provide a sufficient area for cell growth to measure the effect of the mechanical stimulation on the cells, but while keeping the apparatus to a manageable size, an initial substratum length of 40mm was chosen. Consequentially, the range of motion required from the system that allows a 20% strain would be 8mm and this was selected as a specification for the system even though the normal range of motion that was used was half that, resulting in a 10% strain. Closely linked to the

range of motion of the stretching system is the level of accuracy with which it can move. As a preference, this was chosen to be 1% of the normal range of motion of the system, resulting in a desired accuracy of ±40μm.

Another quality of the stretch to consider is its frequency as it is of a cyclic nature and because this frequency has been shown previously by Qu et al. (2006) and Liu et al. (2007) to affect the phenotypic shift caused by the stretch. The normal resting heart rate is around 70 beats per minute (bpm) but in a healthy, young individual the rate can exceed 200 bpm when exercising. The design of this device must therefore, as a minimum, be able to achieve 70 cycles per minute (1.17 Hz) so as to replicate the average resting heart rate but higher values would be useful in order to investigate the effect of heart rate in the model.

As the shape of the pulse wave has been shown by, for example, Haghighipour et al. (2010) to influence the effect of the stretch on the VSMCs resident in a blood vessel, the stress profile created by the mechanical stimulation system is also important and should be controlled. This has been shown to be approximately of a saw-tooth wave shape, with the rate of increase of stress being faster than the decrease, as shown in figure 5.1. A stress waveform of this shape is, in theory, relatively basic to replicate as it only requires a constant rate of stretch. In order to do this the system must be able to move in the stretching phase, where the rate of motion is greatest, at 28mm/s in order to achieve a 20% strain at 70 cycles per minute. This, therefore, also dictates the last of the desired qualities from the system; the speed of motion of the stretching apparatus must be at least 28mm/s.

The system must also have sufficient mechanical power to stretch the cell substratum as described above. This can be achieved by using a motor with a suitable amount of power or to ensure that the substrate is adequately stretchable. The latter can be accomplished by reducing the width or thickness of the membrane, but as a reduction in width would limit the area for cell growth a reduction in membrane thickness would be preferable. Ensuring ample power is available for stretching the membrane can also be performed by limiting the amount of energy wasted in the system by, for

example, the use of high efficiency power transmission components. In addition, as the number of samples stretched in parallel is increased the more samples are available for analysis, but this also increases the power required by the system to stretch the additional samples.

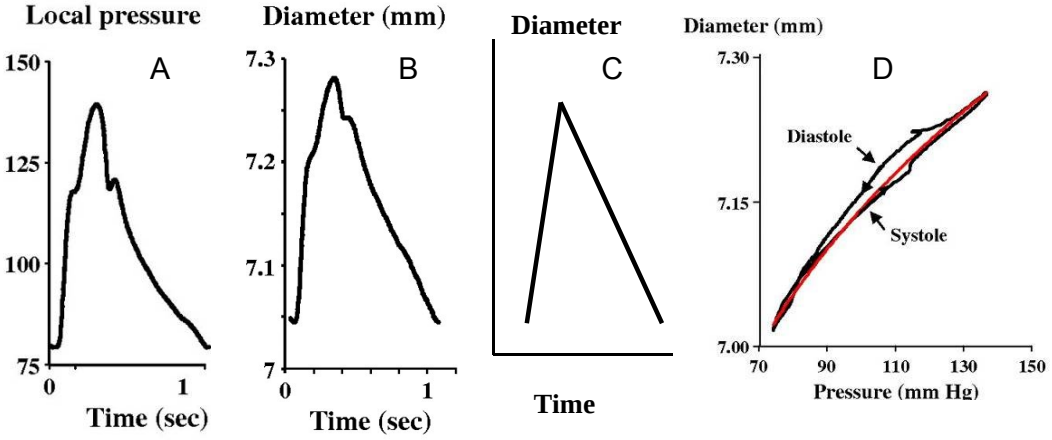

Figure 5.1. A shows the variation in pulse pressure with time, resulting in the stretch in B in a typical artery. This stretch waveform found in vivo *can be replicated, to a reasonable level of accuracy, by a generic saw-tooth wave shown in C. For reference, the relationship between pulse pressure and diameter of the artery is shown in D. A, B and D were adapted from London and Pannier's review (2010).*

5.2.1.2 Capacity to Maintain a Cell Culture

Mechanical deformation of a cell's substratum occurs continuously *in vivo* and it is therefore a requirement to be able to observe this effect over several days using the system developed in this chapter. For a cell culture to be sustained for this duration it must be provided with the correct environment by the system. This includes producing the correct temperature and maintaining the media at the right pH and containing the appropriate nutrients and dissolved oxygen.

5.2.1.3 Compatibility With Previously Used Cell Substrata

As the work in this chapter is based around the testing of the previously used substrata in the presence of deformation, it is important to be able to use these materials in the mechanical stimulation system. The materials that were useful for this purpose were the solvent-cast and electrospun polyurethane, while the tissue culture polystyrene and woven polyester graft material were too rigid to undergo significant deformation if used *in vivo* so it would be unrealistic and prohibitively difficult to use them in the deformation system.

The two PU materials used were of a very similar nature in terms of bulk properties as the only difference was a thin layer of fibres on the electrospun samples. Both could be created in, or cut to a size compatible with that required by the deformation system. In addition, as both were produced in a thin film format the force required to stretch either type of sample was minimised.

5.2.1.4 Suitable For Use With an Upright Microscope

The final consideration of the system was that it should be compatible with a microscope in order to be able to obtain images of the resident cell samples during the course of an experiment. This is important so as to both determine that the cells resident on a substrate are undergoing mechanical deformation when the substrate is and also to observe the effect of this deformation over time, rather than at a small number of time points that would be possible if the stretching regime had to be stopped before analysis.

The main design requirement for satisfying this condition was that the enclosure of the chamber that houses the cell sample being stretched must allow a path of light from the light source of the microscope, through the wall of the chamber, through the cell sample on the substrate, out the other side of the chamber and into the microscope objective. As the substrate samples used in this work are relatively

optically clear they should not cause a problem. However this does also mean that specific parts of the wall of the enclosure must be transparent.

The type of microscope system used was of the upright variety as this was the most versatile system available and had benefits in requiring the placement of the cell sample near the upper window of the cell chamber. The benefits of this included being able to keep the cell samples upright, with cells on top of the substrate, and still being able to visualise them without the need for the substrate to be transparent. This microscope, however, also had a limitation in that the total mass of the deformation system placed on the microscope stage had to be less than 3kg so as not to overload the translatory motors of the stage.

In order to take photomicrographs during the deformation regime it is also important that the cell sample is in the same location for each image taken, a difficult feat considering the sample would be required to be in constant motion, or as close to this as practicable. This can be accomplished, in part, by stretching the two opposing ends of the substrate in equal and opposite directions, therefore leaving the central section of the membrane relatively stationary. It is this central section that should have the most uniform stress profile and, as such, is the most useful for observing the effect of the stress on the cells. This arrangement and the stasis of the central region of the membranes during stretch would have an additional benefit in preventing this region of interest from having to travel through the media and therefore limiting the associated fluid shear forces affecting the cell sample.

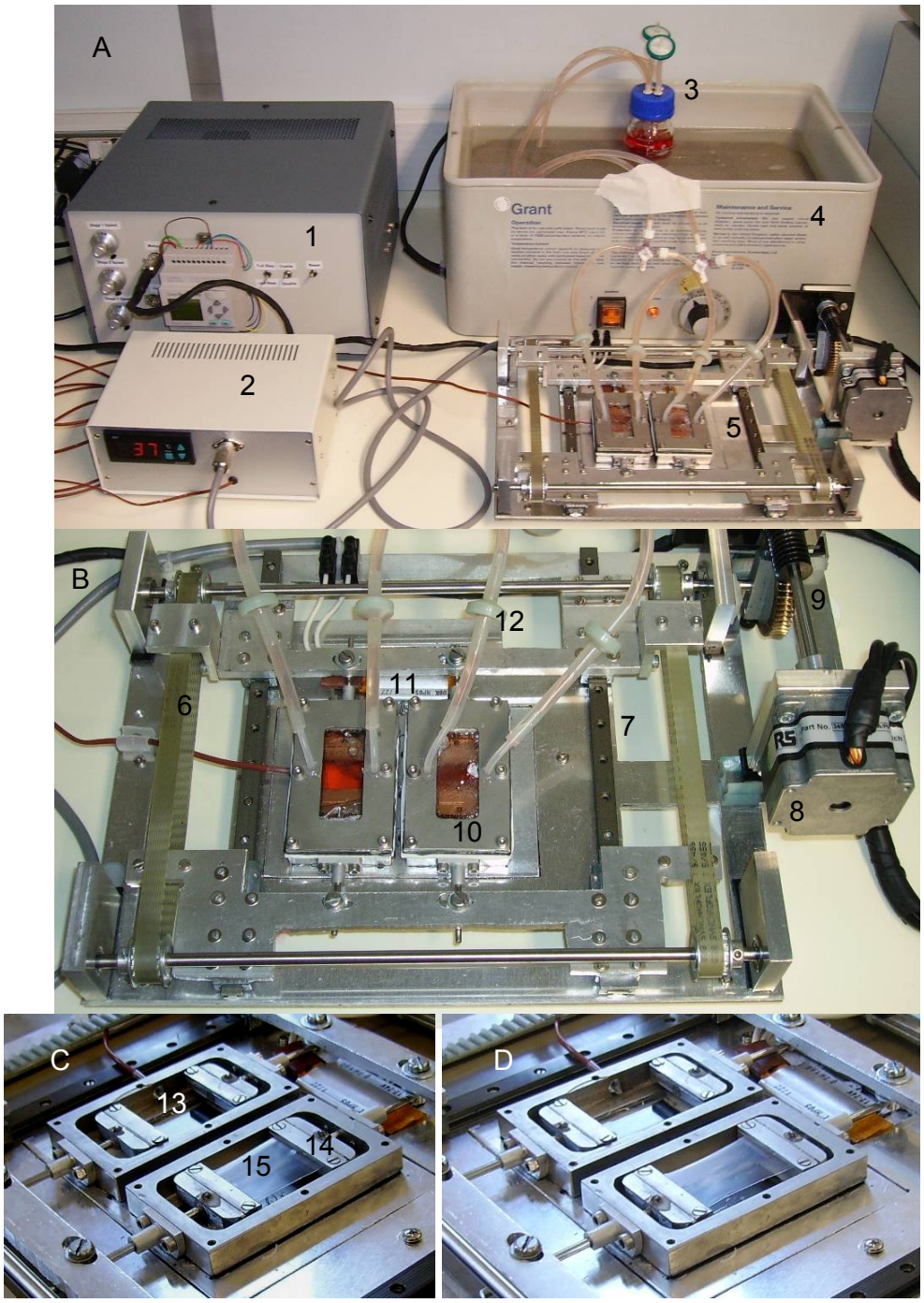

Figure 5.2. Photographs of the mechanical stimulation apparatus, A; the complete system, B; the main stretching part, C; open chambers with membrane not stretched and D; with membranes stretched by 10%. Labels: 1-motor controller, 2-temperature controller, 3-media reservoir, 4-water bath, 5-main stretching part, 6-belt and pulleys, 7-rail, 8-stepper motor, 9-worm and pinion gears, 10-cell sample chambers, 11-heating element, 12-one-way valve, 13-thermocouple, 14-membrane grip, 15-membrane.

5.2.1.5 The Final Design

Using all of the criteria described above, the final system was designed and constructed as shown in figure 5.2. This can be seen to be composed of the main section of the system where the cell samples on the stretched substrates reside, the motor controller and the temperature controller. In addition to this was a temperature controlled water bath for maintaining the temperature of the media reservoir.

The main section of the stretching system was constructed mainly from aluminium so as to be light enough to not overload the microscope stage but strong enough to enable the transmission of the mechanical deformation force to the substrata without causing the system to twist. Nonessential sections of the base were removed to further reduce the mass without compromising the structural integrity.

The system was designed to incorporate two cell sample chambers. This number was selected based on the required size of the cell substrates and on the range of motion of the microscope stage on which the system was to be used while allowing all areas of the cell sample to be imaged. The cell sample chambers were made from surgical grade stainless steel in order to be non-toxic to the cell populations. Their lengths and widths were prescribed by the required size of the deformed substrates, while the thickness of the stainless steel substrate clamps contained inside and on opposite sides of the chambers dictated the thickness of the chamber itself. Both the lid and base of the chambers possessed central windows composed of microscope slides to allow for microscope imaging of the contained samples. The lid attached to the base with a silicone gasket to ensure the chamber remained hermetically sealed while the substrate clamps were connected to the external environment by rods which passed through the chamber walls using a system of O rings, again to allow the chambers to remain sealed. By manipulating the external ends of these rods the substrates could be stretched or allowed to contract.

The method of stretching that was developed was a novel one in terms of cellular substrate deformation systems. It takes advantage of the highly efficient belt and

pulley system which allows for less power wastage and a subsequently smaller and lighter motor to be used. The motion of the belt was also used to the advantage of the requirement for stretching the ends of the cell substrate in equal and opposite directions. When a belt and pulley system rotates in a particular direction the upper and lower halves of the belt move in opposite directions and by attaching either end of the substrate to the opposing halves of the belt the substrate ends move in the same manner. Two belt and pulley systems were used to provide a smooth motion and equal strain to the two membranes without twisting the system. Aluminium bridges were used to join the substrate-attached rods to the belts of the pulley system and were supported by carriages which ran along two parallel rails to keep the motion of the substrate deformation linear. The pulley system was driven by a hybrid stepper motor (Mclennan Servo Supplies Ltd., Surrey, UK) via a worm and pinion gear with a gear ratio of 1:50. This ratio not only allowed the motor to provide the relatively large forces required to stretch the substrates at the rate required but also lead to the motor running at more appropriate speeds than would be the case at a lower gear ratio and consequentially avoided vibrations from the resonance of the motor at these lower speeds.

The inherent ability of the stepper motor to provide discrete alterations in position was used to dispense with a closed loop feedback system to monitor the motor position and therefore the degree of stretch of the substrates and as such no position sensors were required. The drive signal of the motor consisted of a series of pulses, each of which incremented the position of the motor by one step as long as the load on the motor did not exceed its output force. The load on the motor was kept sufficiently low by use of the high gear ratio worm and pinion gears, meaning that steps of the motor were not missed and there was no error between the expected and actual motor position. Another advantage of the worm and pinion gears was that, while the motor could drive the stretch of the substrates, the stretched substrates could only provide a resistance to the turning of the motor but could not actually cause it to rotate. Therefore, if the motor was to temporarily lose power and was free to rotate, the contractile force of the substrates could not cause the motor to turn and lose its positional accuracy for when the power resumed.

A control unit with which to provide the drive signal to the motor was constructed. The main component of the unit was the motor drive card, also from Mclennan Servo Supplies Ltd., which, after a number of modifications, was able to provide the motor with a series of pulses for it to rotate. The frequency of these pulses was proportional to an input DC voltage and, as the frequency of the pulses directly dictates the speed of the motor, the input voltage of the drive card could be used to control the motor speed. In addition, the drive card provided an output signal with every four full steps or eight half steps of the rotation of the motor. It could also be used to reverse the direction of rotation of the motor.

An FL1E programmable relay (IDEC Electronic Ltd, Basingstoke, UK) was used to control the motor through the drive card. It consisted of four separate relays which could provide four signals. One was used to switch on the signal to change the motor direction, while the remaining three were used to provide three distinct but constant voltages to control the motor speed. These three voltages were manually selectable with independent potential dividers constructed using a variable resistor in each. This arrangement allowed the motor to be driven in both directions at up to three different speeds, providing a motion closely reminiscent of a sine wave or merely a saw-tooth wave, as shown in figure 5.3. As the pulse pressure and strain wave is closely represented by the latter, this is the type that was chosen to be used, with a fast stretching phase and a relatively slow relaxation. The programmable relay was also able to use the position output of the motor control card to control the motion of the motor by reversing the direction once the required stretch had been obtained.

A temperature of 37ºC was obtained inside the sample chambers by use of a 70W heating element (DBK Technitherm Ltd, Llantrisant, UK). A central section of the base plate of the main system was made to be removable and placeable into an insulated recess in the base plate. The two sample chambers were attached to the removable section of the base with thermal coupling compound (Fischer Elektronik, Germany) at the interface, leaving an area of this section for the attachment of the heating element, which was also connected with the same compound. The heat

generated by the element could conduct to the base and walls of the sample chambers and heat the enclosed media. Heat was also prevented from transmitting to the rest of the base plate by the presence of the insulator at the interface between the two. In addition, the heating of the media reservoir in the separate water bath prevented the inflowing media from cooling the system or from creating temperature gradients across the sample chamber. The temperature of the sample chambers was measured by a j-type thermocouple encased in a PTFE coating which was introduced into the middle of the side of one of the sample chambers and protruded a short distance into the chamber such that the temperature measured was that of the media and not of the chamber wall. The temperature was monitored by a temperature controller (RS Components Ltd, Corby, UK) which controlled the heating element based on the signal from the thermocouple and the set temperature.

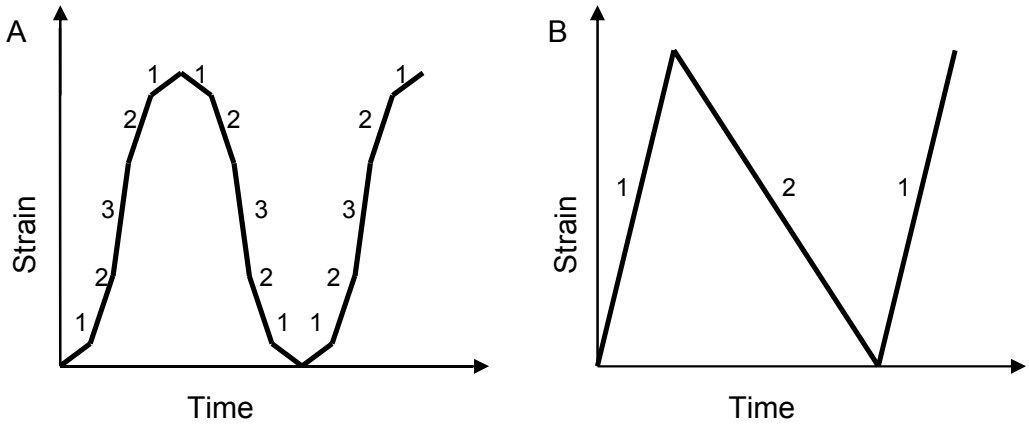

Figure 5.3. Possible strain waves producible by the stretching apparatus with three distinct rates of stretch, numbered 1-3. A; replica of a sine wave. B; saw-tooth wave closely replicating the stretch regime found in vivo.

Fresh medium was pumped through the sample chambers from the reservoir via silicone tubing attached through the lids of both in order to keep the cell samples supplied with nutrients and oxygen and to remove waste products. The buffering of the media could not be accomplished purely from the constituent bicarbonate because the system was not able to fit inside a CO_2 incubator and no other CO_2 source was available. As such it was provided by the addition of HEPES at a

concentration of 25mM. The media flow was attained either by using a peristaltic pump or by harnessing the motion of the stretching motion. The latter option was possible because the chambers each acted like a set of bellows with the rods attached to the samples being continuously moved into and out of the chamber. By introducing the rods further into the chamber the pressure inside the system would increase slightly and decrease again when they were retracted. One-way valves were attached to the silicone tubing, on both the inlet and outlet of both chambers, oriented in the same flow direction, which allowed media to flow out of the chambers when the pressure rose and into it when the pressure decreased. The medium in the reservoir was replaced every three days.

5.2.2 Testing and Calibration of Mechanical Stimulation Apparatus

Firstly, the temperature of the media inside the cell chambers was tested using a separate temperature probe which was placed inside either chamber at various points and the lids closed over the probe's wire. Water was pumped through the chambers using a peristaltic pump (Ismatec, IDEX Health & Science SA, Glattbrugg, Switzerland) at various flow rates from a water reservoir, representing the media reservoir. The temperature was recorded in each position along with the time taken to reach the desired 37ºC from room temperature, with various water flow rates as well as with and without separate heating of the water reservoir.

Next, the viability of cell samples maintained inside the stretching unit was determined using a measurement of their proliferation rate. In order to remove the effects on proliferation due to media flow and substrate stretch cell samples at approximately $5x10^3$ cm^{-2}, approximately 10% confluence, on cast Z1A1 polyurethane substrata were incubated at the base of the chambers of the stretching unit. This arrangement kept the maximum distance between the media inlet to the chamber and the cell sample. It also allowed the substrate grips to move without disturbing the substrate which allowed testing of whether the motion of the grips, or rather the motion of their connecting rods through the chamber walls, affected the

viability of the cells due to the introduction of incompatible materials or through compromising the sterility of the system. The flow of the HEPES-containing media was created by the Ismatec peristaltic pump set at various rates of 1, 2 and 4ml/min. Positive controls for cell viability were composed of equivalent cell samples placed in 60mm diameter tissue culture petri dishes with media without HEPES, while negative controls consisted of similar samples but with the addition of two 20mm lengths of copper wire. Cell samples were removed after three days in culture, fixed and mounted in a DAPI-containing mountant (Invitrogen, Paisley, UK). Cell densities were measured, as before, with fluorescence photomicrographs obtained with an Axio Imager Z1 microscope (Carl Zeiss Ltd, Welwyn Garden City, UK).

Observations of the relationship between the motion of the motor and that of the substrate grips were conducted in order to determine whether there were any discrepancies and to calibrate the stretching of the substrata. The main section of the stretching unit was placed upon the stage of the Axio Imager Z1 microscope for which the unit was designed. The positional accuracy of the microscope objective was used to determine the location of the substrate grips before and after moving the motor by a predetermined amount. The calibration of the motion of the substrate clamps could then be used to create the desired stretch regime of the substrates.

The effect of this stretch on a substrate was subsequently investigated. Sections of solvent-cast Z1A1 PU approximately 34mm x 55mm were placed into both sets of grips in the stretching unit such that a length of 45mm was exposed. This exposed length of membrane was selected as it was the maximum possible length that would fit inside the chambers and allow the desired strain of 10% and it was postulated that the larger the membrane area, the greater the area available for analysis would be. A matrix of marks was applied to the PU sheets and imaged using the upright microscope prior to and after it being stretched by 10%. The change in the relative position of these marks was used to determine the magnitude and direction of the strain on the membrane at all points across its surface.

Lastly, while running the stretching apparatus at 1.17Hz with a strain of 10%, the bellow effect of the chambers was investigated and the subsequent flow rate was measured. This was a simple matter of allowing the chamber to pump water through into a collection vessel where its volume could be measured after various durations of pumping. Although flow rate could not be increased without external support or by changing the stretching regime, the flow rate could be decreased by applying resistance to the media flow through the tubing. This was performed by attaching a simple screw valve to the outlet of the media reservoir which constricted the flow of media to both chambers simultaneously.

5.2.3 Contractile Protein Measurement: Immunocytochemical Analysis

Solvent cast, aligned and unaligned electrospun Z1A1 PU membranes, 25mm x 45mm in size, were created and sterilised as described in the previous chapters. Using sterilised tools these substrata were placed inside the grips in the sample chambers of the mechanical stimulation unit. Aligned electrospun substrates were placed into the unit with the orientation of fibre alignment both parallel and perpendicular to the stretch direction. Identical membranes were placed into 60mm diameter petri dishes as a control. Human aortic smooth muscle cells from passage 2 or 3 were allowed to attach to these substrata at a density of approximately 10^4 cm^{-2} for 1 hour after which the sample chambers and petri dishes were filled with the required amount of media, DMEM with 25mM HEPES in the chambers and DMEM without HEPES in the dishes. The dishes were placed into an incubator maintained at 37ºC with 5% CO_2 while the chambers were assembled on the stretching apparatus, perfused with media from the reservoir and the chambers heated. The non-return valves were utilised, as described previously, to provide recirculation of media between the reservoir and chambers. A stretching regime, as developed from analysis of the motor-grip motion relationship, with a frequency of 1.17Hz, as shown in figure 5.6, was applied to the samples in the mechanical stimulation unit

continuously for four days while the control samples were maintained in the incubator for the same time.

At the end of the stretching and incubation period cell samples were removed from the chambers and dishes, placed into fresh 60mm petri dishes, washed twice with PBS and fixed in paraformaldehyde. They were subsequently permeabilised and stained for either alpha smooth muscle actin or calponin before DAPI staining as described in the previous chapter. Fluorescence micrographs of the cell samples were obtained with an Axio Imager Z1 microscope and analysed for protein content using ImageJ.

5.3 Results

5.3.1 Mechanical Stimulation System Testing

The ability of the system to maintain the required thermal environment within the chambers was tested using water and the temperature found to be accurate and uniform to within 0.1ºC. With a perfusion rate of 10ml/min, far in excess of that required, the system was still able to maintain this degree of accuracy. The desired temperature was obtained swiftly after commencement of heating, taking approximately 1 minute starting from room temperature.

Any toxic effects of the constituent components of the system on the cell samples was analysed using measurements of proliferation rates. In addition three media perfusion rates were tested for their effects on cell viability. As seen in figure 5.4 the positive control for cell viability provided proliferation rates similar to those found in samples maintained in the mechanical stimulation system with media flow rates of 2ml/min and 4ml/min. However significantly lower proliferation rates were found in samples in the system perfused at 1ml/min, while substantial apoptosis was present in the negative control. The most appropriate perfusion rate for use in subsequent

experiments was therefore 2ml/min as this was the lowest found to provide sufficient nutrients and as such less likely to cause effects due to fluid shear stresses.

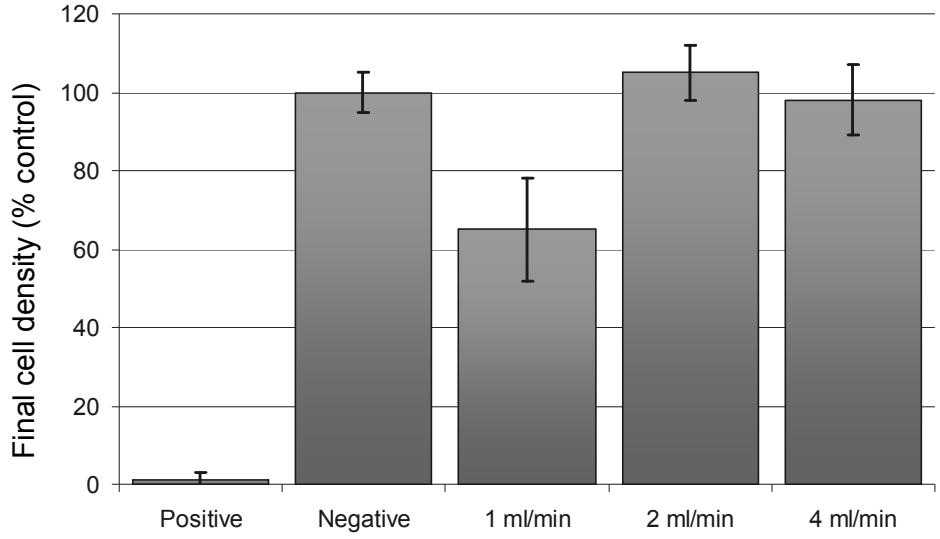

Figure 5.4. Mean viability ±SD of cells in the chamber at various media perfusion rates relative to controls (in TCP with (positive) and without (negative) copper wire). Media flow rates below 2ml/min were found to limit cell viability. All viabilities were measured to be significantly different to the positive control ($p<0.05$) as determined using ANOVA.. n=20

The relationship between the motion of the motor and that of the substrate grips was determined using the position sensor of the microscope and is displayed in figure 5.5. As described in the graph, there is a certain degree of hysteresis in the motion of the grips and through observation of the system during the stretching regime the cause of this lag in their motion was due to the buckling of the base plate and resistance to motion of some of the components rather than stretching of the belts. The motion of the upper and lower grips in their respective directions was not quite equal, perhaps due to incorrect tensioning of the belts or because of a greater resistance to motion of one set of grips. However, the combined motion of the two sets of grips provided the desired stretch in the membrane, with the only effect being a slight motion of the centre of the substrata when stretched.

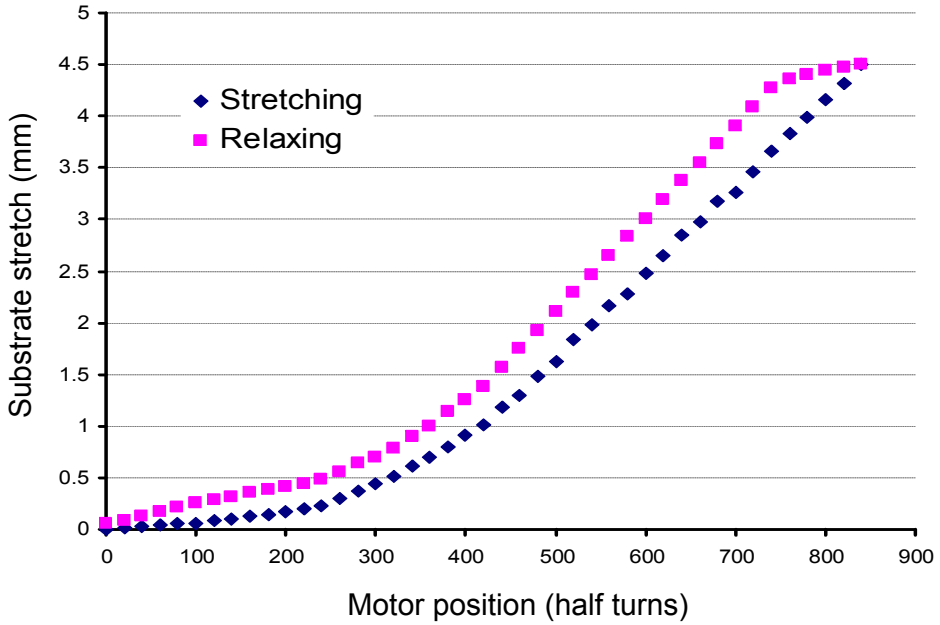

Figure 5.5. Relationship between motor position and substrate stretch in both the stretching and relaxing motions. The delay in the stretch of the substrate after the motor's motion is due to the force required to initiate the motion of various parts of the machinery and due to bending of the base plate.

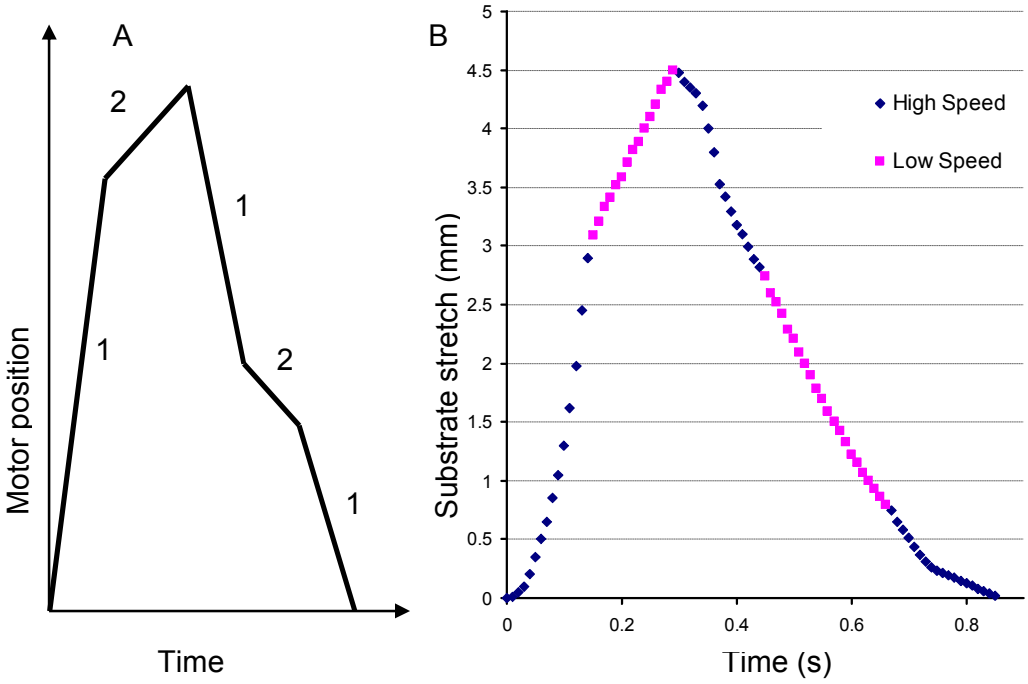

Figure 5.6. A; The modified motor motion required to create the stretch wave seen in B. This replicates the stretch regime seen in vivo *and shown in figure 5.1 more closely that the simple saw-tooth wave.*

Subsequent to determining the relationship between the motor and substrate grips' motions was the investigation of the degree of accuracy with which the grips could be moved. This could be defined as the motion of a grip caused by the smallest incremental motion of the motor, a half step or 1/400 of a rotation, or by the smallest amount of motion of the motor that is detectable by the control unit from the output of the motor drive card, which is equal to eight half steps. Through measurement of the geometry of the system, the theoretical resolution with which the grips can be moved is 3.5μm, while the resolution with which this can be measured through feedback from the drive card is 28μm. The actual resolution, as measured using the microscope when the membrane was approaching 10% strain was 2.8μm and that determinable using the motor feedback was 22.4μm.

As the desired saw-tooth strain waveform shown in figure 5.3 was not achievable from a similar motion of the motor, the latter had to be modified to produce that required in the former. This is illustrated in figure 5.6 where the stretching phase had to be subdivided into two subphases, the first being at a higher rate in order to provide the necessary deformation of the system quickly so that the membranes could be stretched. Similarly, the relaxation phase had to be divided into three sections running at two different motor speeds.

The stress profile of the substrates during stretch was determined through the analysis of the relative motion of their surfaces. The area in the centre of the membrane that experienced a strain of between 8 and 12% and whose principal direction of strain did not deviate from the direction of length of the membrane by more than 10º was found to be approximately 10mm wide and 12mm long. This was therefore the area that was used for cell analysis in future measurements.

With the system set up and running the stretch profile described above, the ability of the motion to promote a flow of media using the non-return valves was tested. Under normal conditions, without the use of the flow-limiting valves, the flow rate was found to be 5.4ml/min per chamber and there was no statistically significant difference between the flow rates from the two chambers. By gradually closing the

valve, restricting the flow from the media reservoir, the flow rate per chamber was reduced to 2ml/min and this arrangement was used in the experiments for determining contractile protein contents of stretched cell samples.

5.3.2 Measurement of Contractile Proteins

Figure 5.7 shows the effect of uniaxial cyclic stretch of cell substrata on the attached cells' contractile protein content. In nearly all samples the effect of this mechanical stimulation was a statistically significant increase in the cell content of both alpha smooth muscle actin and of calponin. The largest increase in αSMA and calponin content due to stretching was seen in cells attached to aligned electrospun PU when the direction of stretching was parallel to the alignment of the fibres. Cells on cast and unaligned electrospun materials displayed a similar increase in contractile protein content when stretched, but with those on cast membranes experiencing a greater proportional increase due to their low content of the proteins when in static culture. The only samples that did not experience this increase were on electrospun polyurethane with aligned fibres when stretched in the direction perpendicular to that of the alignment of the fibres. In these samples there was no significant difference in the content of either protein between the stretched and static samples.

Although images of hASMCs were obtained in order to evaluate the cellular content of αSMA and calponin, these were not adequate for providing a detailed morphological analysis of the cells in the different environments, as it has been the case in the previous work where cellular processes were not visible after staining for these two proteins. However, the cellular shape did seem to follow the same pattern as in the previous chapter; that is cells that produced more of these two contraction-related proteins appeared to develop a more spindle-shaped morphology. As the number of cell samples obtained from the stretching apparatus is limited, future work is required to gain a more complete understanding of the variations in cellular morphology in the dynamic environment utilised in this work.

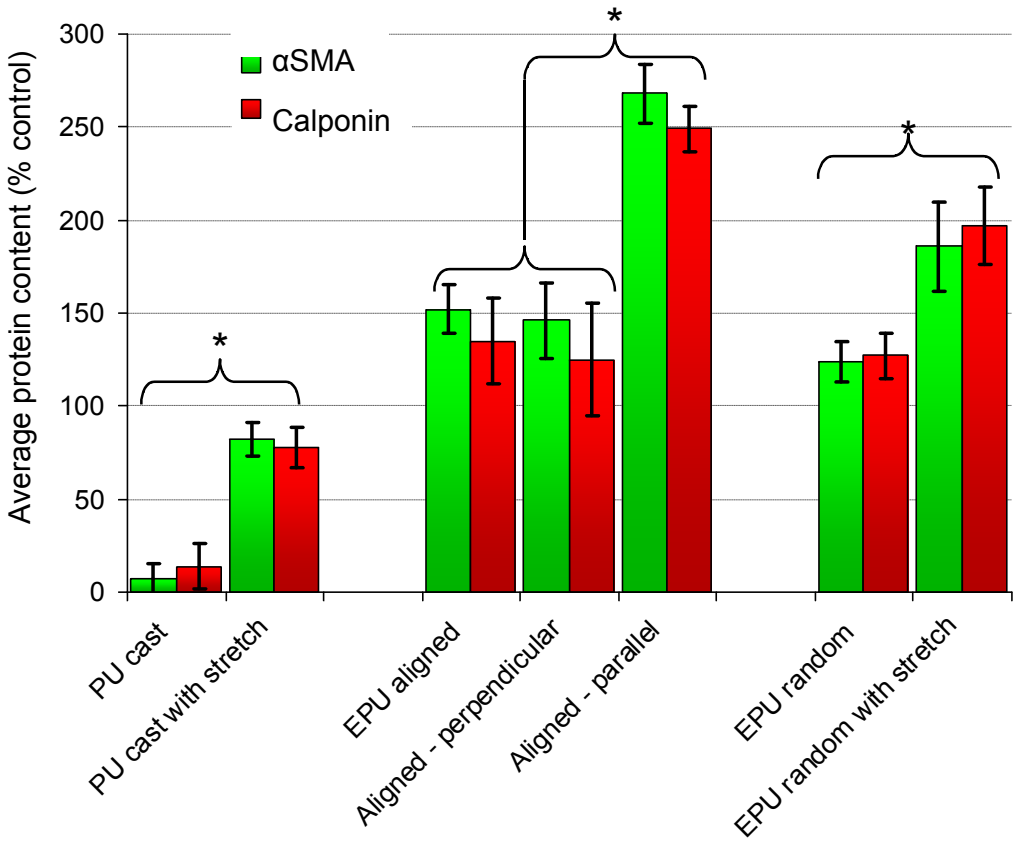

Figure 5.7. Graph showing the effect of cyclic stretch on cellular content of contractile proteins relative to cells on TCP in the absence of serum. Cellular contents of the two proteins were normalised for cell number by counting the number of cells per image using ImageJ. Significant increases in αSMA and calponin content due to stretch were seen in cells on cast PU, aligned electrospun PU when the direction of stretch was parallel to that of the fibre alignment and on unaligned electrospun PU, ($p<0.05$) as determined using the Student's t-test. However, no change was detected when cells on aligned electrospun PU were stretched perpendicular to their fibre direction. n=160.

5.4 Discussion

A mechanical stimulation unit was designed and built to investigate the effect of uniaxial stretch of a substrate on the resident cells. It was designed to provide an equal and opposite stretch to either end of a membrane using a novel belt and pulley system driven by a stepper motor. The integral cell sample chambers were designed to be able to maintain the optimum conditions for cell viability for extended periods of time.

The system was designed to be compatible with an Axio Imager Z1 upright microscope through a number of features. Firstly the system, excluding the motion and temperature control units and the media reservoir, was made to be light enough to not overload the microscope stage motors, that is, less than 3kg. The final load on the stage, when taking into account the force from the trailing leads and tubing, was equivalent to approximately the weight of a 2.9kg mass. This low mass was achieved through the use of low density structural materials and the design of the base plate. However, the resultant strength of the framework was not sufficient to prevent the base plate buckling when a force was applied to the membranes. This caused a problem when imaging the membrane during stretch using the microscope because, as the base plate was attached to the microscope at one edge, the bending would cause the central area of the stretching system to move up and out of the focal plane of the microscope. The main cause of the torsion was from the stiffness of the moving parts of the system rather than the force required to stretch the membranes. This could, in future, be overcome by more precise assembly of the mechanical components such that the stretching force required is less. If this is not sufficient it could also be overcome by using a stronger albeit heavier base plate which could be partially supported by stretchable cables from a stand-alone frame so that the force on the microscope stage does not exceed the safe limit.

The system was also compatible with the microscope due to the optically clear windows at the upper and lower face of the cell sample chambers and the translucent, almost transparent PU samples used. In addition, the positioning of the cell samples

near the top of the chambers allowed the use of higher magnification objectives than would otherwise be possible as the working distance of an objective typically varies inversely with its magnification. The objective with the maximum magnification that was available and had a working distance large enough that it could be used to obtain an image of the cell sample inside the chambers was a x10 objective with a 5.2mm working distance. This allowed the clear visualisation of the cell shape and location with a reasonable accuracy in imaging of larger subcellular structures such as the nucleus and even provided detail on the cytoskeletal arrangement, however clear images of smaller organelles were not obtainable with this objective. The next highest objective in terms of magnification was the x20 objective with a working distance of 2.0mm. This was not compatible with the system as the distance between the cells and the objective was too large. This distance is defined by the thickness of the glass and of the top section of the membrane grip, the former was approximately 1mm and the latter even greater than this. Both of these distances would need to be reduced to permit the use of the x20 objective, however a reduction in the thickness of the glass could lead to it deflecting during the stretching regime, causing a disturbance in the path of light used by the microscope and leading to distorted imaged, while a reduction in the thickness of the grips may lead to a loss of the retention of the membrane during stretching.

The analysis of the cytotoxic effect of the chamber on the cells has shown that the materials used to construct the chambers are non-toxic to the cells. In addition, no leakage of the chambers was detected and no contamination with bacteria or fungus was found, proving that the chamber lid seal and the tubing connectors were watertight. More importantly, this showed that the O ring system through which the membrane grip rods passed did not allow the passage of media or foreign bodies. Also, these studies have provided an approximate minimum media flow rate that provides sufficient nutrients to the cell samples. The chambers were of a size that allowed sufficiently large samples to be investigated while allowing both of them to be observable under a microscope with a limited stage range of motion. The positioning of the tubing connectors in the upper surface of the chamber lids allowed the expulsion of air bubbles more promptly than other positioning would. These

bubbles have a tendency to develop over time and can cause a disruption to the path of light travelling through the chambers and therefore the image acquired by the microscope.

By heating a detachable section of the base plate to which the chambers were attached and through the conduction of the heat to the media in the chambers, the cell samples' temperatures could be controlled. The thermocouple used to regulate the temperature was tested with a separate temperature probe and found to be accurate. The system was also found to produce a uniform and consistent temperature across the whole of both chambers even when relatively high media flow rates were used. This temperature consistency is crucial for ensuring that the whole cell sample in both chambers maintains the correct metabolic rate and that this does not interfere with the results obtained. One slight drawback to the system is that, when heating up from room temperature when using low media flow rates, the medium temperature was found to increase beyond the set value of 37ºC, by up to 2ºC for up to a minute before settling back down. This could be due to the relatively large distance between the heating element and the thermocouple or the relatively large thermal mass of the chambers, however, the latter could also be the cause of the stable temperature during use.

The system was found to be able to reliably replicate the typical strain regime found *in vivo* through use of a series of constant stretch rates. It was able to exceed all criteria specified for it, such as range of motion, speed of motion, force applied and positional accuracy. The generation of three distinct motor speeds was a limit of the control system but did not actually affect the output to a great extent, and in principal a much more complex stretch waveform could have been produced if required. As previously stated another limitation of the system was the resistance to motion of various components, most notably the carriages and rail system, and this lead to torsion of the system which not only affected the ability to use the microscope to monitor the cell samples during stretch but also lead to a modified motor motion regime being used to produce the desired stretch waveform. However, this last point

lead to the advantage that the strain regime produced replicated that found *in vivo* to a much greater extent than the simple saw-tooth wave would have done.

The bellow effect of the chambers and non-return valves was used together with a constriction valve to produce the minimum media flow rate that did not impact on cell viability while producing the minimum effect of fluid shear stress on the cell sample. The motion of the substrate grips was also postulated to aid in the mixing of the media so that stagnant volumes were not created that would lead to cell starvation or hypoxia. Oxygenation of the media reservoir was not a problem and the constant circulation of the media, perhaps alongside the relatively high gas permeability of the silicone tubing was sufficient to provide the correct oxygenation.

Cell samples on a variety of substrata were exposed to cyclic uniaxial stretch using the mechanical stimulation system. All samples when stretched experienced an increase in average cell content of the contraction proteins αSMA and calponin with the exception of the aligned electrospun samples when stretched in the direction transverse to the direction of alignment of the fibres. This increase in contraction-related proteins is an indicator of a move to a more contractile phenotype of the cells when stretched.

As described in the introduction to this chapter and in the work by Li (2002), the way that a cell can sense mechanical perturbations in its substratum is through the surface focal adhesions. These accumulations of structural and signalling proteins initiate a signalling pathway that can lead to many different cellular responses, one such response being the production of contractile markers.

Through observations of the change in contraction-related proteins through stretching of the non-aligned substrata, cast PU and randomly-oriented electrospun PU, it can be seen that the increase in both samples is similar. This is not surprising when considering the interaction between the focal adhesions and the surface. The specific areas on either surface that the cell attaches to will most probably move in a similar manner and as such so will the focal adhesions. One consideration is that the

arrangement of focal adhesions in the cells on a cast and unaligned electrospun material will be in considerably different locations before the commencement of stretching as the cells in one sample will have a flattened and spread morphology while the other will be spindle-shaped, as described in the previous chapter. It is assumed, however that the cells on the cast PU will assume a more spindle shaped morphology as they differentiate. More work is required to investigate the interaction between the VSMCs and the substrata during stretch, such as in the work by Barbee et al. (1994), which would include an observation of the change in geometry of the fibres in the electrospun samples when deformed as well as studying how the morphology and focal adhesion location of both samples changes during stretching.

The similar increase in contractile protein content in the cells on non-aligned samples is more interesting when considering that the cells on the electrospun materials start by having a higher content of these proteins. This could imply that the mechanism for the increase due to topographical cues and due to mechanical stimulation is relatively independent or at least that if the two stimuli act through the same signalling pathway the limit to its effect on the protein production has not been reached.

In the case of stretching cells on aligned electrospun materials a different situation is observed. There is a large difference in the effect of the stretch on the contraction-related proteins in the two sample types with stretch applied either parallel or perpendicular to the direction of fibre alignment. No significant increase in the average cell content of either αSMA or calponin was seen when substrates were stretched perpendicular to the fibre direction over static samples. However, when samples were stretched parallel to the fibre direction the resident cells experienced a substantial increase in these proteins over the equivalent static samples. The increase in these latter samples was approximately twice the increase seen from the stretching of non-aligned substrates. For this reason it would appear that there is a degree of synergy occurring between the effects of fibre alignment and mechanical deformation when the two are aligned.

It is possible that the effect on the protein content is due to the difference in fibre deformation when stretched in the two orthogonal directions. Although it was not studied with the use of a scanning electron microscope it is conceivable that a stretch of the fibres along their direction of alignment would result in the straightening of the fibres and loss of their undulant shape while a stretch across the fibre lengths would result in them curving sideways while being restrained by the points where the individual fibres are attached to their neighbours. In order to accommodate the stretch of the bulk material the individual fibres must be able to stretch, on average, by an equal amount in both of these two ways. The attachment of the cells to the electrospun fibres has also not been extensively investigated but through the use of light micrographs of VSMCs attached to these surfaces and comparison of the relative sizes of both cells and fibres it is likely that a cell would attach to numerous adjacent fibres rather than a single fibre. As such it is probable that a cell without any specific alignment itself would experience a very similar stretch in the two orthogonal directions regardless of fibre orientation.

However, another distinction between the two directions parallel and perpendicular to the fibre direction, other than the orientation of the fibres, is the orientation of the attached cells, which typically align along the fibres. As such, when the deformation is applied to the substrate in the two orthogonal directions it is also applied to the cells either across or along their lengths. For this to be the case for the duration of the experiment the cells would need to maintain their alignment with respect to the electrospun fibres and not realign due to the stimulus from the stretch. The work by Houtchens et al. (2008) shows that, while mechanical strain can align VSMCs perpendicular to the direction of stretch, it is unable to change the alignment of cells caused by surface microgrooves of a range of sizes, while the study by Loesberg et al. (2005) indicates that the same is true for fibroblasts. For this reason it is probable that cells aligned along the fibre direction in the current work will remain so for the duration of the experiment regardless of the direction of the applied mechanical stimulation. In this case it appears that the most likely cause for the difference in contractile protein expression in cells on aligned fibres stretched in either direction is

the effect of stretching the cells along or across their length. As shown in the previous chapter, in particular figure 4.3, the actin filaments in aligned cells are also aligned in the same direction. It seems that via the application of force through the focal adhesions of the cell and along the actin filaments, the phenotype of the cell is regulated. This regulation could also be via activation of a signalling pathway possibly involving the Rho family of GTPases (Numaguchi et al, 1999 and Li and Xu, 2007), or mitogen-activated protein kinases (MAPK) as shown by Hall (2005), Tock et al., (2003) and Worth et al. (2004).

It also appears that stretching of an aligned cell across its width does not elicit the same response as when stretched along the length and as such the same signalling pathways are not activated. In this case it seems that this type of stretch does not apply a tension along the actin filaments and the focal adhesions are more free to move in this direction as the filaments would need to rotate as opposed to extend in order to accommodate the motion. This would lead to a lesser force experienced by both the focal adhesions and actin fibres and as such a lower response to the strain is obtained. The intermediate case is that described previously, where the cells on non-aligned substrates have a random orientation, or no orientation at all and this results in an intermediate increase in contraction-related proteins as the actin filaments would also be at random angles to the direction of stretch, receive varying degrees of tension and eliciting a range of levels of stimulation of the signalling pathways that lead to cell differentiation. However, there have been many reports, including those by Chen et al. (2003) and Standley et al. (2002), into the alignment of VSMCs in a direction perpendicular to that of mechanical stretch when no other directional stimuli are present, and this would have an impact upon this proposed mechanism. There is a wealth of additional work that is required to verify this hypothesis and the interaction of the cell with the electrospun fibres during stretch needs to be studied in much greater detail, starting with an observation of the alignment of cells under these conditions in addition to viewing the stretch of the cells themselves in real-time.

This study also provides additional proof that electrospun Z1A1 polyurethane could provide a useful material for use in vascular graft applications or perhaps in tissue

engineering of vascular materials. This is due to the determination that, in addition to the electrospun fibrous PU producing a contractile phenotype through its use as a substrate, when the mechanical forces present *in vivo* are added to the *in vitro* model the contractile phenotype is developed further still. This is especially the case when aligned electrospun materials are utilised and oriented in a circumferential direction, much like in the native vessel, such that the hemodynamic forces would work synergistically with the effects of the fibrous substrate. The mechanical loading of the substrates also shows that this technique could be utilised to develop these tissue engineered scaffolds as introduced by others such as Zhang et al. (2009).

5.5 Conclusion

The phenotypic response of human aortic smooth muscle cells to cyclic uniaxial strain of their substrata was studied using a custom made mechanical stimulation system. A variety of substrates were used, including cast and electrospun polyurethane. A differential effect of the substrate stretch on the attached cells was observed with substrate type and strain direction. The effect on contractile protein content of cells on aligned substrates was negligible when the strain direction was perpendicular to the fibre alignment of the substrate, while when the two were parallel the effect was maximal. An intermediate effect in the cells was observed when the substrate was composed of either cast PU or unaligned electrospun polyurethane. It is postulated that the differential effect of stretch was, in part, due to the orientation of the cell with regard to the strain direction.

This work is the first in which the effects of substrate geometry and applied mechanical deformation on the phenotypic state of a VSMC population were studied in parallel. These results are an important part in better understanding the development of intimal hyperplasia and how it can be treated.

CHAPTER 6

CONCLUSIONS

6.1 General Conclusions

There are a number of limiting factors in utilising autologous material in vascular bypass graft applications. These include the difficulty, time, risk and damage/morbidity caused by the removal of the vessel used for the bypass, the fact that these can often already be diseased or unavailable for other reasons and also because they do not always have ideal patency rates. For this reason it is important that a suitable synthetic vascular graft material is developed as those currently used have even poorer patency rates than the patient's own tissue in many applications.

The reason for the failure of currently used graft materials is due to thrombus formation and anastomotic intimal hyperplasia which are caused, respectively, by improper haemocompatibility and lack of material compliance. By selecting a polymer that has a more appropriate thromboresistance and which can limit the growth of VSMCs on its anastomotic regions a more respectable patency rate may be obtained. Polyurethane was selected as a starting material to work towards this goal as it has an excellent resistance to thrombosis and a wide range of available material stiffnesses. In order to be able to progress with this polymer towards a viable graft material, the following questions were raised and answered.

How does the stiffness of the polyurethane graft material affect the patency of the graft?

As stated previously, the failure of an ePFTE or PET vascular graft can, in part, be attributed to its lack of mechanical compliance. For this reason the polymer polyurethane was investigated as a potential vascular graft material as it possesses a much lower elastic modulus than the other two. However, the migration rates of cells over a surface have been shown to be influenced by the stiffness of the surface. In addition, the migration rate is also known to be dictated by the density of adsorbed molecules on the surface, particularly those involved in cell attachment and this in turn can vary from polymer to polymer and even between two different grades of the same polymer. The migration of VSMCs onto the luminal surface of the graft is an

important early event in the development of intimal hyperplasia in the graft anastomoses and the subsequent failure of the graft. As such this rate, and its dependence on both the graft material stiffness and the amount of fibronectin, a protein very relevant to this situation, adsorbed on its surface was investigated.

It was found that at certain combinations of substrate stiffness and adsorbed fibronectin densities the migration rate of the attached hASMCs was at a maximum. The values for these two substrate properties where this occurred were reciprocally related. In other words the maximum migration rate occurred at lower Fn densities on stiffer materials and at higher densities on more compliant ones. These maxima were subsequently determined to occur at the same cell-substratum attachment strengths, adding weight to the tensegrity hypothesis, predicting an optimum attachment strength for cellular migration.

The importance of these results lies in the insight that they give into the implications of material properties on the migration rate of the attached cells. By controlling this process it may be possible to influence the progression of anastomotic intimal hyperplasia. The migration of the surrounding VSMCs onto the graft may be limited and as such perhaps this will have an influence on the development of the tissue growth and subsequent stenosis. Conversely, if the same control can be gained over the endothelial cells in the adjacent vessel migrating onto the graft, the endothelialisation of the implanted graft could be achieved to a higher level than is currently seen.

What is the effect of the polymer processing method on the formation of the tissue growth?

Since the earliest attempts at constructing synthetic vascular grafts it has been clear that certain processing techniques for the polymeric materials lead to more viable grafts than others. Following on from this a material processing technique for constructing polyurethane vascular grafts was sought. Electrospinning was the method chosen for investigation due to its ability to produce polymers with a fibrous

geometry, that most closely resemble the native vessel. It has been shown previously that this fibrous structure can have an influence on the behaviour of the attached cells.

An electrospinning rig was constructed that was capable of creating fibrous polyurethane materials with fibre geometries on the scale of those found in the native vessel. It was also found that both randomly orientated and aligned fibres could be produced. The response of VSMCs to these materials when used as their substrates was investigated by measurements of the morphology of the cell, contractile protein content, proliferation and migration rates. All of these measurements illustrated that the cells on these fibrous materials developed a phenotype consistent with those in a healthy vessel and as such were less likely to contribute to the development of intimal hyperplasia. If these materials were to be used in a vascular graft application, perhaps the response of the resident cells after migration onto the graft surface would be more quiescent than hyperplastic. This is especially true for aligned electrospun PU for which the effect on phenotype of the resident cells was the greatest.

These results show the importance of cell-substrate interactions in terms of the geometry of the material. They also provide some further understanding into the development of intimal hyperplasia in the first instance, as the interaction of the medial VSMCs with their surrounding ECM may promote their contractile phenotype and a disruption of this interaction may lead to dedifferentiation to a more synthetic one and subsequent wall thickening.

Does the compliant nature of the polymer affect the behaviour of the tissue that resides upon it?

The compliant nature of the blood vessel, the lack of such in the commonly used prosthetic vascular grafts and the subsequent mismatch have been highlighted numerous times in this work to be a causative influence on the failure of such grafts. This was the main reason that polyurethane was selected as the material for investigation. However, although this is expected to have a positive effect on the

hemodynamics of the blood flow in the region of the anastomosis it would also have an effect on the cells in this area. As such it is important that the behaviour of the cells attached to a compliant vascular graft material are tested in a dynamic system, one which replicates the cyclic distension caused by the varying pulse pressure.

A mechanical stimulation system was designed and constructed which was capable of incubating a cell sample attached to a deformable substrate while providing a wide range of stretch waveforms to the substrate. This was used to replicate the mechanical environment *in vivo* using the previously tested cast and electrospun polyurethane. It was found that for cast and randomly aligned electrospun PU samples cyclic stretching was to lead to a more differentiated cell type, as measured by contractile protein content. However, on aligned electrospun PU the effect was not significant when the stretch direction was perpendicular to the fibre, and subsequently the cell alignment direction. While when the two were parallel the effect on the contractile state was the greatest recorded.

Not only do these results add weight to the evidence that these electrospun materials would provide useful vascular graft materials they also provide a valuable insight into how VSMCs respond to mechanical stimuli. The former is true because the effect of the fibrous electrospun materials on the phenotypic state of the cells was beneficial in static culture but is even more so in this dynamic system, one more representative of the situation *in vivo*. This is particularly in the case of circumferentially aligned materials where the circumferential strain imposed from the distension of the vessel will align with the fibre orientation. The latter is the case as the difference in the response to the mechanical stimulus of the cells on the different substrata shed some light onto its effect on the cells in the different situations.

6.2 Future Work

The optimum final goal of this work would be to develop a vascular graft material that could be tested *in vivo* and then subsequently be used as an actual bypass graft. However, before this can occur many more tests would be required. For instance, the fibronectin solutions utilised in the investigation of Fn densities on the migration rate of VSMCs are distinctly different from whole blood with its multitude of dissolved proteins and due to the complex clotting cascades that occur. Investigations of migration rates of VSMCs on the various polymers exposed to blood may give insight into how these materials respond *in vivo*. In addition, the response of the electrospun materials to their contact with blood may provide insight into the effect of their geometric properties on the normally promising thromboresistive nature of polyurethane. This would also provide a basis to investigate the response of VSMCs to the electrospun materials once coated in a layer of blood borne proteins. However, a precursor to this further work could be the application of Fn solutions to the surfaces of the electrospun polyurethane to investigate how this affects the response of the cell when attached to the material. In addition, to further this, the polymer used in the electrospinning process could be varied, as discussed in section 4.5. This variation in both polymer stiffness and adsorbed Fn density, but in the context of an electrospun material, would bring the work conducted in chapters 3 and 4 together even closer and provide a fuller picture of how the choice of polymer and its processing technique can affect the nature of the cells that are attached to it.

There is much more work to be conducted into the interaction of VSMCs with the electrospun materials. Firstly, the more detailed micrographs of their interaction would be beneficial, perhaps obtained using a scanning electron microscope or atomic force microscope. Secondly, a videomicrograph of their movements over the electrospun material would provide a much-needed insight into the way that they interact with the fibrous structure. Although much data were generated using the mechanical stimulation unit, there is still a wealth of data to be obtained in order to better understand the interaction of the cell with the substrate when undergoing this type of stimulus, for example, observations of the cells on the surfaces when

undergoing the stretch. The hypothesis generated in the previous chapter relating to the way in which cells experience stretch dependant upon their orientation was dependant upon the expectation that a cell, when aligned in a particular direction due to the effect of the fibrous substrate orientation, would not reorient itself due to the cue from the mechanical deformation. Real-time analysis of this situation would reveal whether this is the true situation. Lastly, if these materials are to be used as a basis for a tissue engineered scaffold, the pore sizes of the matrix would need to be modified to allow the appropriate level of cellular infiltration, as shown by Balguid et al. (2009) because the infiltration in the current material is minimal.

The impermeability of the electrospun materials would, however, be advantageous when considering the addition of endothelial cells to the model, as these cells are required to remain at the luminal surface of the vessel and should not be allowed to migrate into the vessel walls. Investigation of this situation would require a co-culture and a more complex electrospun material. This could perhaps be obtained by electrospinning a tight mesh of fibres, much the same as generated in this work, and then overlaying them with a loser mesh, again by electrospinning. The most obvious way to produce a fibrous material with larger pores would be to try to alter the electrospinning parameters, but this would generally increase the fibre diameter, which is undesirable in that if could affect the cell-fibre interaction. However, this loose mesh could perhaps be generated with the alternate spinning of two different polymer fibres and the subsequent dissolution or otherwise removal of one, leaving the other intact. SMCs could then be applied to the face of the electrospun sheet with the larger pore size and incubated until cell infiltration had occurred. The sample would then be inverted and endothelial cells applied to the other surface, where they should form a monolayer. This co-culture construct could provide invaluable information into the interaction of the two cell types and perhaps demonstrate how such a construct could be of use in a clinical environment.

6.3 Final Conclusions

As the patency rates of many commonly used prosthetic graft materials can be disappointing, the work conducted for this thesis illustrates the benefits of utilising alternative materials and processing methods. The effect of material compliance and the associated protein adsorption were shown to affect the early stages of the failure of the graft, while the fibrous nature when processed using electrospinning showed that the latter stages could also be controlled, particularly when the dynamic nature of the vascular system is considered.

In addition to investigations into the development of vascular graft materials, much of the work in this thesis also has great relevance to the construction of tissue engineered blood vessels. The material stiffness has been shown to affect cell migration rates, a crucial process in the initial cell seeding of the construct, while the fibrous geometric nature of an electrospun scaffold could be utilised to obtain the desired properties of the resident cells in the final product.

REFERENCES

Aikawa M, Sivam P N, Kuro M, Kimura M, Nakahara K M, Takewari S, Ueda M, Yamaguchi H, YazakiY, Periasamy M, Nagai R, 1993. Human smooth myosin heavy chain isoforms as molecular markers for vascular development and atherosclerosis. Circ. Res. **73**: 1000-1012.

Altman G, Horan R, Martin I, Farhadi J, Stark P, Volloch V, Vunjak-Novakovic G, Richmond J, Kaplan D L, 2002. Cell differentiation by mechanical stress. The FASEB Journal **16:** 270-272

Asanuma K, Magid R, Johnson C, Nerem R M, Galis Z S, 2003. Uniaxial strain upregulates matrix-degrading enzymes produced by human vascular smooth muscle cells. Am J Physiol Heart Circ Physiol. **284**: 1778–1784

Bader D L, Knight M M, 2008. Biomechanical analysis of structural deformation in living cells Med Biol Eng Comput. **46**: 951–963

Bahadur P, 2001. Block copolymers – Their microdomain formation (in solid state) and surfactant behaviour (in solution). Curr. Sci. India. **80**: 1002-1007.

Balguid A, Mol A, van Marion M H, Bank R A, Bouten C V C, Baaijens F P T, 2009. Tailoring Fiber Diameter in Electrospun Poly(ε-Caprolactone) Scaffolds for Optimal Cellular Infiltration in Cardiovascular Tissue Engineering. Tissue Engineering A **15**: 437-444.

Batchelor W B, Robinson R, Strauss B H, 1998. The Extracellular Matrix in Balloon Arterial Injury: A Novel Target for Restenosis Prevention. Progress in Cardiovascular Diseases, **41**: 35-49.

Barbee K E, Macarak E J, Thibault L E, 1994. Strain Measurements in Cultured Vascular Smooth Muscle Cells Subjected to Mechanical Deformation. Annals of Biomedical Engineering, **22:** 14-22

Baumgarten P, 1971. Electrostatic spinning of acrylic microfibers. J Colloid Interface Sci, **36**(1): 71-9.

Basso N, Heersche J N M, 2002. Characteristics of In Vitro Osteoblastic Cell Loading Models. Bone. **30**: 347–351.

Beamish J A, Fu A Y, Choi A, Haq N A, Kottke-Marchant K, Marchant R E, 2009. The influence of RGD-bearing hydrogels on the re-expression of contractile vascular smooth muscle cell phenotype. Biomaterials, **30**: 4127–4135.

Berns G. S., M. W. Berns, 1982. Computer-based tracking of living cells. Exp Cell Res. **142**: 103–109.

Bia D, Cabrera Fischer E I, Zocalo Y, Pessana F, Armentano R, 2006. Differences in conduit and buffering function among arteries, venous grafts and synthetic prosthesis: Implicances in the development of intimal hyperplasia. Latin Americal Applied Research, **36**: 29-36.

Birchall I E, Field P L, Ketharanathan V, 2001. Adherence of human saphenous vein endothelial cell monolayers to tissue-engineered biomatrix vascular conduits. J Biomed Mater Res. **56**: 437–443.

Birukov K G, Shirinsky V E, Stepanova O V, Tkachuk V A, Hahn A W A, Resink T J, Smirnov V N, 1995. Stretch affects phenotype and proliferation of vascular smooth muscle cells. Molecular and Cellular Biochemistry **144**: 131-139.

Birukov K G, Bardy N, Lehoux S, Merval R, Shirinsky, Tedgui V P, 1998. Intraluminal pressure is essential or the maintenance of smooth muscle caldesmon

and filamin content in aortic organ culture. Arteriosclerosis, Thrombosis, and Vascular Biology, **18**: 922–927.

Boerboom R A, Rubbens M P, Driessen N J B, Bouten C V C, Baaijens F P T, 2008. Effect of Strain Magnitude on the Tissue Properties of Engineered Cardiovascular Constructs. Annals of Biomedical Engineering, **36**: 244–253.

Bouta E M, McCarthy C W, Keim A, Wang H B, Gilbert R J, Goldman J, 2011. Biomaterial guides for lymphatic endothelial cell alignment and migration. Acta Biomaterialia **7**: 1104–1113.

Brossollet L J, 1992. Mechanical issues in vascular grafting: a review. Int J Artif Organs, **15:** 579 –584.

Brown T D, 2000. Techniques for mechanical stimulation of cells in vitro: a review. Journal of Biomechanics **33**: 3-14.

Butcher J T, Barrett B C, Nerem R M, 2006. Equibiaxial strain stimulates fibroblastic phenotype shift in smooth muscle cells in an engineered tissue model of the aortic wall. Biomaterials **27:** 5252–5258.

Cacou C, Palmer D, Lee D A, Bader D L, Shelton J C, 2000. A system for monitoring the response of uniaxial strain on cell seeded collagen gels Medical Engineering & Physics, **22**: 327–333.

Cao Y, Poon Y F, Feng J, Rayatpisheh S, Chan V, Chan-Park M B, 2010. Regulating orientation and phenotype of primary vascular smooth muscle cells by biodegradable films patterned with arrays of microchannels and discontinuous microwalls Biomaterials **31**: 6228-6238.

Chamley-Campbell J H, Campbell G R, 1981. What controls smooth muscle phenotype? Atherosclerosis, **40**, 347-357.

Chen Q, Li W, Quan Z, Sumpio B E, 2003. Modulation of vascular smooth muscle cell alignment by cyclic strain is dependent on reactive oxygen species and P38 mitogen-activated protein kinase. Journal of Vascular Surgery, **37**: 660-668.

Chu, L., L. A. Tempelman, C. Miller, and D. A. Hammer, 1994. Centrifugation assay of IgE-mediated cell-adhesion to antigen-coated gels. AICHE J. **40**: 692-703.

Dancu M B, Berardi D E, Vanden Heuvel J P, Tarbell J M, 2004. Asynchronous Shear Stress and Circumferential Strain Reduces Endothelial NO Synthase and Cyclooxygenase-2 but Induces Endothelin-1 Gene Expression in Endothelial Cells. Arterioscler Thromb Vasc Biol. **24**: 2088-2094.

Dardik A, Yamashita A, Aziz F, Asada H, Sumpio B E, 2005. Shear stress-stimulated endothelial cells induce smooth muscle cell chemotaxis via platelet-derived growth factor-BB and interleukin-1α. J Vasc Surg, **41**: 321-31.

Decaestecker C, Debeir O, Van Ham P, Kiss R, 2007. Can anti-migratory drugs be screened *in vitro*? A review of 2D and 3D assays for the quantitative analysis of cell migration. Med. Red. Rev. **27**: 147-176.

Deitzel J M, Kleinmeyer J, Harris D, Tan N C B, 2001. The effect of processing variables on the morphology of electrospun nanofibers and textiles. Polymer **42**: 261-72.

Deligianni D D, Katsala N, Ladas S, Sotiropoulou D, Amedee J, Missirlis Y F, 2001. Effect of surface roughness of the titanium alloy Ti-6Al-4V on human bone marrow cell response and on protein adsorption. Biomaterials 22 1241-1251.

Diener A, Nebe B, Luthen F, Becker P, Beck U, Neumann H G, Rychly J, 2005. Control of focal adhesion dynamics by material surface characteristics. Biomaterials. **26**: 383-392.

DiMilla P A, Barbee K, Lauffenburger D A, 1991. Mathematical model for the effects of adhesion and mechanics on cell migration speed. Biophys. J. **60**: 15-37.

DiMilla P A, Stone J A, Quinn J A, Albelda S M, Lauffenburger D A, 1993. Maximal migration of human smooth muscle cells on fibronectin and type IV collagen occurs at an intermediate attachment strength. J. Cell Biol. **122:** 729-737.

Dong Z, Kennedy S J, Wu Y, 2011. Electrospinning materials for energy-related applications and devices. Journal of Power Sources, **196**: 4886–4904.

Doshi J, Reneker D H, 1995. Electrospinning process and applications of electrospun fibers. J Electrostatics, **35**:151-60.

Drew J S, Moos C, Murphy R A, 1991. Localization of isoactins in isolated smooth muscle thin filaments by double gold immuno labeling. Am. J. Physiol. 260 Cell Physiol. **29**: C1332-C1340.

Francois P, Vaudaux P, Nurdin N, Mathieu H J, Descouts P, Lew D P, 1996. Physical and biological effects of a surface coating procedure on polyurethane catheters. Biomaterials **17**: 667-676.

Fruchart J-C, Nierman M C, Stroes E S G, Kastelein J J P, Duriez P, 2004. Circulation, **109**, 15-19

Fujita K, Komatsu K, Tanaka K, Ohshima S, Asami Y, Murata E, Akita M, 2006. An in vitro model for studying vascular injury after laser microdissection. Histochem Cell Biol **125**: 509–514.

Gahtan V, Wang X, Ikeda M, Willis A I, Tuszynski G P, Sumpio B E, 1999. Thrombospondin-1 induces activation of focal adhesion kinase in vascular smooth muscle cells. J Vasc Surg, **29:** 1031-1036.

Ganguli A, Persson L, Palmer I R, Evans I, Yang L, Smallwood R, Black R, Qwarnstrom E E, 2005. Distinct NF-κB Regulation by Shear Stress Through Ras-Dependent IκBα Oscillations. *Circ Res*. **96**: 626-634.

Garrett, J. T., C. A. Siedlecki, and J. Runt, 2001. Microdomain morphology of poly(urethane urea) multiblock copolymers. Macromolecules. **34**: 7066-7070.

Gerthoffer W T, 2007. Mechanisms of Vascular Smooth Muscle Cell Migration. *Circ. Res.* **100**: 607-621.

Godin M, Bryan A K, Burg T P, Babcock K, Manalis S R, 2007. Measuring the mass, density, and size of particles and cells using a suspended microchannel resonator, Appl. Phys. Lett. **91**, 123121-3.

Goodman S L, Simmons S R, Cooper S L, Albrecht R M, 1990. Preferential adsorption of plasma proteins onto apolar polyurethane microdomains. J. Colloid Interf. Sci. **139**: 561-570.

Grinnell F, Feld M K, 1981. Fibronectin adsorption on hydrophilic and hydrophobic surfaces detected by antibody binding and analyzed during cell adhesion in serum-containing medium. J. Biol. Chem. **257**: 4888-4893.

Haghighipour N, Tafazzoli-Shadpour M, Shokrgozar M A, Amini S, 2010. Effects of Cyclic Stretch Waveform on Endothelial Cell Morphology Using Fractal Analysis. Artificial Organs **34**: 481-490.

Hall A, 2005. Rho GTPases and the control of cell behaviour. Biochem Soc Trans. **33**: 891– 895.

Hasaneen N A, Zucker S, CaoJ, Chiarelli C, Panettieri R A, Foda H D, 2005. Cyclic mechanical strain-induced proliferation and migration of human airway smooth muscle cells: role of EMMPRIN and MMPs. **19**: 1507-1509.

Hayati I, Bailey A I, Tadros T F, 1987. Investigations into the mechanisms of electrohydrodynamic spraying of liquids. 1. Effect of electric-field and the environment on pendant drops and factors affecting the formation of stable jets and atomization. J Colloid Interface Sci. **117**: 205-21.

Hipper A, Isenberg G, 2000. Cyclic mechanical strain decreases the DNA synthesis of vascular smooth muscle cells. Eur J Physiol. **440**: 19–27

Houtchens G R, Foster M D, Desai T A, Morgan E F, and Wong J Y, 2008. Combined Effects of Microtopography and Cyclic Strain on Vascular Smooth Muscle Cell Orientation *J Biomech*. **41**: 762–769.

Hsieh T M, Ng C W B, Narayanan K, Wan A C A, Ying J Y, 2010. Three-dimensional microstructured tissue scaffolds fabricated by two-photon laser scanning photolithography. Biomaterials, **30**, 7648-7652.

Hu, Y, Bock, G, Wick, G, Xu, Q, 1998. Activation of PDGF receptor alpha in vascular smooth muscle cells by mechanical stress. FASEB Journal, **12**: 1135–1142.

Humphrey J D, Na S, 2002. Elastodynamics and Arterial Wall Stress. Annals of Biomedical Engineering, **30**: 509–523.

Hungerford J E, Little C D, 1993. The developmental biology of vascular smooth muscle as studies with a new monoclonal antibody directed against an embryonic quail vascular smooth muscle antigen. J. Cell Biochem. **17**: 198.

Ingber D E, 1993. Cellular tensegrity: defining new rules of biological design that govern the cytoskeleton. J. Cell. Sci. **104**: 613-627.

Ingber D E, 2003a. Tensegrity I. Cell structure and hierarchical systems biology. J. Cell Sci. **116**: 1157-1173.

Ingber D E, 2003b. Tensegrity II. How structural networks influence cellular information processing networks. J. Cell Sci. **116**: 1397-1408.

Isenberg B C, Tsuda Y, Williams C, Shimizu T, Yamato M, Okano T, Wong J Y, 2008. A thermoresponsive, microtextured substrate for cell sheet engineering with defined structural organization. Biomaterials, **29**: 2565–2572.

Jaeger R, Bergshoef M M, Batlle C M I, Schonherr H, Vancso G J, 1998. Electrospinning of ultra-thin polymer fibers. Macromol Symp. **127**: 141-50.

Jeong S I, Kim S Y, Cho S K, Chong M S, Kim K S, Kim H, Lee S B, Lee Y M, 2007. Tissue-engineered vascular grafts composed of marine collagen and PLGA fibers using pulsatile perfusion bioreactors. Biomaterials **28**: 1115–1122.

Jesudason R, Black L, Majumdar A, Stone P, Suki B, 2007. Differential effects of static and cyclic stretching during elastase digestion on the mechanical properties of extracellular matrices. J Appl Physiol. **103**: 803–811.

Jiang, G, Huang A H, Cai Y, Tanase M, Sheetz M P, 2006. Rigidity sensing at the leading edge through αvβ3 integrins and RPTPα. Biophys. J. **90**: 1804-1809.

Jiang H, Fang D, Hsiao B S, Chu B, Chen W, 2004. Optimization and characterization of dextran membranes prepared by electrospinning. Biomacromolecules, **5**: 326-33.

Kakisis J D, Liapis C D, Breuer C, Sumpio B E, 2005. Artificial blood vessel: The Holy Grail of peripheral vascular surgery. J Vasc Surg. **41**: 349-54.

Karim M A, 1998. In vivo role of the extracellular matrix during vascular repair. Basic Res Cardiol. **93**: 50 – 54.

Keese C R, Wegener J, Walker S R, Giaever I, 2004 Electrical wound-healing assay for cells *in vitro*. PNAS, **101**: 1554-1559.

Kim B S, Mooney D J, 2000. Scaffolds for engineering smooth muscle under cyclic mechanical strain conditions. Journal of Biomechanical Engineering **122**: 210–215.

Koo L Y, Irvine D J, Mayes A M, Lauffenburger D A, Griffith L G, 2002. Co-regulation of cell adhesion by nanoscale RGD. J. Cell. Sci. **115**: 1423-1433.

Kotani J, Awata M, Nanto S, Uematsu M, Oshima F, Minamiguchi H, Mintz G S, Nagata S, 2006. Incomplete Neointimal Coverage of Sirolimus-Eluting Stents. Journal of the American College of Cardiology, **47**: 2108-2111.

Kuro M, Nagai R, Tsuchimochi H, Katoh H, Yazaki Y, Ohkubo A, Takaku F, 1989. Developmentally regulated expression of vascular smooth muscle myosin heavy chain isoforms. J. Biol. Chem. **264**: 18272-18275.

Labow R S, Erfle D J, Santerre J P, 1995. Neutrophil-mediated degradation of segmented polyurethanes. Biomaterials, **16**, 51-59

Langelier E, Rancourt D, Bouchard S, Lord C, Stevens P -P, Germain L, Auger F A, 1999. Cyclic Traction Machine for Long-Term Culture of Fibroblast-Populated Collagen Gels. Annals of Biomedical Engineering, **27**, 67–72.

Laurent S, Girerd X, Mourad J J, Lacolley P, Beck L, Boutouyrie P, Mignot J P, Safar M, 1994. Elastic modulus of the radial artery wall material is not increased in patients with essential hypertension. Arterioscler Thromb Vasc Biol, **14**: 1223-1231.

Lee C H, Shin H J, Cho I H, Kang Y, Kim I E, Park K, Shin J, 2005. Nanofiber alignment and direction of mechanical strain affect the ECM production of human ACL fibroblast. Biomaterials **26**: 1261–1270.

Lemson M S, Tordoir J H M, Daemen M J A P, Kitslaar P J E H M, 2000. Intimal hyperplasia in vascular grafts. Eur. J. Vasc. Endovasc. Surg. **19**: 336-350.

Li C, Xu Q, 2007. Mechanical stress-initiated signal transduction in vascular smooth muscle cells in vitro and in vivo. Cellular Signalling, **19**: 881–891.

Li L, Chaikof E L, 2002. Mechanical Stress Regulates Syndecan-4 Expression and Redistribution in Vascular Smooth Muscle Cells. Arterioscler. Thromb. Vasc. Biol. **22**: 61-68.

Li Y J, Haga J H, Chien S, 2005. Molecular basis of the effects of shear stress on vascular endothelial cells Journal of Biomechanics **38**: 1949–1971.

Lillie M A, Shadwick R E, Gosline J M, 2010. Mechanical anisotropy of inflated elastic tissue from the pig aorta. Journal of Biomechanics **43**: 2070–2078.

Liu B, Qu M, Qin K, Li H, Li Z, Shen B, Jiang Z, 2007. Role of cyclic strain frequency in regulating the Alignment of Vascular Smooth Muscle Cells *in vitro.* Biophys J. **94**: 1497-507.

Liu Y, Ji Y, Ghosh K, Clark R A F, Huang L, Rafailovich M H, 2008. Effects of fiber orientation and diameter on the behavior of human dermal fibroblasts on electrospun PMMA scaffolds. J Biomed Mater Res. **90A**: 1092–1106.

Liu Y, Franco A, Huang L, Gersappe D, Clark R A F, Rafailovich M H, 2009. Control of cell migration in two and three dimensions using substrate morphology. Experimental Cell Research **315**: 2544-2557.

Liang C C, Park A Y, Guan J L, 2007. *In vitro* scratch assay: a convenient and inexpensive method for analysis of cell migration *in vitro.* Nature Protocols. **2**. 329-333.

Liang D, Hsiao B S, Chu B, 2007. Functional Electrospun Nanofibrous Scaffolds for Biomedical Applications. Adv Drug Deliv Rev. **59**: 1392–1412.

Lo C M, Wang H B, Dembo M, Wang Y L, 2000. Cell movement is guided by the rigidity of the substrate. Biophys J. **79**: 144-152.

Loesberg W A, Walboomers X F, van Loon J J W A, Jansen J A, 2005. The effect of combined cyclic mechanical stretching and microgrooved surface topography on the behavior of fibroblasts. J Biomed Mater Res. **75A**: 723–732.

London G M, and Pannier B, 2010. Arterial functions: how to interpret the complex physiology. Nephrol. Dial. Transplant. **25**: 3815–3823.

Lowry O H, Rosebrough N J, Farr A L, Randall R J, 1951. Protein measurement with the Folin phenol reagent. J. Biol. Chem. **193**, 265–75.

Lubarsky G V, Davidson M R, Bradley R H, 2004. Elastic modulus, oxidation depth and adhesion force of surface modified polystyrene studied by AFM and XPS. Surface Science **558**, 135–144

Ma X, Wang Y, Stephens N L, 1998. Serum deprivation induces a unique hypercontractile phenotype of cultured smooth muscle cells Am. J. Physiol. **274**: C1206– C1214.

Macdonald D E, Deo N, Markovic B, Stranick M, Somasundaran P, 2002. Adsorption and dissolution behavior of human plasma fibronectin on thermally and chemically modified titanium dioxide particles. Biomaterials. **23**: 1269-1279.

Meechaisue C, Dubin R, Supaphol P, Hoven VP, Kohn J, 2006. Electrospun mat of tyrosine-derived polycarbonate fibers for potential use as tissue scaffolding material. J Biomater Sci Polym Ed. **17**: 1039-56.

Megelski S, Stephens J S, Chase D B, Rabolt J F, 2002. Micro- and nanostructured surface morphology on electrospun polymer fibers. Macromolecules **22**: 8456-66.

Mitra A K, Gangahar D M, Agrawal D K, 2006. Cellular, molecular and immunological mechanisms in the pathophysiology of vein graft intimal hyperplasia. Immunology and Cell Biology **84**, 115–124.

Miyamotoa K, Atarashia M, Kadozonoa H, Shibataa M, Koyamaa Y, Okaia M, Inakumaa A, Kitazonob E, Kanekob H, Takebayashia T, Horiuchia T, 2009. Creation of cross-linked electrospun isotypic-elastin fibers controlled International Journal of Biological Macromolecules, **45**: 33–41.

Nestor A L, Cicila G T, Karol S E, Langenderfer K M, Hollopeter S L, Allison D C, 2006. Linkage analysis of neointimal hyperplasia and vascular wall transformation after balloon angioplasty. Physiol Genomics, **25**: 286–293.

Nicolas A, Besser A, Safran S A, 2008. Dynamics of cellular focal adhesions on deformable substrates: consequences for cell force microscopy. Biophysical J. **95**: 527-539.

Niessen P, Clement S, Fontao L, Chaponnier C, Teunissen B, Rensen S, van Eys G, Gabbiani G, 2004. Biochemical evidence for interaction between Smoothelin and filamentous actin. Experimental Cell Research, **292**, 170-178.

Norman J J, Desai T A, 2006. Methods for Fabrication of Nanoscale Topography for Tissue Engineering Scaffolds. Annals of Biomedical Engineering, 34, 89–101

Numaguchi K, Eguchi S, Yamakawa T, Motley E D, Inagami T, 1999. Mechanotransduction of rat aortic vascular smooth muscle cells requires RhoA and intact actin filaments. Circulation Research **85**, 5–11.

Ogawa J, Fujiwara H, Kawamura A, Katsuragawa M, Htay T, Fujiwara T, Hasegawa K, Yamasak K, Tanaka M, Sasayama S, 1997. Acute cellular damage in medial smooth muscle cells following experimental coronary angioplasty in Dog. Damage of cytoskeleton and apoptosis. Heart Vessels, **12**: 157-166.

Oishi K,1 Itoh Y, Isshiki Y, Kai C, Takeda Y, Yamaura K, Takano-Ohmuro H, Uchida M K, 2000. Agonist-induced isometric contraction of smooth muscle cell-populated collagen gel fiber. Am J Physiol Cell Physiol. **279**: C1432–C1442.

Okada S S, Tomaszewski J E, Barnathan E S, 1995. Migrating vascular smooth muscle cells polarise cell surface urokinase receptors after injury in vitro. Experimental Cell Research, **217**: 180-187.

Palecek S P, Loftus J C, Ginsberg M H, Lauffenburger D A, Horwitz A F, 1997. Integrin-ligand binding properties govern cell migration speed through cell-substratum adhesiveness. Nature. **385**: 537-540.

Pedersen J A, Swartz M A, 2005. Mechanobiology in the Third Dimension. Annals of Biomedical Engineering, **33**: 1469–1490.

Peyton S R, Putnam A J, 2005. Extracellular matrix rigidity governs smooth muscle cell motility in a biphasic fashion. J. Cell. Physiol. **204**: 198-209.

Pitsch R J, Goodman G R, Minion D J, Madura II J A, Fox P L, Graham L M, 2000. Inhibition of smooth muscle cell proliferation and migration in vitro by antisense oligonucleotide to c-*myb*. J. Vasc. Surg. **23**: 783-791.

Pratt B M, Harris A S, Morrow J S, Madri J A, 1984. Mechanisms of cytoskeletal regulation. Modulation of aortic endothelial cell spectrin by the extracellular matrix. Am. J. Pathol. **117**: 349-354.

Punchard M A, Stenson-Cox C, O'Cearbhaill E D, Lyons E, Gundy S, Murphy L, Pandit A, McHugh P E, Barron V, 2007. Endothelial cell response to biomechanical forces under simulated vascular loading conditions. Journal of Biomechanics, **40**: 3146–3154.

Putnam A J, Schultz K, Mooney D J, 2001. Control of microtubule assembly by extracellular matrix and externally applied strain. Am. J. Physiol. Cell. Physiol. **280**: C556-C564.

Qu M J, Liu B, Wang H Q, Yan Z Q, Shen B R, Jiang Z L, 2006. Frequency-Dependent Phenotype Modulation of Vascular Smooth Muscle Cells under Cyclic Mechanical Strain. J Vasc Res **44**: 345–353.

Rajagopalan, P., W. A. Marganski, X. B. Brown, and J. W. Wong, 2004. Direct comparison of the spread area, contractility, and migration of balb/c 3T3 fibroblasts adhered to fibronectin- and RGD-modified substrata. Biophys. J. **87**: 2818-2827.

Reusch P, Wagdy H, Reusch, R, Wilson E, Ives, H E, 1996. Mechanical strain increases smooth muscle and decreases nonmuscle myosin expression in rat vascular smooth muscle cells. Circulation Research **79**, 1046–1053.

Rosales O R, Isales C M, Barrett P Q, Brophy C Sumpio B E, 1997. Exposure of endothelial cells to cyclic strain induces elevations of cytosolic Ca^{2+} concentration through mobilization of intracellular and extracellular pools. Biochem. J. **326**: 385-392.

Roy P, Rajfur Z, Pomorski P, Jacobson K, 2002. Microscope-based techniques to study cell adhesion and migration. Nature Cell Biology, **4**: E91-96.

Sell S A, McClure M J, Garg K, Wolfe P S, Bowlin G L, 2009. Electrospinning of collagen/biopolymers for regenerative medicine and cardiovascular tissue engineering. Advanced Drug Delivery Reviews, 61, 1007–1019

Sharifpoor S, Simmons C A, Labow R S, Santerre P J, 2010. A study of vascular smooth muscle cell function under cyclic mechanical loading in a polyurethane scaffold with optimized porosity Acta Biomaterialia, **6**: 4218–4228.

Shyu K, 2009. Cellular and molecular effects of mechanical stretch on vascular cells and cardiac myocytes Clinical Science **116**, 377–389.

Simmers M B, Pryor A W, Blackman B R, 2007. Arterial shear stress regulates endothelial cell-directed migration, polarity, and morphology in confluent monolayers. Am J Physiol Heart Circ Physiol **293**: H1937–H1946.

Sipkema P, van der Linden P J W, Westerhof N, Yin F C P, 2003. Effect of cyclic axial stretch of rat arteries on endothelial cytoskeletal morphology and vascular reactivity. Journal of Biomechanics **36**: 653–659.

Smith, J T, Tomfohr J K, Wells M C, Beebe Jr. T P, Kepler T B, Reichert W M, 2004. Measurement of cell migration on surface bound fibronectin gradients. Langmuir. **20**: 8279-8286.

Standley P R, Camaratta A, Nolan B P, Purgason C T, Stanley M A, 2002. Cyclic stretch induces vascular smooth muscle cell alignment via NO signalling. Am J Physiol Heart Circ Physiol **283**: 1907–1914.

Stephansson S N, Byers B A, García A J, 2002. Enhanced expression of the osteoblastic phenotype on substrates that modulate fibronectin conformation and integrin receptor binding. Biomaterials. **23**: 2527-2534.

Streuli C, 1999. Extracellular matrix remodelling and cellular differentiation. Current Opinion in Cell Biology, **11**: 634–640.

Subbotin V M, 2007. Analysis of arterial intimal hyperplasia: review and hypothesis. Theoretical Biology and Medical Modelling, **4**: 41.

Sweeney N O, Cummins P M, Birney Y A, Redmond E M, Cahill P A, 2004. Cyclic strain-induced endothelial MMP-2: role in vascular smooth muscle cell migration. Biochemical and Biophysical Research Communications. **320**: 325–333.

Tanaka H, Hirose M, Osada T, Miwa H, Watanabe S, Sato N, 2000. Implications of Mechanical Stretch on Wound Repair of Gastric Smooth Muscle Cells In Vitro Digestive Diseases and Sciences, **45**: 2470–2477.

Taylor G, 1969. Electrically driven jets. Proc Natl Acad Sci London, A313: 453-75.

Telemeco T A, Ayres C, Bowlin G L, Wnek G E, Boland E D, Cohen N, Baumgarten C M, Mathews J, Simpson D G. Regulation of cellular infiltration into tissue engineering scaffolds composed of submicron diameter fibrils produced by electrospinning. Acta Biomaterialia **1**: 377–385.

Thakar R G, Ho F, Huang N F, Liepmann D, Li S, 2003. Regulation of vascular smooth muscle cells by micropatterning. Biochemical and Biophysical Research Communications, **307**: 883–890.

Tiwari A, Cheng K S, Salacinski H, Hamilton G and Seifalian A M, 2003. Improving the Patency of Vascular Bypass Grafts: the Role of Suture Materials and Surgical Techniques on Reducing Anastomotic Compliance Mismatch. Eur J Vasc Endovasc Surg, **25**: 287-295.

Tock J, Van Putten V, Stenmark K R, Nemenoff R A, 2003. Induction of SM-α-actin expression by mechanical strain in adult vascular smooth muscle cells is mediated

through activation of JNK and p38 MAP kinase. Biochemical and Biophysical Research Communications **301**: 1116–1121.

Todaro, G. J., G. K. Lazar, and H. Green, 1965. The initiation of cell division in a contact-inhibited mammalian cell line. J. Cell Physiol. **66**: 325–333.

Tozzi P, Hayoz D, Oedman C, Mallabiabarrena I, von Segesser L K, 2001. Systolic axial artery length reduction: an overlooked phenomenon in vivo. Am J Physiol Heart Circ Physiol. **280**: 2300–2305.

Truskett V N, Watts M P C, 2006. Trends in imprint lithography for biological applications. Trends in Biotechnology, **24**, 312-317.

Tsuchida H, Wilson S E, Ishimaru S, 1997. Healing Mechanisms of High-Porosity PTFE Grafts: Significance of Transmural Structure. Journal of Surgical Research, **71**: 187-195.

Tsui J C S, Dashwood M R, 2002. Recent Strategies to Reduce Vein Graft Occlusion: a Need to Limit the Effect of Vascular Damage. Eur J Vasc Endovasc Surg 23, 202–208.

Uttayarat P, Chen M, Li M, Allen FD, Composto R J, Lelkes P I, 2008. Microtopography and flow modulate the direction of endothelial cell migration. Am J Physiol Heart Circ Physiol. **294**: 1027–1035

Uttayarat P, Perets A, Li M, Pimton P, Stachelek S J, Alferiev I, Composto R J, Levy R J, Lelkes P I, 2010. Micropatterning of three-dimensional electrospun polyurethane vascular grafts. Acta Biomaterialia **6**: 4229–4237.

Uyama Y, Inoue H, Ito K, Kishida A, Ikada Y, 1991. Comparison of different methods for contact angle measurements, J. Colloid Interface Sci. **141** (1), 275–279.

van Eys G J, Niessen P M, Rensen S S, 2007. Smoothelin in Vascular Smooth Muscle Cells. Trends in Cardiovascular Medicine, **17**, 26-30.

Venkatraman S, Boey F, Lao L L, 2008. Implanted cardiovascular polymers: Natural, synthetic and bio-inspired. Progress in Polymer Science, **33**, 853–874.

Veress A I, Weiss J A, Gullberg G T, Vince D G, Rabbitt R D, 2002. Strain Measurement in Coronary Arteries Using Intravascular Ultrasound and Deformable Images. Journal of Biomechanical Engineering, **124**: 734-741.

Vernon R B, Gooden M D, Lara S L, Wight T N, 2005. Microgrooved fibrillar collagen membranes as scaffolds for cell support and alignment Biomaterials **26**: 3131–3140.

Wei J, Igarashi T, Okumori N, Igarashi T, Maetani T, Liu B, Yoshinari M, 2009. Influence of surface wettability on competitive protein adsorption and initial attachment of osteoblasts. Biomed. Mater. **4**: 1-7.

Williams C, Brown X Q, Bartolak-Suki E, Ma H, Chilkoti A, Wong J Y, 2011. The use of micropatterning to control smooth muscle myosin heavy chain expression and limit the response to transforming growth factor β1 in vascular smooth muscle cells Biomaterials **32**: 410-418.

Wong J W, Velasco A, Rajagopalan P, Pham Q, 2003. Directed movement of vascular smooth muscle cells on gradient-compliant hydrogels. Langmuir. **19**: 1908-1913.

Worth N F, Rolfe B E, Campbell J H, Campbell G R, 2004. Rho and smooth muscle cell phenotype International Congress Series **1262**: 111 – 114

Xu C Y, Inai R, Kotaki M, Ramakrishna S, 2004. Aligned biodegradable nanofibrous structure: a potential scaffold for blood vessel engineering. Biomaterials **25**: 877–886.

Xue L, Greisler H P, 2003. Biomaterials in the development and future of vascular grafts J Vasc Surg. **37**: 472-80.

Yeung T, Georges P, Flanagan L A, Marg, Ortiz M, Funaki M, Zahir N, Ming W, Weaver V, Janmey P A, 2005. Effects of substrate stiffness on cell morphology, cytoskeletal structure, and adhesion. Cell Motil. Cytoskel. **60**: 24-34.

Yim E K F, Reano R M, Pang S W, Yee A F, Chen C S, Leong K W, 2005. Nanopattern-induced changes in morphology and motility of smooth muscle cells. Biomaterials, **26**: 5405–5413

Yoshigi M, Clark E B, Yost H J, 2003. Quantification of Stretch-Induced Cytoskeletal Remodeling in Vascular Endothelial Cells by Image Processing Cytometry Part A, **55A**: 109–118.

Yost M J, Simpson D, Wrona K, Ridley S, Ploehn H J, Borg T K, Terracio L, 2000. Design and construction of a uniaxial cell stretcher. Am J Physiol Heart Circ Physiol. **279**: 3124–3130.

Zhang C X, Yuan X Y, Wu L L, Han Y, Sheng J, 2005. Study on morphology of electrospun poly(vinyl alcohol) mats. Eur Poly J. **41**:423-32.

Zarghama R, Touyz R M, Thibault G, 2007. α8 Integrin overexpression in de-differentiated vascular smooth muscle cells attenuates migratory activity and restores the characteristics of the differentiated phenotype Atherosclerosis, **195**: 303–312.

Zeebregts C J, Kirsch W M, van den Dungen J J, Zhu Y H, van Schilfgaarde R, 2004. Five years' world experience with nonpenetrating clips for vascular anastomoses. The American Journal of Surgery, **187**: 751–760.

Zeidan A, Nordström I, Albinsson S, Malmqvist U, Swärd K, Hellstrand P, 2003. Stretch-induced contractile differentiation of vascular smooth muscle: sensitivity to actin polymerization inhibitors. Am J Physiol Cell Physiol **284**: 1387–1396.

Zhang X, Wang X, Keshav V, Wang X, Johanas J T, Leisk G G, Kaplan D L, 2009. Dynamic culture conditions to generate silk-based tissue-engineered vascular grafts. Biomaterials, **30**: 3213–3223.

Zhang Y Z, Su B, Venugopal J, Ramakrishna S, Lim C T, 2007. Biomimetic and bioactive nanofibrous scaffolds from electrospun composite nanofibers. International Journal of Nanomedicine, **2**: 623–638.

Zhang Z, Marois Y, Guidoin R G, Bull P, Marois M, How T, Laroche G, King M W, 1997. Biomaterials **18**, 113-124.

Zilla P, Bezuidenhout D, Human P, 2007. Prosthetic vascular grafts: Wrong models, wrong questions and no healing. Biomaterials, **28**: 5009–5027.